UNIVERSITY OF THE PELOPONNESE
DEPARTMENT OF HISTORY, ARCHAEOLOGY
AND CULTURAL RESOURCES MANAGEMENT

NATIONAL CENTER
FOR SCIENTIFIC RESEARCH
"DEMOKRITOS"

NATIONAL
OBSERVATORY
OF ATHENS

Master of Science in
«Cultural Heritage Materials and Technologies»

DELANEY BRINK
(R.N. 1012202002002)

DIPLOMA THESIS:

ANCIENT THOURIA LAGYNOS: AN ORGANIC RESIDUE CASE STUDY

SUPERVISING COMMITTEE:
- Prof. Nikolaos Zacharias
- Assoc. Prof. Stamatis Boyatzis

EXAMINATION COMMITTEE:
- Prof. Nikolaos Zacharias
- Assoc. Prof. Stamatis Boyatzis
- Dr. Eleni Palamara

KALAMATA, JULY 2022

Acknowledgements

I would like to express my deepest thanks to my supervisors and the members of the examination committee: Professor Stamatis Boyatzis, Professor Nikolaos Zacharias, and Dr. Eleni Palamara. Without their boundless support, guidance, and useful critiques throughout the course of this research, this project would not have been possible. Without Professor Boyatzis, this project would not have lived up to its potential; thank you for sacrificing your time again and again so that I could make and fix mistakes. Professor Zacharias was a fountain of endless patience and guidance that allowed this project to bloom into something amazing. And it was only thanks to Dr. Palamara's understanding and creativity that I was able to explore all of my academic interests with this project. Special thanks to doctoral researcher Celia Valantou without whom I would still be struggling to understand the complexities of Greek archaeology.

It is my pleasure to thank the Archaeological Museum of Messenia, the Department of Conservation of Antiquities and Works of Art (*CAWA*) Laboratory at the University of West Attica, and the Laboratory of Archaeometry at the University of the Peloponnese. These institutions enabled the foundations necessary for the execution and completion of this work. Additional thanks are given to Dr. Arapogianni, Dr. Malapani, Mr. Katakos, and the Greek Ministry of Culture for access to the Ancient Thouria Site and the Thouria lagynos vessel. I would also like to thank Ms. Spala for her assistance in understanding the conservation and preservation of the lagynos vessel.

I would also like to express my most heartfelt gratitude to my friends and family without whom I could not have completed this thesis. I would also like to express my sincerest affection to Izma and Nala who provided unparalleled emotional support during times of stress.

Table of Contents

List of Tables

List of Figures

Abstract

A lagynos vessel ascribed to Hellenistic Times from the Ancient Thouria archaeological site was found undamaged in a tomb that was uncovered during a rescue excavation. Based on the vessel type and appearance, it was assumed to have contained wine or oils which were presumably used in a funerary context. As the vessel was discovered in a rescue excavation, it is important to understand the context of the vessel in addition to its contents. In order to verify the identity of the vessel's possible organic residue, archaeometric analysis was required. Due to the delicate and unique state of the lagynos, the archaeological soil inside of the vessel was analyzed in order to prevent damage to the vessel itself. The study was conducted through the use of minimally invasive optical microscopy, SEM-EDS, RAMAN spectroscopy, and FTIR spectroscopy. In order to evaluate the results, the archaeological soil was compared against reference soils collected from the Thouria area at various distances from the tomb. Based on the results of the analysis, it is assumed that there are organic remains inside of the vessel and that the vessel was unmoved post-deposition in the tomb until its rediscovery in 2018. Thus, it is the goal of this study to determine if archaeological soils can be utilized to verify the presence of organic remains without the destruction of intact ceramic bodies or potsherds fragments.

Keywords: Thouria; organic residue; lagynos; FTIR; archaeological soil; minimally invasive

Introduction

During a rescue excavation at the Ancient Thouria archaeological site in 2018, a lagynos vessel in the white-ground style was found undamaged and intact inside of a tomb. As there have only been a few vessels of this style discovered intact, the function and usage of the white-ground lagynoi have not been studied in detail; however, based on the vessel's typology and appearance it was hypothesized to have contained liquids intended for funerary or ritual use which were most likely wines or oils. That being said, as the preservation state of the Thouria lagynos is delicate, an examination of the assumed residue could not be performed using traditional organic residue analysis methodology. As a result, new methods for analysis using archaeological soils from inside of the vessel have been proposed in order to evaluate if the vessel did, in fact, contain liquids through the use of minimally invasive optical microscopy, SEM-EDS, RAMAN spectroscopy, and FTIR spectroscopy. Thereby the purpose of this study is to determine if archaeological soils, which were collected from inside of the lagynos, can theoretically also be utilized in the examination of previously liquid organic residue *without* the destruction of intact ceramic bodies or potsherds fragments.

The methodology of this study can be separated into three sections: sample selection, methodology evaluation, and organic residue identification. In order to evaluate which archaeological soil fragments were suitable for analysis, visual examination and optical microscopy were required to narrow the sample group from 30 to 7; these samples, collectively referred to as the Refined Analysis Group, were examined using SEM-EDS and Raman spectroscopy in order to evaluate the plausibility of organic residue. Additionally, 5 reference samples from the ancient Thouria site were also examined to

provide context. Following this, the two sample groups were then analyzed using several different FTIR methodologies in order to identify and verify the samples containing organic residue and to determine if the organic residue differs from that of the reference samples. Following identification, the organic peaks were examined and compared against those of the reference samples from the Thouria area and known biomarkers from wines and oils.

As such, this study consists of seven main chapters which outline the background of the study, the analytical process, and the corresponding conclusions. In order to introduce the background cultural information for the study, Chapter One details the history of the Peloponnese and the Ancient Thouria archaeological site. The second chapter details the technical aspects of ceramic studies and organic residue analysis. The materials utilized during the study and their collection process are detailed in Chapter Three. The fourth chapter entails the methodologies performed during the study. The results of these analyses are presented in Chapter Five; Chapter Six entails the discussion of these results. The final chapter compiles the results of this study and proposes steps for future analysis.

Chapter 1. Cultural Background

1.1 Messenia

Messenia is situated in the southwestern corner of the Peloponnese and encompasses the region from the Alpheios River on the north to the Messenian gulf on the south and from Mount Taygetos on the east to the Ionian Sea on the west (Fig. 1) (Loy & Wright, Jr., 1972, p. 36). Historic records of the southwest Peloponnese start to slowly appear beginning during the end of the Mycenaean Age and into the beginning of the Byzantine era which covers a time period from roughly the 11th century B.C.E. to the 4th century C.E.; following this range of time, there is a sharp increase in historical documentation of the area (Simpson & Lazenby, 1972, pp. 81-82).

Figure 1: Local Map. Peloponnesian location map in Greek and Roman times (Simpson & Lazenby, 1972, p. 83).

There is little surviving evidence of Messenia before the 4th century B.C.E which is consistent with the fact that there are few historic documents for the area as a whole before the 6th century B.C.E.; in addition, even less is known about Messenians as a whole due to their subjection under Spartan control during this time period (Simpson & Lazenby, 1972, pp. 81-82). The 5th century B.C.E. saw the emergence of the Messenians in the political landscape of Greece as word of their revolt spread to the rest of Greece (Luraghi, 2009). The new Messenian group was composed of Helots and *perioikoi* who seceded from Sparta (Luraghi, 2009). The members of these groups would go on to occupy the site known today as Ancient Thouria (Fig. 2).

Figure 2: Close-Up Map. Messenia location map in Greek and Roman times (Simpson & Lazenby, 1972, p. 95).

1.2 Ancient Thouria

The Ancient Thouria Archaeological Site as it is known today is most closely associated with the classical phase of the settlement as a "περίοικος πόλη", a designation used to describe peripheral or neighbouring communities that existed at the outskirts of an important site, which reflects the city's position as one of the most important settlements in western Messenia (Villafane Silva, 2015, p. 16); this is further supported by the fact that, after 369 B.C.E. when Messene was founded, Thouria was considered the second richest city in the region. The importance of the city is evident from the naming of the gulf from Avia and Fares to the valley of Pamisos as *Thouriatis gulf* (Αραπογιάννη, 2017).

At present, the ruins of the ancient settlement can be located about 10 km northwest of Kalamata, on the right side of the road Kalamata - Tripoli, and approximately 2.5 km north of the current town Thouria (Ancient Thouria Excavation Website, 2016). The site is situated on a long, extended ridge that runs north to south along the highway and reaches a height of 100 meters above the plain (Αραπογιάννη, 2017). Ancient Thouria occupies a strategic position in a naturally fortified area with a direct connection to the fertile river valley; this location was ideal for the cultivation of a variety of agricultural products as a result of seasonal flooding from the nearby rivers, Ari and Pamisos (Panagiotidis, et al., 2019, p. 258). Part of the city was unearthed in 2007 and has been under systematic excavation since 2009 under the direction of Dr. Arapogianni and the auspices of the Archaeological Society at Athens (Ancient Thouria Excavation Website, 2016).

Historic Occupation

Although the Ancient Thouria Archaeological site is most commonly associated with the classical period, the importance of the city of Thouria can be traced further in history under a variety of different identities in literature and history. The settlement itself has been identified by epigraphic plates that mention the name of the ancient city which have been connected to historical documents. In addition, archaeological evidence indicates that the city was occupied, beginning in the Bronze Age, as a significant Mycenean center, however, historic and mythic sources indicate a wider scope of occupation (Αραπογιάννη, 2018, pp. 48-50).

Historical accounts of Ancient Thouria are fragmented and often separate from that of the history of Messene which has been recounted by historians of the time like Thucydides (1.101.2) and Polybius (XXV. 1 and XXIII.17.2), in addition to travelers like Pausanias (IV.1-29 and IV.31.1-2); these historical writings have provided detailed accounts centered on the events of the Messinian Wars while giving little information about individual events in Thouria (Panagiotidis, et al., 2019, p. 259); (Simpson & Lazenby, 1972). In addition to historic accounts, several mythic and literary sites have been attributed to the city of Ancient Thouria which provide additional insight into the area's history.

The tablets of Linear B from Pylos mention "re-υ-ko-to-ro", a strong Mycenean center, located in the eastern part of Nestor's dominion. It has been assumed that Thouria and Lefktron (Λεύκτρον) are in the same location based on literature and the location of the Mycenean cemetery near to the Ancient Thouria site (Bennet, 2005, pp. 143-174); (Simpson, 2007, p. 112). In addition, historical writings from Pausanias (4.31.1-2),

correlate the site to Homeric Antheia; alternatively, Strabo (VIII, 4,5) identifies the city with Homeric Epia from the word “αιπύς” meaning high or steep in ancient Greek, which is supported by the fact that Thouria was built on a high hill (Αραπογιάννη, 2017). That being said, the city is mentioned as Antheia for the first time by Homer in the Iliad, where it is praised as "*Antheia with its dense meadows*"[1] (Αραπογιάννη, 2017). The transition of the city being identified as Antheia to being called Thouria can be attributed to historical events; as the conquerors Lacedaemonians settled in the place - following the first Messenian wars when the Messenian residents were forced to exile by the conquering Lacedaemonians - during the last quarter of the 8th century B.C.E. they instated a new name "*Thouris*", which means “settlement’s peak”, in order to displace the Mycenaean place name "*Antheia*" (Panagiotidis, et al., 2019, p. 258).

During the Classical period, Thouria was under the influence of the Lacedaemonians as a “*perioikos*” city that was occupied by Messenian inhabitants -which were loyal to the Lacedaemonians - who enjoyed privileges over other Messenian subjects (Αραπογιάννη, 2018, pp. 48-50). After the earthquake of 464 B.C.E., Thucydides (I. 101-1) writes that the inhabitants of the city tried to liberate themselves from the Spartans and - after joining the Messenian helots - took refuge and fortified themselves in a stronghold located on Mount Ithome. However, the Messenian inhabitants were defeated and forced to move to Nafpaktos with the assistance of the Athenians.

In the next century, after the foundation of Messene in 369 B.C.E., Thouria was no longer dependent on the Lacedaemonians and instead became a member of the free

[1] “ἠδ’ Ἄνθειαν βαθύλειμον” (Ilid. I, 151, 293).

Messenian state as evidenced by the Delphic inscription[2] (325 B.C.E. or 315 B.C.E.) (Αραπογιάννη, 2017); (Ancient Thouria Excavation Website, 2016). Later, in 182 B.C.E. Thouria along with Pharai and Avia were detached from Messene and became members of the Achaean League as independent cities. After being defeated in 146 B.C.E. in Corinth by the Romans, the league was dismantled. According to Pausanias (IV.31.1-2), after the battle of Aktio in 31 B.C.E, the victor Augustus subjugated Messenia, and by extension Thouria, to the Lacedaemonians of Sparta again as punishment because the Messinians had taken the side of his opponent, Antonios (Αραπογιάννη, 2017). Later in 25 C.E., during the rule of Tiberius, the lands were ceded back to the Messenians and the border between Messenia and Laconia was defined (Takitos, *Annales* 4.43). From this point, it is unclear whether the city was under Lacedaemonian or Messinian rule. However, from numismatic and epigraphic evidence it appears that in the 2nd century (193-217 C.E.) it can be assumed that the city was still under the heavy Lacedemonian influence (Αραπογιάννη, 2018, pp. 48-50).

Topography & Archaeology of Ancient Thouria

The geography of the excavated sections of Ancient Thouria provides a key insight into the exploration of the area by archaeologists over time. In 1903, A. Ekiot, a Greek physiologist, discovered the village of Paleokastro which was located on the western side of the acropolis of Thouria which included abundant architectural materials; additional foundations of ancient buildings were also identified under the monastery (Αραπογιάννη, 2017, p. 24). Following this first discovery by explorers, much of the monuments and ruins

[2] Inscription SGDI 2619 now in the Archaeological Museum of Messenia, found in 1926 (Valmin, 1930, pp. 1-16).

were destroyed or removed which eventually resulted in the transformation of the archaeological site's topography into an agricultural geography which preserved the site from urbanization (Αραπογιάννη, 2017). In 1926, M. N. Valmin, a Swedish archaeologist, explored the area during a topographic study of Ancient Messenia based on a study by Leake (Valmin, 1930, pp. 12-19); (Leake, 1830, pp. 345-346). The geological area was reexamined in 1957 and again in 1961 by R. H. Simpson, who published a general map placing emphasis on survey of the archaeological Mycenean area (Simpson, 1966, pp. 113-131); (Simpson, 2007, pp. 111-120). An additional study was made of the visible ancient relics by G. Sachs, a German archaeologist, during a journey through Messenia during 2003-2005 (Sachs, 2006, p. 38). In 2007, experimental excavations were carried out at the site to locate the ancient monuments under the direction of Dr. X. Arapogianni, Head of the 5th Ephorate of Prehistoric and Classical Antiquities of Messenia (Αραπογιάννη, 2018, pp. 48-50). Following the discovery of indications of significant antiquities within the field of research, a systematic excavation has been in progress under the direction of Dr. Arapogianni and the auspices of the Archaeological Society at Athens beginning in 2009 and is still ongoing (Αραπογιάννη, 2017, pp. 49-50); (Ancient Thouria Excavation Website, 2016).

Based on these surveys, it was determined that many occupation phases are layered on top of each other across the ancient site; the most ancient layer dates back to 2500-2000 B.C.E. and is located in the southern part of the hill. In the same area as the ancient acropolis, an ancient wall with rectangular towers built in accordance with the isodomic opus quadratum system has been dated to the 4th c. B.C.E. (Αραπογιάννη, 2017, p. 29). In addition, two tomb burial mounds ((height 4-5m. and diameter 10m. each) dating to

prehistoric times have been uncovered in the “Kasfoulia” area directly opposite from the Mycenaean necropolis of the "Ellinikà" (Rambach, 2007, pp. 137-150); (Stewart, 2011, p. 59). Of the tombs in this area, the best preserved contained three unmarked burials which have been dated to approximately 2050 B.C.E. This dates them at least 500 years older than the tombs of the Mycenaean cemetery (Fig. 3) (Mitsopoulos-Leon & Österreichisches Archäologisches Institut (Wien), 2001, pp. 293-298). A monumental Mycenean vaulted tomb, similar to that of the great tombs of Mycene, was discovered to the west of the Mycenaean cemetery of the "Ellinikà" (Themelis, 2010, pp. 89-90). This grave was originally dated to 1600-1400 B.C.E and underwent several second uses after 900-700 B.C.E. with increased usage during the late classical period as a site of ancestor and hero worship (Αραπογιάννη, 2017, pp. 29-35). Occupation of the area continued in the following centuries based on evidence shown by the scattered pottery of Early Geometric 1060-1900 B.C.E. and Geometric 900-700 B.C.E. periods, which have been superficially discovered throughout the ancient city and within the embarkment of the Mycenaean acropolis (Themelis, 2010, p. 93); (Themelis, 1965, p. 207). The evidence shows that habitation in the area continued during the Historical and Byzantine periods, into that of the Ottoman rule (Malapani, 2021, p. 42).

Figure 3: Thouria Graves. The three cist graves from "Kassoulis" area (Αραπογιάννη, 2017, p. 42).

Although a portion of the site has been explored, the historical cemetery of the ancient city has not been located with certainty. That being said, the possibility of such a cemetery has been verified by the discovery of a tombstone inscribed "ΝΙΚΑΝΔΡΙΑ ΧΑΙΡΕ" which has been dated to approximately 1st B.C.E. – 1st C.E. (Αραπογιάννη, 2017). In addition, six box-shaped tombs of early Hellenistic times, filled with rich offerings, were discovered in 2017 during the expansion of a rural road at "Kassouli" which is located near the small temple of Agias Barbara on a flat area north of the citadel of Thouria (Malapani, 2021, p. 42). These tombs are part of the ancient city's cemetery that extends into that area and contains indications of other tombs in the area. This discovery has supported the hypothesis of the existence of an extensive cemetery located in the area. That being said, this discovery does not exclude the existence of cemeteries or tomb clusters in other locations in the wider area of the ancient city (Αραπογιάννη, 2018, pp. 48-50) (Αραπογιάννη, 2017, pp. 40-44). It should be noted that a cist grave was uncovered by a

rescue excavation north of the Acropolis in 2018, however, the site has not been explored (Fig. 4) (Malapani, 2021, p. 42).

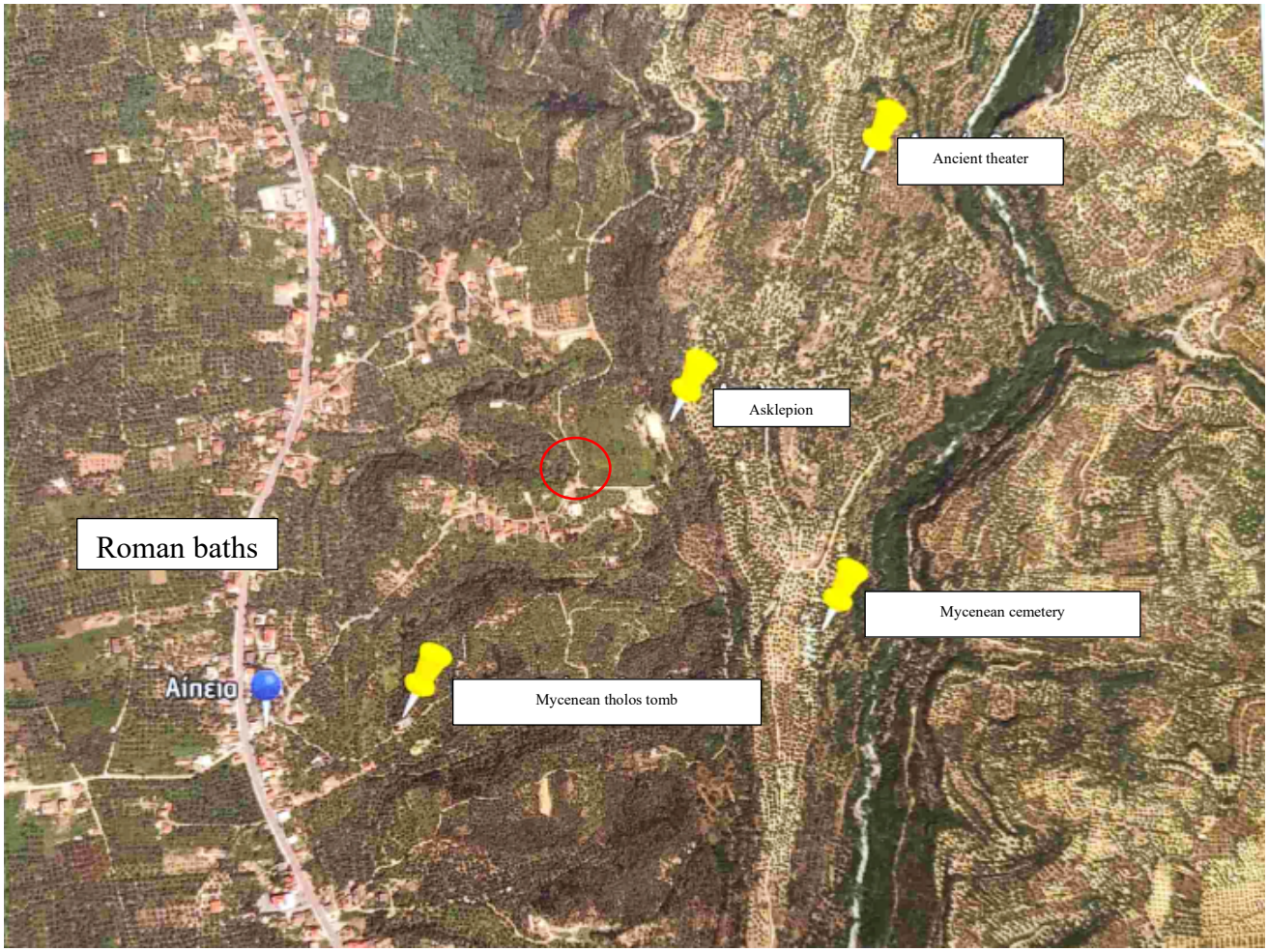

Figure 4: Thouria Site. The main sites of Thouria and the site of the cist grave of the 2018 rescue excavation shown in red (Αραπογιάννη, 2017, p. 25).

1.3 Archaeological Findings

It was at the Ancient Thouria site that a completely intact white-ground lagynos vessel was discovered beyond the excavation area during construction work in 2018; the recovery of the artifact will be discussed in further detail in a later section (3.1). As Corinth was part of the Achaean League during the 2nd century, it can be assumed that there were

trading routes between Corinth and Thouria during this period (Αραπογιάννη, 2018, pp. 48-50); this is supported by the presence of the white-ground lagynos in Thouria (Fig. 15).

Typology

The term "lagynos" has been defined as a type of one-handled, thin-necked pitcher made from a great variety of fabrics from the 3rd to the 1st century and was commonly used as a pouring vessel (Lund, 2013, p. 256). One such lagynoi variety is the white-ground lagynos that, although present throughout the Hellenistic period, was the most prevalent in the 2nd and 1st century B.C.E. (Vogeikoff-Brogan, 2000, pp. 301-302). In addition to a large amount of intact white-ground lagynoi which were discovered in Asia Minor along with indicators of production (Figs. 5 & 6), these vessels are also present in other areas of the Aegean including Corinth (Figs. 7 & 8) (Vogeikoff-Brogan, 2000, p. 302). Archaeological evidence of white-ground lagynoi fragments and whole vessels at Corinth during this period suggests that the practice of importing them was just beginning at the time of Corinth's destruction in 146 B.C.E. (Vogeikoff-Brogan, 2000, p. 302).

Figure 5: White-Ground Lagynos. Lagynos from the Musée du Lourve (Musée du Lourve, 2021)

Figure 6: White-Ground Lagynos. Lagynos from the British Museum (The British Museum, 2021).

Figure 7: White-Ground Lagynos. Lagynos from the Metropolitan Museum of Art (The Metropolitan Museum of Art, 2021).

Figure 8: White-Ground Lagynos. Lagynos from the Archaeological Museum of Messenia.

Although the lagynoi vessel shape has been present in a variety of styles and decorations throughout the Hellenistic period (Blázovics, et al., 2019, p. 148), white-ground lagynoi with wreath decorations have been predominately dated to the 2nd and 1st century (Walters, et al., 1925, p. 513); (Richter, 1953, p. 130); (Leroux, 1913, p. 39). This style of lagynos is characterized by the distinctive decorative style seen on this flask: wreaths or garlands and ribbons or taeniae suspended from fibulae or olives, *magadis* or harp, an oval-shaped net or basket or instrument, and an oinochoe or lagynos (Walters, et al., 1925, p. 513); (Richter, 1953, p. 130); (Leroux, 1913, p. 39). The interpretation of the design is highly debated but the iconography is consistent: wreaths with bows (Figs. 10 & 11), a stringed instrument (Fig. 9), an oval-shaped frame with woven cross-pieces (Fig. 11), and a pouring vessel (Fig. 12). These decorations are painted in a thin orange-brown paint on top of a white-ground base (Vogeikoff-Brogan, 2000, p. 302). This color and decoration iconography can be used as an indication of the vessel's purpose, as will be further discussed below.

Figure 9: Lagynos Decoration. White-ground lagynos, decoration depicting a stringed instrument.

Figure 10: Lagynos Decoration. White-ground lagynos, decoration depicting a funerary wreath.

Figure 11: Lagynos Decoration. White-ground lagynos, decoration depicting a funerary wreath and an oval shaped frame with cross pieces.

Figure 12: Lagynos Decoration. White-ground lagynos, decoration depicting a lagynos.

Iconography & Usage

As the vessels have typically been discovered intact within tombs, it can be assumed that they played a part in funerary practices; this is further supported by the iconography on the vessels

themselves. The wreath decorations can be assumed to be funerary wreaths of either olive or laurel leaves. This was a common facet of funerary rituals in Classical times (Garland, 1985, p. 116). Some have assumed that these wreaths were used in funerary rites to symbolize hope for continued life after death (Oakley, 2004, p. 206). In addition to wreaths, pouring vessels also play a physical part in the funerary practices in addition to iconographic representations on the lagynoi. During the funerary ritual a libation ceremony in honor of the deceased was often performed; in this act, liquids such as oil, wine, or other substances were offered to the dead. This offering is identified by iconographic information like that of funerary scenes on lekythoi and in written sources such as Euripides and Aeschylus (Garland, 1985, p. 37). The musical instruments depicted on the vessels were probably included as a depiction of luxury as images of music have been used as indicators of status and wealth in funerary contexts in the 3rd and 2nd centuries B.C.E. (Alexandrescu, 2019, p. 185). Similar iconography has also been depicted on Attic lekythoi (Figs. 13 & 14) which, like the lagynoi, have only been found in a funerary context and have a characteristic white-ground surface (Oakley, 2004, p. 9). In both cases, the white-ground coating is also indicative of funerary purpose as, although the forms of the vessels are utilitarian in their usage, the delicate white-ground coating was never intended for anything other than burial ceremonies (Beazley, 1938, p. 6).

Although the production technology of the decorations of the lagynoi is unknown, the white-ground coating of the lekythoi is assumed to have been produced in a similar manner (Eliasson, 2020, p. 2). The white coloring was produced from a very fine white clay, called kaolinite, which was applied with a brush while the vase was rotated on a wheel; this was done to produce a uniform layer on the vessel (Noble, 1960, p. 315). The clay often flaked off after firing as a result of the thin layers (Noble, 1960, p. 316). The diluted brown paint was then brushed on

after the firing of the lagynoi using a small, thin brush (Noble, 1960, p. 315). As this paint is applied over the white clay slip, it is often eroded, faded, or completely absent due to sunlight, water, or corrosive soils (Noble, 1960, p. 316).

Figure 13: Lekythoi. White-ground Attic lekythoi with musical instrument decorations (Princeton University, 2022).

Figure 14: Lekythoi. White-ground Attic lekythoi with wreath and lagynoi decorations (The Metropolitan Museum of Art, 2021).

Although the lekythoi and lagynoi share similar characteristics, their timeframe, location, and usage are very different. For instance, unlike the white-ground lagynoi which have been discovered in a variety of locations, the white-ground lekythoi have only been found in Classical Athens and were often deliberately shattered at the grave (Grinsell, 2012, p. 483). This was a practice intentionally performed so that the vessel might symbolically "die" (Oakley, 2004, p. 205). In fact, in Hellenistic times funerary rituals included breaking earthenware vessels outside of the dead person's home, along the route followed by the funeral procession, and at the graveside

(Grinsell, 2012, p. 483). As such, the fact that the majority of the white-ground lagynoi have been found intact inside graves is an indicator of their very different usage and purpose compared to that of the white-ground lekythoi. Thus, the position of the unbroken white-ground lagynoi within the grave is a reflectance of the purpose and importance of the vessel. Just as the decorations and color indicate the vessel exists for a funerary purpose, the placement of the vessel itself indicates its intended user was not the funerary participants, but the dead themselves (Garland, 1985, p. 120).

Although the context of its usage is understood, the actual content of the vessel is still greatly debated. The lagynoi shape is considered a pouring vessel based on its long, slender neck which tapers upwards to end in a narrow annular rim. Unlike other lagynoi, the white-ground lagynos possesses a smooth, flat handle that begins just below the rim and runs to the widest part of the body; the body is defined by its squat stature and slanted shoulders which result in a carinated shape and the widest part of the vessel containing a characteristic sharp angle (Lund, 2013, pp. 256-257). This is consistent with Westholm's Type 2 classification of lagynoi (Lund, 2013, pp. 256-257); (Vogeikoff-Brogan, 2000, p. 302). Based on the physical characteristics of the vessel, it is debated whether the lagynoi contained oil or wine (Walters, et al., 1925, p. 513); (Richter, 1953, p. 130); (Leroux, 1913, p. 39). As both wine and oil are associated with funerary rights during this time period, the contents of the white-ground lagynos cannot be definitively stated based on the vessel's appearance or situational context (Garland, 1985, p. 37). Thus, further analysis is required to examine and identify the contents the vessels once contained.

1.4 Thouria Lagynos

The vessel recovered from the rescue excavation in Ancient Thouria stands approximately 20cm in height and has a width of 16cm from the widest point of the vessel body. The vessel mouth has an opening of 4cm in diameter. The bottom of the vessel is approximately 10cm in diameter[3]. Based on the vessel's dimension and physical appearance, the Thouria Lagynos is considered a Type 2 lagynos based on Westholm's classifications (Lund, 2013, pp. 256-257); this is consistent with the classification of the aforementioned lagynoi from the British Museum and the Metropolitan Museum of Art (Walters, et al., 1925, p. 513); (Richter, 1953, p. 130).

Figure 15: Ancient Thoura Lagnos. Lagynos from the Archaeological Museum of Messenia.

The body of the ceramic is coated in a layer of white slip; the technical aspects of the artifact production will be discussed in further detail in a later section (2.2). The vessel is decorated with seven images that were applied with a brown paint. The icons depict four wreaths with bows (Figs. 16, 18, 20, & 21), one-stringed instrument (Fig. 17), one oval-shaped frame with woven

[3] The measurements of the vessel are estimates which were taken post-examination of the vessel at the Archaeological Museum of Messene.

cross-pieces (Fig. 21), and a single lagynos of a similar shape to the vessel (Fig. 19). Additional paint has been applied to the edge of the vessel's body at the widest point in a decorative pattern depicting two thin circles and a thicker outer border circle.

Figure 16: Funerary Decoration. White-ground lagynos, decoration depicting funerary wreath #1.

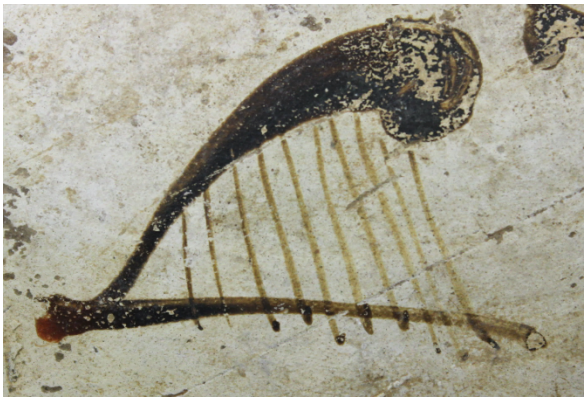

Figure 17: Funerary Decoration. White-ground lagynos, decoration depicting a stringed instrument.

Figure 18: Funerary Decoration. White-ground lagynos, decoration depicting funerary wreath #2.

Figure 19: Funerary Decoration. White-ground lagynos, decoration depicting a lagynos.

Figure 20: Funerary Decoration. White-ground lagynos, decoration depicting funerary wreath.

Figure 21: Funerary Decoration. White-ground lagynos, decoration depicting funerary wreath #4 and oval shaped frame with cross pieces.

The colors of the icons are darker and less vibrant than that of the other documented lagynos vessels. This can be attributed to the fact that the vessel was discovered within a tomb and has not undergone extensive conservation. The vessel has been ascribed to Hellenistic Times with an approximate dating around 2nd-1st century B.C.E. based on typological comparison and the assumed time period of the tomb it was discovered in (Vogeikoff-Brogan, 2000, pp. 301-302).

Chapter 2. Theoretical Background of Ceramic Studies

In order to understand the significance and unique characteristics of the white-ground lagynos vessel, it is important to understand how ceramics are produced in general during this period. Although production technology and methodology differ by region, the general aspects of pottery production and the *chaîne opératoire* of ceramics are fairly standardized across the Mediterranean (Skibo, 2013, pp. 7-8). In each step of the ceramic life cycle- from the collection of raw materials to the final decorations-, the process can be manipulated or adjusted to create a wholly unique product (Gosselain, 2018, p. 4). Ceramics can be attributed to specific time periods, cultures, and even geological areas based on physical, elemental, and technological characteristics which are considered markers of identity (Gosselain, 2018, p. 9).

2.1 Pottery Production

Although ceramics can be produced in a variety of ways, the basic phases of ceramic production follow a standard pattern: raw material collection, clay processing, shaping, drying & firing, and decoration (Fig. 22). These primary phases are composed of a series of sub-phases which must be completed within a specific order before moving onto the next phase.

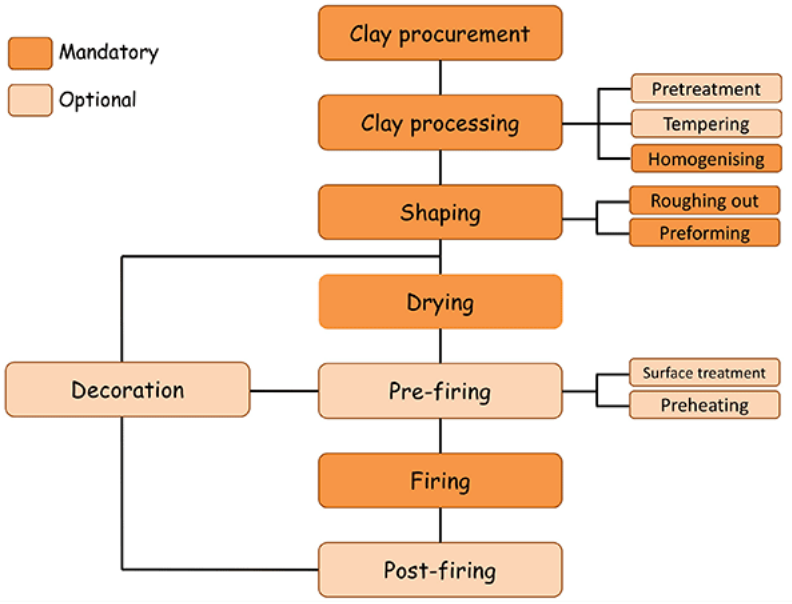

Figure 22: Pottery Production Phases. The different phases and subphases of a pottery chaîne opératoire as illustrated by O. Gosselain (2018, p. 4).

Raw Materials

In order to produce ceramics, specific raw materials are required. These include clay, non-clay materials, and fuels. Although clay is a primary component of ceramic production, it is broadly defined as a fine-grained, earthen material that, when mixed with liquid, develops plasticity (Goffer, 2007, p. 240). At the most basic level, clay is composed of silica, alumina, and water; however, the ratio and presence of other chemical components such as iron, calcium, and alkali salts influence the physical characteristics of the final material (Shepard, 1956, p. 6). Raw, dry clay is combined with water to create a clay paste which is used for ceramic processing and production. In addition to raw clay, non-clay materials such as fillers, non-plastic fillers, inclusions, tempers, and additives can be added to clay paste (Goffer, 2007, p. 240). The addition and availability of these materials can be dependent on the ceramic's production location and can include a variety of materials such as sand, volcanic ash, crushed rocks, grog, shards, seashells,

and organic matter (Shepard, 1956, p. 25). Modern ethnographic studies of traditional ceramic production techniques have shown that potters may identify and select the raw materials used based on obvious physical properties like color, plasticity, number of non-plastics, drying characteristics, or a salty taste; however, it should be noted that the historical selection of these materials is often related to religious, superstitious, cultural, or technical traditions (Arnold, et al., 1991, p. 71). These items can also be present in raw clay as impurities which can impact the properties of the final ceramic (Shepard, 1956, p. 18). Depending on the desired product, different raw clay materials in an area are combined to create a clay paste (Arnold, et al., 1991, p. 70).

Processing

Following the collection of components, these raw materials can be combined to create a clay paste. During processing, the properties of clay pastes are modified through the removal or addition of non-clay materials; following processing the clay paste is manufactured into a shape (Shepard, 1956, p. 18). Depending on the processing methods and final combination of raw materials, the final manufactured ceramic fabrics will have very different properties.

A ceramic fabric is typically classified as fine or coarse which is dictated by the consistency and homogeneity of the clay paste. These fabrics are achieved through the modification of the source clay based on local technologies like levigation or tempering (Goffer, 2007, p. 241). Levigation is the process of separating fine and coarse particles of clay by mixing the dry raw clay with water and allowing the particles to settle; the coarser particles settle first and are subsequently removed from the clay paste (Goffer, 2007, p. 493). This is typically performed to produce a fine clay paste for manufacturing. This is also done to improve the stability of the clay fabric as natural impurities can weaken the plasticity and stability of the final ceramic (Shepard, 1956, p. 25).

Alternatively, tempering is the addition of non-plastic materials to the clay paste in order to alter the plasticity and firing properties of the final ceramic (Goffer, 2007, p. 520). This process typically produces coarse clay paste for manufacturing. Although temper may seem counterproductive, as the addition of non-plastics can weaken the final ceramic body, temper materials can be used to counteract shrinkage and facilitate drying which reduces the risk of cracking (Shepard, 1956, p. 25). The characteristics of the clay can also be changed through the addition of inclusions, which, unlike temper -which is composed of non-clay materials-, are composed of non-plastic materials which can be naturally found in clays (Goffer, 2007, p. 241). The final quality of the prepared clay paste can be altered through additional processing.

The working quality of the clay paste can be improved through methods like soaking, wedging, and working (Shepard, 1956, p. 53). Soaking allows water to fully permeate the clay paste which allows for uniform drying and shrinkage (Goffer, 2007, p. 241). Wedging is performed to create a uniform and homogenized texture; this is performed by cutting slabs in the plastic clay paste and working the pieces together which creates a more equal distribution of material throughout the clay (Shepard, 1956, p. 53). This can be done to improve the controllability, formability, and plasticity (Skibo, 2013, pp. 39-40). Working is done to test the properties of the clay before firing; this can be performed by allowing a sample of the paste to dry or to fire a small disk to test for defects or impurities (Shepard, 1956, pp. 50-51). These processes are performed before shaping in order to improve the workability of the clay (Skibo, 2013, pp. 39-40). Although there are many methods for preparing and processing the clay, the methods differ amongst pottery workshops and regions (Arnold, et al., 1991, p. 70).

Shaping & Drying

The prepared plastic clay paste is formed and shaped into objects (Goffer, 2007, p. 241). There are a variety of shaping methods that can be employed to create vessels that have important characteristics for usage and purpose (Skibo, 2013, pp. 2-3). The shaping of the vessels is most commonly done through hand-forming, molding, or wheel turning (Goffer, 2007, p. 241). Hand forming can be done through coiling, pinching, or paddling soft clay to form a vessel (Shepard, 1956, pp. 54-61); the process is simple and requires few additional materials or tools for production. Alternatively, molding requires a mold in which to press raw clay to form a cast (Goffer, 2007, pp. 498-499). Although this method can produce intricately decorated vessels, there are limitations due to the need to remove the dry vessel from the mold for firing. The final method, wheel turning, requires more technique to produce viable vessels but the results can be achieved much quicker than other methods. This is because the throwing ceramics on the wheel utilizes rotational and centrifugal force for efficient and uniform shaping (Shepard, 1956, pp. 59-62). Once the final form of the vessel has been determined through the use of these methods, the wet ceramic body must be allowed to dry completely, commonly referred to as bone dry, before firing. Surface treatments are often applied on ceramics before this phase; the phase of dry but not yet bone dry is known as leather dry or leather hard (Skibo, 2013, p. 77); (Shepard, 1956, p. 65). In any case, the vessel must be allowed to dry completely before firing; if a ceramic is heated too quickly before all of the water has been removed from the fabric, the water can become steam and expand with explosive effects on the ceramic (Skibo, 2013, p. 122).

Surface Treatments & Decoration

Surface treatments are applied to the wet or leather-hard vessel in order to provide a more finished surface for slipping, decorating, or firing. These treatments, also called finishing, most commonly consist of burnishing, beating, or polishing (Shepard, 1956, p. 65). Finishing serves to remove irregularities on the surface leftover from forming and shaping the vessel. The type of finishing treatment depends on the final characteristics of the ceramic; a fine-ware ceramic will be treated differently than a coarse or earthenware ceramic. Fine ware ceramics are treated with burnishing or polishing which are similar processes but require different tools. Burnishing is the process of smoothing or polishing the surface of a leather hard ceramic by rubbing it with a hard tool such as a smooth stone (Shepard, 1956, p. 65); polishing is often done using a cloth or by hand (Shepard, 1956, pp. 66-67). In both cases, it is important that the ceramic is not yet bone dry or scratching may occur on the fine ceramic surface (Goffer, 2007, p. 465). Alternatively, beating is performed on coarse ware ceramics before firing in order to remove large inclusions or temper from the surface before firing. The soft but not leather-dry clay is hit with a paddle or stone to force the rough inclusions below the surface ((Tite, et al., 2001) 1982, 115). Once the vessel surface has been smoothed, it may be fired as is or additional surface treatments may be applied.

Slipping is the application of a thin mixture of clay and water to the surface of the vessel following finishing and drying. The slip is applied to further smooth the surface or to improve the impermeability of the vessel (Goffer, 2007, p. 242). In many cases, ceramics are often slipped with a different type of clay in order to achieve a high gloss finish on the surface of the pottery (Shepard, 1956, pp. 67-69). Calcareous and non-calcareous slips can be used in conjunction with oxidizing or reducing environments to create a variety of colored surfaces (Tite 1982, 118). Non-calcareous slips on calcareous bodies in an oxidizing environment are common in the Aegean region due to

the artistic contrast produced (Tite 1982, 119); this contrast will be explained in greater detail later in this chapter. When oxidized, non-calcareous slips will produce a red glaze that contrasts with the white body produced by the calcareous clay. A non-calcareous body that has been burnished and fired in a reducing environment will create a black glaze. The presence of differing quantities of iron and calcium will alter the appearance of the slip during the firing process which can affect the appearance of the final ceramic produced (Tite 1982, 118). The surface may be coated several times until the desired color or smoothness is achieved (Shepard, 1956, pp. 67-69).

Following this process, the ceramic may be fired before final decorations like paint or glaze are applied; if a ceramic is fired following finishing but before decoration is applied, this is called biscuit firing (Goffer, 2007, p. 463); (Shepard, 1956, pp. 127-130). Painting is the application of pigments or colored slips to the surface of the vessel; this can be performed in a decorative pattern or design on select parts of the ceramic (Shepard, 1956, p. 69). In order to create dimensional images, the firing conditions may be manipulated between biscuit firing and final firing in order to produce additional colors. The characteristic "black-and-red glaze" decorative patterns on Attic pottery can be attributed to this process which will be expanded upon further in the firing section (Goffer, 2007, pp. 251-254). Although this process does not technically produce a glaze, which is a glassy material that is applied over the surface of the ceramic, it is still referred to as a glaze; the most common types of glazes are lead or alkaline glaze. These glazes have different physical properties which influence the final appearance of the ceramic (Shepard, 1956, pp. 44-48).

Firing

Finished and decorated ceramics are fired at various temperatures, lengths of time, and atmospheric conditions which changes the physical properties of the ceramic. Each of these factors

greatly influences the final state of the ceramic; if the quantity of oxygen in the atmosphere, the length of the firing, or the temperature is too low, carbon may be burned only from the surface of the ceramic which results in a cooked surface and a dark inner core (Goffer, 2007, pp. 242-243). Alternatively, if the ceramic is fired for too long or at too high of a temperature, it can become brittle and deform (Skibo, 2013, pp. 45-47). It is important to customize each of these factors to the intended characteristics of the ceramic; coarse ware ceramics are fired in very different conditions than that of fine ware in order to manipulate the structural properties of the ceramic such as permeability, thermal shock resistance, and overall strength (Goffer, 2007, pp. 246-250).

Depending on the composition of the ceramic and the firing conditions, ceramics can undergo a chemical change called vitrification during firing; this process is what strengthens ceramics and allows them to become impervious to water (Tite, et al., 2001, pp. 301-312). However, this process is very dependent on temperature, time, and atmospheric conditions (Shepard, 1956, pp. 19-24). Atmospheric conditions of firing are defined as oxidizing, reducing, or neutral. An oxidizing firing atmosphere contains free oxygen while a reducing firing atmosphere contains gases that take oxygen from constituents of the clay (Goffer, 2007, pp. 241-254). What this means is that oxidizing environments have a surplus of oxygen in the atmosphere to fuel the fire like that found in an open fire or vented kiln; reducing conditions have a lack of oxygen in the atmosphere to fuel the fire which results in oxygen being taken from the ceramic itself like that of a closed kiln. Alternatively, neutral conditions do not have an excess or deficit of oxygen (Shepard, 1956, p. 103). However, it is important that neither oxidation nor reduction can take place until the temperature is high enough to facilitate a reaction. Both calcareous and non-calcareous ceramics do not undergo vitrification at temperatures below 800 °C. The initial vitrification develops when the pottery is fired at temperatures ranging from 800-850 °C during which variations in

vitrification can be observed depending on firing conditions and mineral composition (Maniatis & Tite, 1981, p. 68). When fired in a reducing atmosphere both non-calcareous clays and calcareous clays begin to display vitrification at temperatures 50°C lower than in an oxidizing environment. However, at a high firing temperature in the reducing environment the non-calcareous ceramics develop pores that increase in size ranging from fine to medium as correspond to increases in temperature over a range of 800-1000 °C (Maniatis & Tite, 1981, p. 61). Alternatively, in both the reducing and oxidizing environments calcareous clays form crystalline phases at low firing temperatures that melt together to form extensive vitrification that is relatively unchanged at temperatures ranging from 850-1050 °C (Maniatis & Tite, 1981, p. 65). With this in mind, manipulation of different factors such as atmosphere, clay composition, and firing temperature can produce vastly different properties for the final ceramic.

The firing process can be utilized to produce different colors on the surface of the ceramic (Goffer, 2007, pp. 251-254). Although plain clay - which is high in calcium but lacks additional minerals or metal ions - produces white ceramics when heated, the majority of ceramics are colored with secondary clay decorations (Tite, et al., 1982, p. 118). Iron ions are used to produce red colors, white manganese ions are used to make it dark or black. However, the color produced is also dependent on the atmospheric conditions (Goffer, 2007, pp. 251-254). When oxidized, non-calcareous slips will produce a red glaze that contrasts with the white body produced by the calcareous clay. A non-calcareous body that has been burnished and fired in a reducing environment will create a black glaze. The presence of differing quantities of iron and calcium will alter the appearance of the slip during the firing process which can affect the appearance of the final ceramic produced (Tite, et al., 1982, p. 118). It is through understanding how the different factors of firing influence the final ceramic product that complexly decorated ceramics - like that

of the “black-and-red glaze” ceramics characteristic of Attica - have been created (Goffer, 2007, pp. 251-254).

2.2 Decoration Techniques & Methodology

Although not as popular as the black and red figure ceramics, Attic white-ground pottery plays an important role in Greek ceramics with reference to the artistic, the material, and the manufacturing points of view during the Classical Period (Berthold, et al., 2016, p. 1). This special technique was created during the 6th and 5th centuries B.C. in Athens; however, the peak of its popularity is considered to be from approximately 475 B.C. to 400 B.C. (Mertens, 2006, pp. 186-189); (Eliasson, 2020, pp. 1-2). Typical examples of white-ground ceramics produced in Athens and the surrounding area include lekythoi, cups, kraters, and oil flasks; later on in time, this style became synonymous with burial objects of various styles and decorations (Berthold, et al., 2016, p. 1); (Mertens, 2006, pp. 189-190). Therefore, it is not unexpected that the lagynos vessels have been discovered in this style. As only intact lagynoi have been studied, little can be definitively said about how the production techniques or methodology differ from that of the more common lekythoi.

The white-ground technique is characterized by the application of a white clay slip to some portion of a vessel, most commonly to provide a surface for decoration (Mertens, 2006, p. 186). The white slip, consisting of a very fine white clay which is assumed to be a form of kaolin, was applied with a brush while the vase rotated on a wheel; this allowed for an even application of the slip to the vessel. Depending on the desired style, the surface was either burnished to a glossy white or left a matte white (Noble, 1960, p. 315); (Berthold, et al., 2016, p. 2). Although it was

possible to have a very pure white color during this period through refinement methods, commonly a small amount of iron was intentionally added to the slip; following firing, the yellow undertone derived from the iron produced a very deliberate cream color to the ceramic body (Noble, 1960, p. 315); (Berthold, et al., 2016, p. 1).

The white-ground, in contrast to the black or red, was regarded as an excellent drawing surface that was suitable for the application of a range of colors before or after firing (Mertens, 2006, p. 14). A thin, brownish paint, also referred to as a dilute glaze, was used on certain types of white-ground lekythoi; this paint was often used in conjunction with a black glaze to create outlines or decoration on the vessels before firing (Noble, 1960, p. 315). Other colors were not commonly applied to the vessel at this phase in manufacturing; this was because the red pigment common for the time, a red oxide of iron that mixed with water and 10% black glaze matter as a binder, did not adhere well on top of the ground white clay and would often flake off after firing (Noble, 1960, pp. 316-317). Until around 470 B.C, the slip and decoration were fired in the kiln with the vase itself; however, by 430BC, almost all decoration was executed after firing which allowed for the execution of greater detail and the presence of additional colors; however, these colors may no longer be visible on the surface of the white-ground vessels (Mertens, 2006, p. 191).

Studies have shown that there were certain additional colors that Greek vase painters used on white-ground lekythos that were not fired in the kiln. These fairly fugitive mineral or vegetable colors were painted after firing on some Attic white-ground lekythoi in shades that include blue, green, yellow, pink, purple, and matte black (Noble, 1960, pp. 316-317); (Berthold, et al., 2016, pp. 2-4). At present, these colors are often seen as either a complete absence or as extreme fading on vases; the actions of sunlight or water in the soil are considered the most likely cause of removal or degradation. It is assumed that these pigments were never fired in a kiln based on tests performed

on fragmented pieces of white-ground lekythos that were placed in an oxidizing kiln at temperatures up to 950 °C[4]; during this testing, the previously visible pattern on the border of the white lekythos fragments completely disappeared, leaving a blank area outlined by the black glaze linework (Noble, 1960, pp. 316-317). Based on this, additional vessels were evaluated for the assumed presence of additional colors; as supported by the aforementioned test, it is possible that the dull and empty areas on the white-ground lekythoi contained additional color which was applied over or in conjunction with the black and brown glaze lines (Noble, 1960, pp. 316-317); (Berthold, et al., 2016, pp. 2-4). These fugitive colors, which were often completely eroded by groundwater following the burial, have been detected and identified on the bodies of white-ground lekythoi using scanning XRF microanalysis and μ-XRD which were able to detect the presence of pigments and line drawings that were not visible on the surface of the vases; these drawings were assumed to have been applied as a post-firing application based on the elemental composition and maximum firing temperature of the identified pigments (Scott, 477-478); (Berthold, et al., 2016, pp. 2-4).

With this in mind, although many assumptions can be made about the white-ground lagynos production and decoration techniques, it is difficult to state such information definitively. In addition, as the decoration methodology is assumed to be similar to that of the white-ground lekythos of the Attic region, it is not unreasonable to assume that these fugitive colors may have also been present on the white-ground lagynos (Vogeikoff-Brogan, 2000, p. 302). That being said, the analysis of fugitive pigments on Attic white-ground lekythoi makes up a small portion of the

[4] This temperature was determined to be the maximum temperature of firing used during the production of the vessel (Noble, 1960, pp. 316-317).

greater field of ceramic studies in archaeometry which is made up of a wide range of topics and techniques which will be generally discussed in the next section (2.3).

2.3 Ceramic Studies in Archaeometry

For an archaeologist, ceramics provide a unique window into the past; as these objects are resistant to weathering and erosion, have a high tolerance to the passage of time, are easily transportable, and have diverse functionality, ceramics and their *chaîne opératoire* are common objects for study (Kazakis, 2015, pp. 239-240). These factors are traditionally studied based on technical and physical characteristics; a typological analysis of ceramics can be used to determine the general characteristics of a ceramic based on its form, function, and production style. There is well documented evidence of stylistic changes during specific time periods; comparison with known decorations can be used to determine the approximate age of a ceramic (Carter, 2007, pp. 3-14). In addition, there are stylistic variances between the different regions of the Aegean during specific time periods which assists in producing a general region for the ceramic. The typological forms of the ceramic follow this same pattern of change over regions and time periods. These physical changes are often a result of variations in techniques and production methods across regions based on local practices; such changes are also influenced by the clays available to the local potters. As there is a great variety of techniques and production methods across Greece, the physical characteristics of ceramic can provide key insight into the ceramic's history or provenance (Montana, 2020, pp. 1-15). Although ceramics have been typically studied based on physical appearance, modern methods in archaeometry - the scientific study of archaeological materials through physical techniques - have allowed for a greater understanding of ancient ceramics as a whole.

Textural Analysis

The textural analysis is centered on the physical appearance of the ceramic's fabric matrix; this includes the frequency of inclusions, inclusion size, pore size, frequency of pores, and grain size distribution. Just as there are many different types of clay fabric types, the ceramic's matrix is influenced by the different factors of its composition (Maniatis & Tite, 1981, p. 68). These factors are most commonly identified via visual examination through the use of optical microscopy.

Grain size distribution refers to the percentage of fine and coarse inclusions occurring in the ceramic fabric; small grains are considered fine while large grains are classified as coarse. This is often referred to as the percentage of coarseness (Edmonds, et al., 1998, p. 25). A wide range of distribution can be considered the result of insufficient refinement and homogenization of the clay paste or non-plastic temper materials (Hein, 2018, pp. 220-221). This can also greatly influence the distribution of inclusions within the matrix.

Although much of this type of study is focused on the distribution of minerals within the ceramic matrix, it is not centered on the identification of the mineral. The frequency of inclusions refers to the percentage of inclusions within the matrix; these inclusions can be of varied sizes or shapes across a wide range. The size is often classified as very small, small, medium, large, and very large (Hein, 2018, pp. 220-221). Depending on the texture of the inclusions, they can be classified from fine to coarse; this directly correlates to the inclusion type and shape. The most common shapes of the inclusions can be classified as prismatic, columnar, platy, granular, angular, and subangular (Edmonds, et al., 1998, p. 8). Inclusions have a major impact on the pore size distribution (Hein, 2018, pp. 220-221).

Pores are classified as voids in the ceramic matrix; there are two different levels of classification of pore structure depending on the area of the ceramic being examined. The smallest level of pore structure concerned the actual clay minerals, packing, and the development of the micromorphology during vitrification (Edmonds, et al., 1998, p. 25). The frequency and size of pores at this level are subject to a certain variation of firing temperature and duration, which was controlled solely by the experience of the craftspeople through kiln design, fuel replenishment, and observation of the glow colors (Hein, 2018, pp. 220-221). The subsequent level of pore structure is related to the non-plastic inclusions in the clay paste which are not affected by decomposition or vitrification during the firing process (Edmonds, et al., 1998, p. 25). These pores emerge in the ceramic matrix due to incomplete wedging of the clay paste and inclusions before forming and firing; in this case, the more incomplete the incorporation and wedging, the greater the frequency of pores. The resulting air pockets that remain in the clay paste body can commonly increase in size during firing (Hein, 2018, pp. 220-221).

Petrographic Analysis

The petrographic analysis focuses on the identification of the mineral components of the ceramic fabric and the determination of the origins of these materials using microscopy (Montana, 2020, pp. 1-15). The geological information of ceramic inclusions can help isolate a ceramic's origin based on specific minerals found in certain areas; this analysis also provides a greater understanding of how the ceramic is processed based on the fabric quality, texture, and color (Kazakis, 2015, pp. 242-243). The most common type of petrographic analysis is thin section petrography which functions to study of the microscopic features of minerals. This method utilizes thin slices, called thin sections, of a ceramic sample which is examined using a 'polarizing' or 'petrographic' microscope. At a very thin thickness (~30μm), most minerals become more or less

transparent and can be studied by a microscope using transmitted light allowing the extraction of colorful images (Kazakis, 2015, p. 245).

The understanding obtained from thin-section microscopy can also provide information on the life cycle of a ceramic artifact in regard to its production, distribution, and usage (Montana, 2020, pp. 1-15). The microstructure and physiochemical properties examined through petrographic analysis can also provide additional information regarding the manufacturing technique, firing conditions, and technological level of production at a given time and area (Kazakis, 2015, pp. 242-243). Although this technique provides information on the technology used during the manufacturing of the ceramic from a clay paste to a final ceramic which is used in the evaluation of provenance, it cannot determine the origin with the same level of certainty that is provided by mineralogical techniques (Arnold, et al., 1991, p. 71).

Mineralogical Analysis

The mineralogical analysis focuses on the identification of mineral components within a ceramic's fabric; these minerals can provide important contextual information for the production, life cycle, and usage of a ceramic. Certain rocks and minerals in ceramics have trace minerals that can be used to determine their region of origin; the presence and quantity of these minerals vary depending on the unique geological and geographical environment of their source location. This can be attributed to the fact that the rock-forming processes at different sites differ, which makes the trace minerals site-specific (Jehlicka, 2012, pp. 421-423). The concentrations of these minerals can be compared against raw materials and reference ceramics to determine an object's possible origin (Iordanidis, 2009, pp. 292-294). These trace minerals can also be considered characteristic of specific molecules. Unfortunately, the identification of minerals is not always straightforward.

Crystalline and molecular phases are influenced by manufacturing technology and mineralogical components; they are used to determine the identity of specific minerals within a ceramic. As the minerals that are added to temper a ceramic often undergo phase changes with heating to produce polymorphic forms, it is important to analyze the crystalline and molecular phases of the final ceramic to create a larger understanding of ceramic production as a whole (Carter, 2007, pp. 652-674). Certain polymorphs are often viewed as temperature indicators for ceramic firing technology (Odelli, 2020, pp. 1-5). An understanding of these phase changes also provides information on how the ceramic may have altered following burial as the presence of the low-temperature forms of a mineral may indicate deposition after firing (Vandenabeele, 2016, pp. 6-8). The mineralogical analysis provides context on certain factors that must be taken into account when analyzing a ceramic's composition. The intricacies of the instrumentation required for this analysis will be explained later in this section as many different methods are applicable.

Chemical Analysis

Chemical methods of analysis are used to determine the elemental and molecular composition of the ceramic using various analytical techniques. Concentrations of major, minor, and trace elements can be used to determine the chemical composition of the ceramic. Major element compositions are used in the determination of clay type, manufacturing technology, and variation of non-plastic components in coarser pieces (Hein & Kilikoglou, 2020, pp. 1-6). Trace and minor elements are used to determine specific workshops within a group based on the characteristic geological environment of the workshop location. As the accuracy and sensitivity of different chemical analysis methods vary, in some cases one method may be more suitable for only trace or major element identification (Kazakis, 2015, pp. 242-243).

Molecular analysis can be used to identify the microstructures within a ceramic; these microstructures are often associated with specific minerals which are intentionally added into ceramic to influence their strength, plasticity, brittleness, and thermal conductivity (Carter, 2007, pp. 289-308). The microstructure and resulting physiochemical properties examined through mineralogical provenance can also provide additional information regarding the manufacturing technique, firing conditions, and technological level of production at a given time and area (Kazakis, 2015, pp. 242-243). The unique elemental concentrations and microstructure observed are the "chemical fingerprint" of the ceramic (Kilikoglou, 1988, p. 37–40). In order to determine a ceramic's origin, this chemical fingerprint is compared against other known fingerprints in order to determine the chemical variability within a group. These values can be compared against reference values from known production centers to determine the origin of a ceramic, however, this practice is not absolute (Hein, et al., 2002, p. 542–546). In order to distinguish between different ceramic origins, the compositional variability within the ceramics attributed to an individual source must be smaller than the compositional variability of all of the sources analyzed; this comparison of variation amongst individual ceramics accounts for the changes that occur within a production center during processing and manufacture (Kazakis, 2015, pp. 242-243). Thus, these comparisons require an analytical technique that possesses high accuracy and high sensitivity in order to achieve the necessary resolution between the different but compositionally similar populations (Hein & Kilikoglou, 2020, pp. 1-6); the instrumentation for such analytical techniques will be discussed below.

Instrumental Analysis

Although there are many different methods of performing the above-mentioned analytical tests, the most accurate implementation is through the use of instrumental analysis. Scientific

instruments focus on such factors as accuracy or precision in either a qualitative or quantitative nature; however, some instruments are more suited for one factor over another (Hein & Kilikoglou, 2020, pp. 1-6). Some instruments are both qualitative and quantitative however they are often expensive to use. It is also important to consider how destructive or non-destructive an instrument is, as archaeological samples are often fragile. A semi-comprehensive list of instrumentation can be seen in the appendix (Appendix A.1). Many factors can greatly influence the practicality and advantages of using one instrument over another, some of the most important factors, and the instruments best suited to their unique analysis are ranked in the following chart (Fig. 23). With this in mind, it is important to understand the goals and nature of the examination before selecting an instrumental technique.

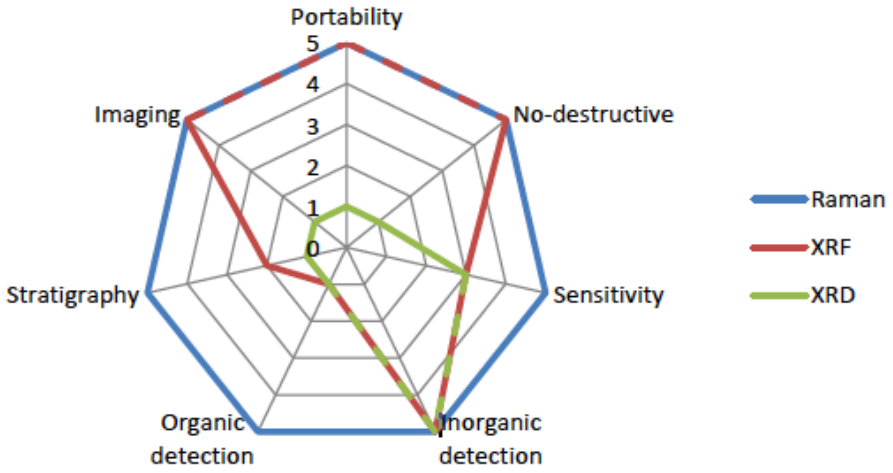

Figure 23: Instrumental Technique Comparison. Comparison of some relevant characteristics associated with three different experimental techniques: Raman (blue), XRF (red), and XRD (green) (Chiriu, 2020, p. 2).

X-ray fluorescence (XRF) spectroscopy is one of the most common techniques to determine the elemental concentration of a ceramic. Through XRF, samples are irradiated with x-rays which result in the ionization of the sample's atoms. This leads to the emission of secondary

x-rays which are characteristic of the different elements present in the sample. A spectrum of the chemical profile is created based on the characteristic emissions and their concentrations (Kazakis, 2015, pp. 242-243). This method is sensitive to major, minor, and trace elements; it also has high quantitative accuracy. It does have low sensitivity for light elements which limits the ability to complete the elemental profile (Chiriu, 2020, pp. 1-3). This minimally destructive method is most suitable for surface analysis (Kazakis, 2015, pp. 242-243).

Alternatively, X-ray diffraction (XRD) is one of the most common methods to determine the molecular structure of a ceramic body. XRD is a qualitative analysis used to study crystalline materials (Chiriu, 2020, pp. 1-3). The crystals of the ceramic are bombarded at different angles with a finely focused monochromatic x-ray beam which results in diffraction. This diffraction pattern is unique and can be used as a fingerprint of the phases present within the sample when compared against known values (Kazakis, 2015, pp. 245-246). However, it is only sensitive to large crystalline structures and may not detect small quantities present in the clay fabric.

Scanning Electron Microscopy/Energy-Dispersive X-ray (SEM/EDS) Spectroscopy is both a qualitative and quantitative non-destructive surface analysis that can be employed for elemental analysis of the minerals present based on the chemical composition of individual grains. With this method, an accelerated beam of electrons is directed at the surface of the sample; this results in the emission of secondary electrons which are collected by a detector. Multiple scans of a sample can be used to create an image of the surface of the sample; in addition, two types of images can be produced based on the detected electrons, secondary and backscatter (Kazakis, 2015, pp. 242-243). These images together can provide information on the ceramic surface homogeneity, presence of temper, and the structure of crystalline materials; this technique is often combined with EDS to gain a full chemical background of these elements. Through EDS the atoms

on the surface are excited to emit characteristic x-rays which are detected using the energy dispersive detector (Carter, 2007, pp. 652-674).

Raman Spectroscopy has gained popularity in the field of cultural heritage analysis for its extreme sensitivity and accuracy as a qualitative method of analysis; however, under certain circumstances it can also be a quantitative method. Raman utilizes vibrational spectroscopy in which scattered light is used to measure the vibrational energy modes of a sample; in other words, the spectrometer observes the change in polarizability of a molecule when it is excited with energy through the measurement of the scattered energy also referred to as the "Raman scattering" phenomenon of infrared radiation (Chiriu, 2020, pp. 1-3). With this, Raman is able of identifying molecules and compounds based on the excitement of bonds and the resulting examination of vibrational wavelengths (Vandenabeele, 2016, pp. 6-8). Unlike the other methods of molecular analysis listed, Raman is able to detect and analyze molecular bonds of both organic and inorganic substances; such methodology is incredibly useful for the understanding of compounds and molecules within the ceramic fabric. In addition, this method is often utilized for its ability to discern amorphous and glassy phases in ceramics which can be difficult to discern by other means (Chiriu, 2020, pp. 1-3). This non-destructive analytical instrument can be performed on ceramic surfaces or cross-sections (Vandenabeele, 2016, pp. 6-8).

Similar to Raman, Fourier Transform Infrared Spectroscopy (FTIR) has also grown in popularity in recent years due to its usefulness in identifying a range of materials for archaeometric analysis (Shillito, et al., 2009, p. 120). Compared to other methods like GC-MS (Gas Chromatography–Mass Spectrometry), FTIR is inexpensive, easy to use, and applicable for the nondestructive examination of a variety of cultural heritage materials; it is an easy and fast technique with minimal sample preparation which makes the technique very useful (Shoval &

Beck, 2005, p. 609). Like Raman spectroscopy, FTIR is also based on molecular vibrations and can examine organic and inorganic materials. However, FTIR works by analyzing the infrared spectrum of absorption (Goffer, 2007, p. 484); this essentially means that with FTIR, IR radiation is passed through a sample; some of the infrared radiation is absorbed by the sample which excites the bonds of the molecule while the rest is transmitted. The resulting spectrum represents the molecular absorption and transmission which creates a molecular fingerprint for the sample (Shillito, et al., 2009, p. 120). FTIR and RAMAN are often treated as complementary methods of examination, although both techniques operate based on the same principle the peaks of the resulting spectra provide different information, which can be utilized in conjunction in order to create a comprehensive analysis of a material (Goffer, 2007, p. 484).

2.4 Current Studies on Organic Residue in Ancient Ceramics

Archaeometric analysis of ceramics, which includes the application of analytical techniques discussed previously, produces extensive data that is commonly utilized for the wider scope of study of past habitation and occupation; this information is frequently studied in search of information about the various aspects of past societies such as socio-economic developments, the organization of production and trade, and the mechanisms of cultural interactions (Skibo, 2013, p. 4). Pottery is a particularly optimal object for this type of analysis as it was used in daily activities, was commonly produced locally, has a relatively limited use life, and is frequently preserved in archaeological contexts (Oudemans, 2007, p. 1). However, discussions on intended vessel function versus actual vessel usage based on archaeological data can be inconclusive (Skibo, 2013, p. 4). As such, methods for the determination of actual pottery use commonly consist of ethnoarchaeology, studies of archaeological context, pollen analysis, analysis of residues, and wear

patterns (Evershed & Heron, 1993, p. 247); organic residue analysis is one such subset of these methods of study.

Organic analysis in archaeometry is the study of organic materials which have been found in an archaeological context and preserved through the site's timeline (Oudemans, 2007, p. 1). In most cases, this encompasses the study of dry food storage, wet food storage, or cooking materials intended for preparation, storage, transport, and trade (Skibo, 2013, p. 4). Dry food storage vessels typically contained products like cereal grains and local agricultural products while wet storage vessels were often used for wines or oils; prepared foods like meats or dairy products were produced with cooking materials (Harush & Grosman, 2021, pp. 3-4). These products easily degrade over time because they are composed of organic compounds like fats, oils, and proteins (Barnard, et al., 2007). With this in mind, organic residue analysis specifically focuses on pieces of organic remains whose identities cannot be easily discerned like that of amorphous or invisible residues (McGovern, et al., 2017, p. 3). This technique is not applicable to all types of ceramics as it can be difficult to determine what products might have been in a vessel based on its typological style alone; thus, organic residue analysis makes up a small subcategory of ceramic studies as a whole (Barnard, et al., 2007). Nevertheless, the information obtained from organic analysis allows for a greater understanding of ceramic materials that could not otherwise be understood.

The characterization of amorphous and/or invisible organic remains by analytical methods -chromatographic, spectrometric, and isotopic techniques- have contributed significantly to a wide range of archaeological questions including our understanding of the invention and adoption of pottery technology and its effect on changing subsidence strategies and foodways (Roffet-Salque, et al., 2017, pp. 627-628); the relationships between form and function can be examined fully with organic residue analysis as the fabric and style of a vessel are often related to the commodities

housed within them (Skibo, 2013, p. 4). As a result, many organic residue studies focus on more than just the actual function of the vessel in relation to its contents but also technologies involved with the production, repair, and decoration of the ceramic (Oudemans, 2007, p. 1); (Roffet-Salque, et al., 2017, p. 628); (Drieu, et al., 2019, p. 182). However, it should be noted that even though many studies of organic residue focus on definite and perceived usage, not all studies of actual versus intended pottery function utilize organic residue analysis. This is because there are many factors - such as temperature, humidity, acidity, and microbial processes to name a few- that influence the survival of an organic residue following the loss or retirement of a ceramic from usage (Fig. 24) (Roffet-Salque, et al., 2017, p. 628). In addition, these factors can make it difficult to assess the overall life cycle of the ceramic as many vessels are not intended for single use but instead undergo repeated usage or recycling based on their form and function (Skibo, 2013, p. 4). That being said, the preservation and identification of an organic residue within a vessel can be used to answer questions regarding production technology, intended functionality, disposal practices, burial processes, preservation environment, and excavation techniques in addition to actual function. In other words, organic residue analysis is applicable for the understanding of more than just vessel contents and can be applicable to the study of a variety of different archaeological questions. Although it is important to understand the archaeological questions associated with organic residue analysis, as mentioned above, the evaluation of these questions is beyond the scope of this discussion which is instead centered on organic residue analysis as an analytical practice.

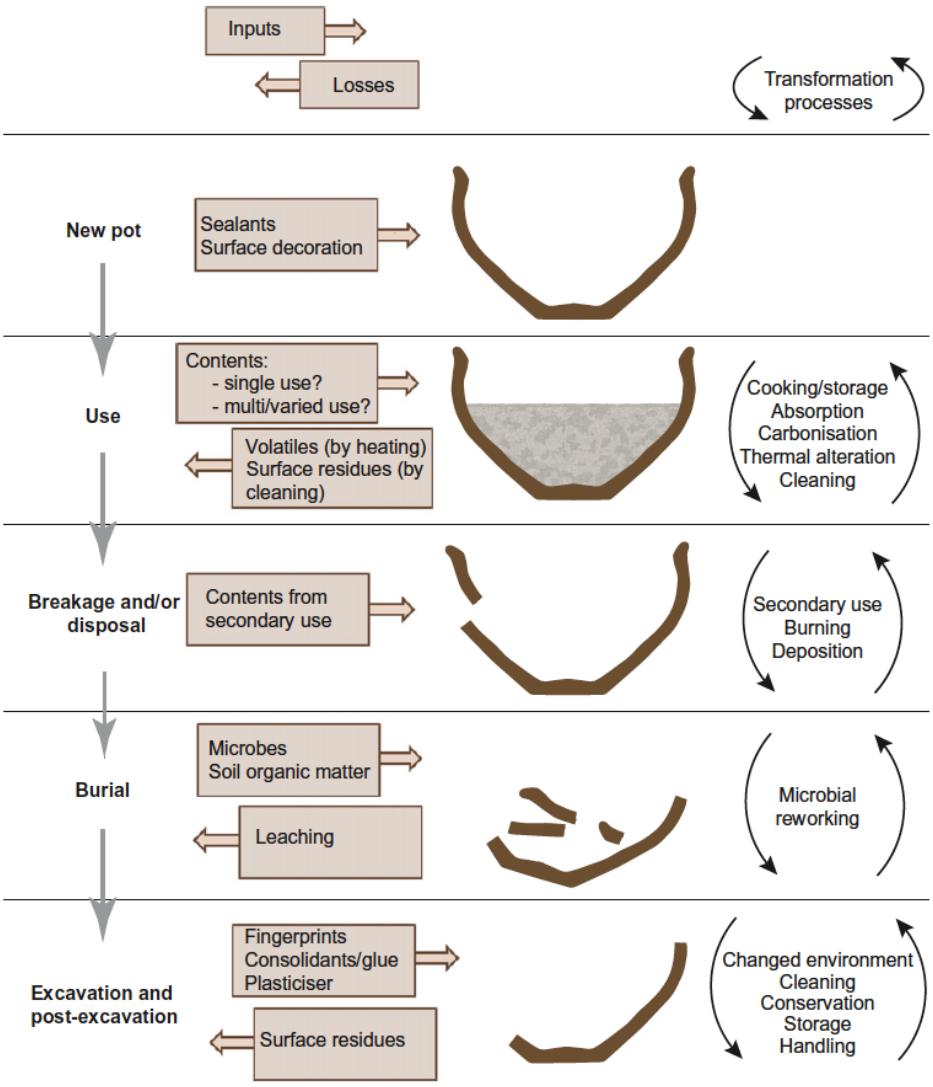

Figure 24: Archaeological Ceramic Transformation Processes. Main inputs, losses and transformation processes affecting the survival and composition of visible and absorbed organic residues in archaeological ceramics (Roffet-Salque, et al., 2017, p. 628).

By definition of residues, organic residues lack the clearly discernible morphological features that characterize other bioarchaeological materials such as wood, bone, leather, seeds, or pollen (Evershed & Heron, 1993, p. 249). As such, the archaeological practice of organic residue analysis can be considered to encompass all research aimed at the detection, identification, and explanation of the chemical characteristics of amorphous organic residues found in direct

association with ancient ceramics (Oudemans, 2007, p. 3). Organic residues typically survive in the archaeological record in one of three ways: as actual contents preserved in situ as a vessel fills with soil; surface residues appearing as visible residues on the interior or exterior of the vessel; or absorbed residues preserved within the vessel walls which are invisible to the naked eye (Evershed, 2008, pp. 903-904). Visible residues, either preserved contents or surface crusting, are not commonly studied due to post-burial and post-excavation loss during the cleaning of sherds and/or contamination (McGovern, et al., 2017, p. 3). Alternatively, absorbed residues are considered more abundant but may be harder to identify; however, it is important to remember that "absence of evidence is not evidence of absence" as organic remains typically degrade over archaeological timescales (Roffet-Salque, et al., 2017, p. 627). Therefore, this discussion will focus exclusively on absorbed residue techniques.

Absorbed organic residues typically originate from the original contents that were either stored or processed in the vessel, representing either a single use or an accumulation of cooking events over a vessel's lifetime (Barnard, et al., 2007). Unglazed fabrics offer the highest potential for the retention and survival of absorbed residues; however, unglazed fabrics are not typically used for storage as the ceramic must be sealed to decrease the permeability of the fabric in order to create effective containers for liquids (Roffet-Salque, et al., 2017, pp. 627-628). This is not to say that unglazed fabric guarantees the survival of an organic residue following the loss or retirement of a ceramic from usage. However, as absorbed residues result from the contact and subsequent absorption of a vessel's contents into the ceramic walls during vessel use, direct contact with the permeable and porous walls allows for a greater chance of retention; this contained residue is often preserved from environmental contamination for millennia until chemically extracted (McGovern, et al., 2017, p. 4). Most organic materials that come into contact with the pottery

during use are composed of lipids, proteins, carbohydrates, and other biopolymers (Evershed & Heron, 1993, pp. 250-251).

However, as the majority of archaeological biomaterials are a result of human activities such as food preparation or preservation, they are rarely found as singular entities or isolated compounds. The majority of residue analysis practices center on the isolation and identification of biomarkers which are utilized to identify specific biological materials (Drieu, et al., 2019); (McGovern, et al., 2020); (Drieu, et al., 2021). Biomarkers are considered substances occurring in organic residues that provide information relating to human activity in the past; in other words, this means the term biomarker can be applied to any class of biomolecules such as DNA, proteins, carbohydrates, lipids, and more (Evershed, 2008, p. 897). However, as most archaeological biopolymers do not survive without degrading over archaeological timescales, most analysis of biomarkers refers to structurally diagnostic forms of the biomolecule such as a stable fragment - like that of a DNA sequence - or a structural component - like that of amino acids or peptides (Roffet-Salque, et al., 2017, pp. 627-628). These structurally significant biomarkers are typically found in conjunction with other degradation products which can make the isolation and identification of specific materials difficult as the levels of preservation and destruction vary depending on the biopolymers in question. It is, therefore, important to consider that the preservation environment of the biomarker has a significant impact on its structural longevity and consequent identification (Evershed, 2008, p. 897). Thereby, absorbed organic residues composed of proteins, lipids, and polyphenols, which are easily preserved within the ceramic matrices, often provide the most stable and uncontaminated structurally significant biomarkers compared to that of other biomolecules.

The organic residues contained within ceramic matrices are typically analyzed through the use of ceramic fragments or potsherds; the use of already broken fragments is preferred from an archaeological standpoint as it allows for the preservation of intact vessels and a greater flexibility for analysis as the ceramic fragments must be scraped or pulverized to expose the inner - assumed to be uncontaminated - pores which contain the preserved organic materials (Shillito, et al., 2009); (Roffet-Salque, et al., 2017); (McGovern & Hall, 2015); (Romanus, et al., 2009); (Barnard, et al., 2007); (Drieu, et al., 2019); (Oudemans & Boon, 1991); (McGovern, et al., 2017). Although many studies have been conducted by only using potsherds, recent innovations in organic residue analysis suggest that this method should be combined with other analytical techniques in order to produce conclusive results; this is because recent studies have shown that the residues contained within a ceramic can be transformed in the period between the original context, the post-depositional process, and the post-recovery process (Fig. 25) (Oudemans, 2007, p. 7). Thus, it is important to evaluate the impact of these processes on potsherds through additional methodologies.

As previously mentioned, biomarkers are the result of human interactions with organic materials in their original context which are then preserved within the ceramic matrix; these interactions can vary depending on the intended use or uses of the vessel. In the majority of potsherd-based studies, preference is given to base fragments - sherds assumed to be from the bottom of the vessel - as it is assumed that the organic residue settled to the bottom of the vessel over time which results in the greatest amount of biomarkers to have accumulated into the ceramic matrix interiors (McGovern, et al., 2017, p. 4); (Romanus, et al., 2009); (Barnard, et al., 2007). However, this understanding of organic material distribution is flawed as it does not account for the accumulation of organic material at the rim of the ceramic body during cooking and boiling (Roffet-Salque, et al., 2017, p. 627). In addition, post-recovery contamination has only recently

been considered in regard to the processing of sherd; the standard practice in many excavations is to clean sherds by washing them with dilute hydrochloric acid to remove the calcium carbonate and other post-burial accretions (McGovern, et al., 2017, p. 3). During this process, ancient organics may be altered, transformed, or destroyed which can result in false or flawed data. In addition to the impacts of pre-loss and post-recovery, it is important to understand the effect deposition has on the organic residue within ceramic as it is typically the longest period of exposure to degradation or contamination. However, when examining the effect of deposition on an organic residue, it is important to consider more than just the potsherd; during this time period there is commonly an exchange of compounds between the soil and the ceramic matrix which can result in additional contamination and degradation (Oudemans, 2007, p. 7); (Roffet-Salque, et al., 2017, pp. 627-628). That being said, distinguishing between the different phases of exposure to degradation and contamination, particularly between post-deposition and post-recovery, can be challenging and it is often difficult to determine at what phase of the transformation process such events occur.

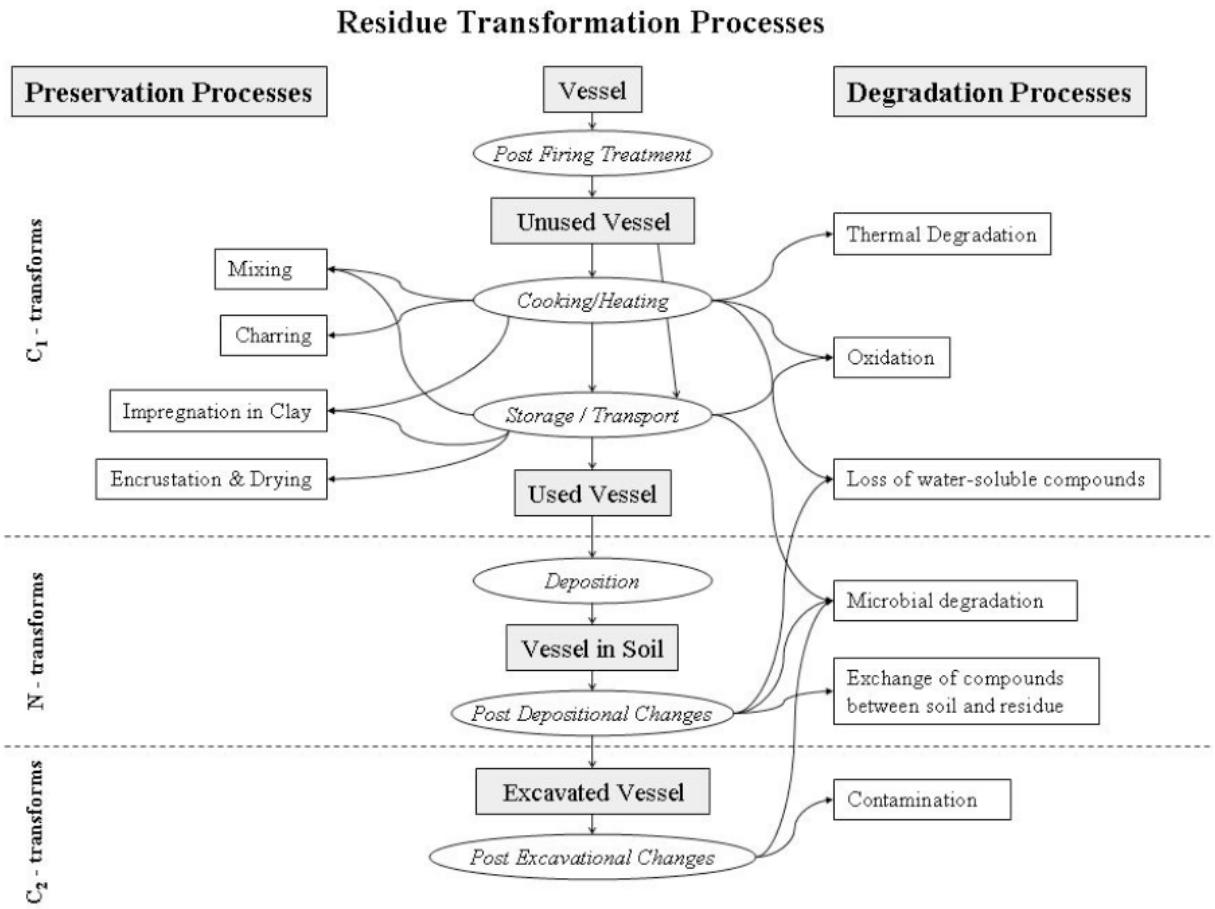

Figure 25: Residue Transformation Processes. Transformation processing includes processes in the original prehistoric context as the so called C1 transforms (cultural transforms), and processes in the post depositional context as the so called N1 transforms (natural transforms), and the post-excavational context as the so called C2 transforms (cultural transforms). Each of the transformation processes creates changes in the chemical composition of the original organic material in the vessel. Some of these changes cause the degradation of specific chemical characteristics (degradation process) while other chemical changes will enhance the preservation of such typical chemical characteristics of the original materials (preservation processes) (Oudemans, 2007, p. 7).

Techniques for determining and distinguishing between the occurrence of post-depositional and post-recovery degradation processes vary greatly; for the purpose of this discussion, only soil-related methodologies will be discussed. In many cases, in order to determine if a residue underwent contamination during the post-depositional and post-recovery process, reference soils are collected and examined in conjunction with the recovered residues (Oudemans,

2007, pp. 5-7); (McGovern & Hall, 2015, p. 593); (Evershed, 2008, p. 907). These reference soils are either from the area around the potsherd fragment or from both inside and outside of an intact vessel; in each instance, the collected samples are used for comparison in order to understand how preservation and degradation processes have impacted the soil itself in addition to the ceramic in which the residue is collected (Oudemans, 2007, pp. 5-7). This is because, following the deposit, there may be an exchange of organic compounds between the residue and the soil that surrounds it (McGovern & Hall, 2015, p. 594). This exchange can go both ways as a form of leaching (in which elements are taken from the ceramic matrix into the soil) or impregnation (in which elements are transferred from the soil into the ceramic matrix) (Oudemans, 2007, pp. 5-7). Thus, it is important to analyze reference soils from the area around the vessel in addition to soils from the interior in order to evaluate the organic compounds present naturally in the area against those being observed inside of the vessel and within the ceramic matrix (McGovern & Hall, 2015, p. 594). In other words, careful consideration must be given at all times to compounds that could originate from soils and additional comparisons need to be made to consider missing compounds that might have been lost during burial. (Oudemans, 2007, pp. 5-7). Although such analysis is only recently becoming common practice, it is nevertheless important to consider the impact of soils on organic residue analysis methodologies.

In addition to their impact on the analysis of organic residues within ceramic matrixes through comparison, archaeological soils can theoretically also be utilized in the examination of previously liquid organic residue *without* the destruction of intact ceramic bodies or potsherds fragments (Roffet-Salque, et al., 2017, pp. 627-628). As previously mentioned, visible residues can be preserved when a vessel is filled with soil following deposition; such an event can also result in non-visible residue as the trapped organic material is absorbed into the ceramic over a

period of time (Evershed, 2008, pp. 903-904). It can be assumed that the organic material is also absorbed into the soil sediment in addition to the clay matrix (McGovern & Hall, 2015, p. 594). Thus, it is possible that organic biomarkers can be preserved in the soil inside the vessel as, under favorable circumstances, organic compounds have been shown to survive in soils and sediments across the archaeological timescale (Evershed, 2008, p. 907). As discussed, previous analyses of archaeological soil have primarily centered on their use as reference material or as independent artifacts; however, it stands to reason that in specific preservation environments, archaeological soils can be considered as the fourth form of organic preservation methodology that can be studied in cases where intact ceramic vessels or potsherds cannot be analyzed by destructive methodology (McGovern & Hall, 2015, p. 594). With this in mind, the present study aims to evaluate if organic residues can, in fact, be detected through non-destructive and non-invasive methodology centered on the use of archaeological soils as an alternative to that of ceramic potsherds or intact vessels. The methodology and results of this analysis will be discussed in the subsequent chapters.

Chapter 3. Materials

3.1 Artifact Discovery

The artifact under study in the present work was discovered fully intact in 2018 within a tomb during a rescue excavation as a result of road maintenance close to the Ancient Thouria city remains (Malapani, 2021, p. 44). As it was not part of a systematic excavation, there is little information about the actual discovery and uncovering of the tomb. The burial and environmental conditions of the excavation area are unknown. As the site was discovered during public maintenance, the tomb was recovered with asphalt when the road was repaired.

3.2 Reference Samples Collection

The location of the tomb was determined in relation to the Ancient Thouria site (Fig. 32). As the rescue excavation occurred in 2018, the current appearance of the site was documented (Fig. 33). Due to the fact that the archaeological soil from around the tomb was inaccessible as a result of refilling and reburial, samples were taken from five different locations at various distances from the site. These sample locations were determined by the visible appearance of the soil and location relative to the excavated grave site (Fig. 34). Five sites for sampling were selected based on these characteristics.

Figure 26: Tomb and Reference Sample Site. The location of the sampling site/tomb location compared to the primary Thouria site [(Ασκληπιειο = Asklepion Temple) (Θεση Ανασκαφης = Excavation site of the tomb)].

Figure 27: Present Tomb Site. Discovery location of the tomb and current appearance post paving.

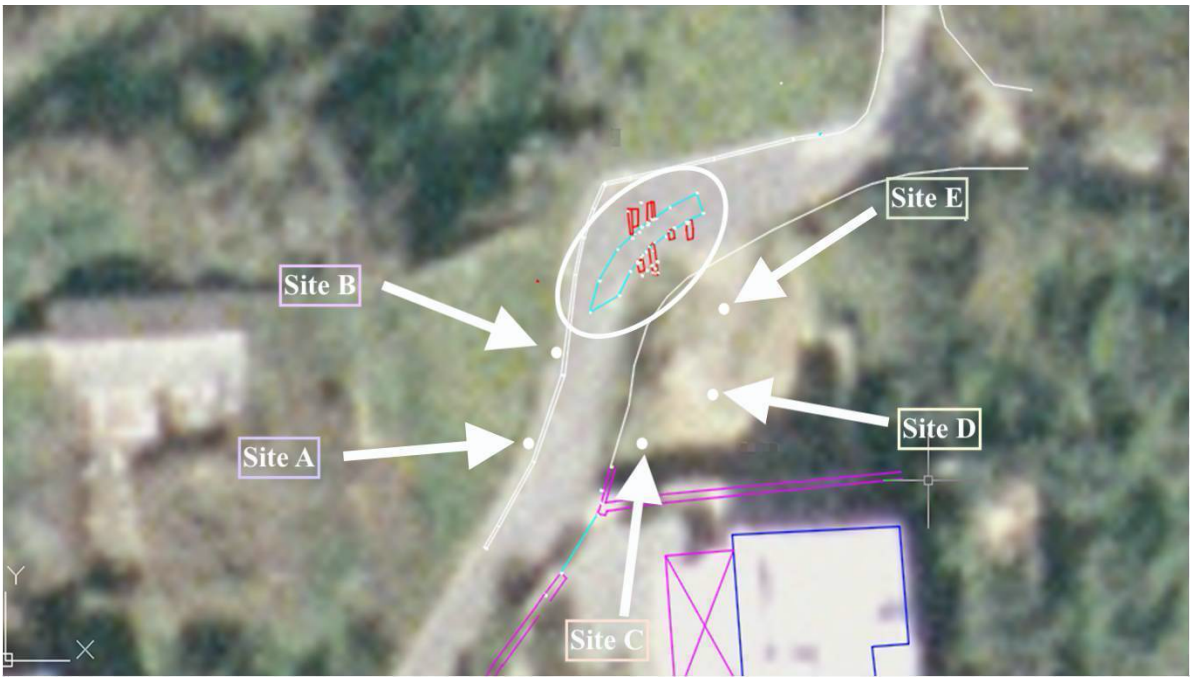

Figure 28: Reference Sites Relative to Tomb Site. The different locations where soil samples were taken compared to the actual site of the grave under the asphalt (white circle indicates tomb site underneath the pavement).

Following the selection of five reference sample sites, approximately 50 g of loose soil was extracted from a depth ranging from 1-5 cm from the surface in each location The location of the sampling site and the close-up of the soil extraction site were documented (Fig. 35). From the loose soil collected, a single sample with the smoothest and flattest surface was selected for analysis as a representative reference sample; this process was repeated for each of the reference sites. The resulting five samples, collectively referred to as the "Reference Group," will be discussed further in a later section (3.3).


A


B


C

Figure 29: Reference Sample Sites. Location of reference sample sites (left) and close up of the sample soil (right). (From top to bottom: Site A, Site B, Site C, Site D, Site E).

3.3 Sample Collection

In order to conduct further analysis focusing on the evaluation of the initial content of the vessel, the soil from inside of the vessel was collected (Fig. 30). This collected soil was sifted for large fragments which may have been next to the walls of the vessel and thus could have absorbed some of the liquid the vessel once contained. During the selection of samples, predominately soil fragments with visibly smooth or flat surfaces were selected. Although several clusters and a sample of the loose soil were collected, approximately 50g of soil, much of the soil from the inside of the vessel remained with the artifact in storage.

From this soil, approximately 30 soil clusters were selected for analysis which will hereto forth be referred to as the “Sample Group”.

Figure 30: Sample Group Source. Soil collected from inside of Lagynos Vessel.

3.4 Initial Documentation & Classification

The collected samples were preliminarily separated into groups of their assumed position within the vessel by the observed basic physical characteristics (Appendix B). Defining characteristics of the smooth side included the angle, curvature, and general evenness; the rough side was determined by particle size and texture (Fig. 31). The color of each sample was also recorded. Fragments without a discernable smooth or rough side were considered loose soil.


10 cm
10 cm
10 cm
10 cm
10 cm
10 cm

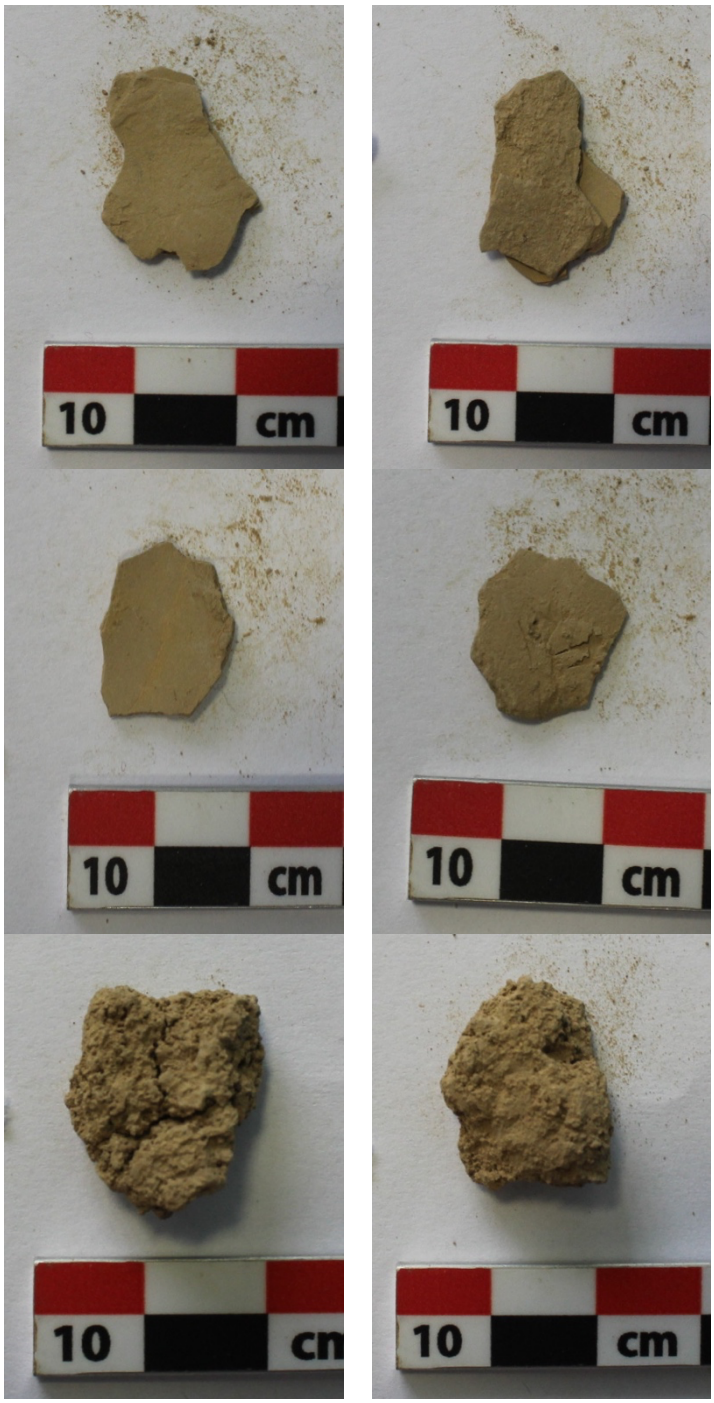

Figure 31: Sample Side Comparison. Comparison of the smooth (left) and rough (right) sides of the Refined Analysis group. (From top to bottom: A1, B1, B4, B6, B7, & C3[5]).

[5] Sample E1 was excluded for lack of discernable smooth and rough sides for documentation.

LED Optical Microscopy

Using optical microscopy, the colors of fragments were determined with the assistance of the Munsell Color Chart by means of visual color comparison (Munsell Color Company, 1975). An image of the fragment's representative fabric was taken at 50x magnification. Through examination of this image, the frequency of inclusions, shape and size of inclusions, coarseness, and porosity of the sample group were determined (Appendix C). Based on these characteristics and the physical appearance of the samples, the sample group was further refined to include only 7 samples; this group will be referred to as the "Refined Analysis Group" from this point forward (Table 1). Only samples with smooth, flat surfaces were selected. The evaluation of characteristics was also repeated for the reference samples also known as the Reference Group to determine which samples shared characteristics with the Refined Analysis Group (Table 2).

Table 1: LED and Munsell of the Refined Analysis Group. A macroscopic analysis of Samples A1 - E1.

Sample	*LED Photo (X50)*	*Munsell Soil Color Chart*	*Frequency of Inclusions*	*Size & Shape of Inclusions*	*Coarseness*	*Porosity*
A1		2.5Y 6/3 Light yellowish-brown	60%	small inclusions; granular, angular, subangular; fine to coarse	coarse	5%
B1		2.5Y 6/3 Light yellowish-brown	70%	small inclusions; granular, angular, subangular; fine to coarse	coarse	10%
B4		2.5Y 6/3 Light yellowish-brown	10%	small inclusions; granular; fine	fine	0%
B6		2.5Y 6/3 Light yellowish-brown	10%	very few small inclusions; granular; fine	fine	0%
B7		2.5Y 6/3 Light yellowish-brown	5%	very few small inclusions; granular; fine	fine	0%
C3		2.5Y 6/4 Light yellowish-brown	30%	small inclusions; granular, subangular; fine to coarse	fine	10%
E1		2.5Y 6/3 Light yellowish-brown	10%	small inclusions; granular, angular, subangular; fine to coarse	fine	40%

Table 2: LED and Munsell analysis of the Reference Group. A macroscopic analysis of Samples REF_A1 - REF_E1.

Sample	*LED Photo (X50)*	*Munsell Soil Color Chart*	*Frequency of Inclusions*	*Size & Shape of Inclusions*	*Coarseness*	*Porosity*
REF_A1		10YR 5/3 Brown	50%	medium and small inclusions; granular, angular, subangular; fine to coarse	coarse	5%
REF_B1		7.5YR 5/4 Brown	80%	large, medium, and small inclusions; platy, angular, subangular; fine to coarse	coarse	10%
REF_C1		2.5Y 6/4 Light yellowish-brown	70%	small inclusions; granular, angular, subangular; fine to coarse	coarse	0%
REF_D1		2.5Y 6/4 Light yellowish-brown	80%	small inclusions; granular, angular, subangular; fine to coarse	coarse	0%
REF_E1		2.5Y 6/3 Light yellowish-brown	60%	small inclusions; granular, angular, subangular; fine to coarse	coarse	15%

3.5 Artifact Conservation

Following its recovery, the lagynos vessel was dried, weighed, and stored in a polypropylene box at the Conservation Department of the Archaeological Museum of Messenia for over a year after the excavation. After being removed from storage, the vessel's condition was documented and the outside was cleaned using a solution of distilled water and ethylene in a 3:1 ratio. Following this, the inside of the artifact was mechanically cleaned using distilled water injections to remove the excess soil and prepare for the

desalination treatment; this soil was collected and dried. In order to desalinate the vessel, the lagynos was soaked for 24 hours in distilled water before being dried in an oven at 60°C for 24 hours. A consolidation treatment was then applied so as to preserve the vessel's integrity (Spala, 2021).

3.6 Macroscopic Examination

The vessel was intact, of great archaeological significance, and had already undergone conservation (Fig. 32). Therefore, extracting micro-samples or conducting any destructive chemical analysis was not possible due to preservation concerns. Instead, the vessel's decorations and damages were fully documented.

Figure 32: Lagynos vessel. Documentation of damage to the top of the vessel.

The lip and handle of the lagynos show chipped paint (Fig. 33). The ridge in the center of the handle has worn spots with high amounts of paint chipping.

Figure 33: Lagynos Vessel Rim and Handle. Documentation of damage to the upper areas of the vessel.

The bottom of the vessel shows scratch marks in a variety of locations and sizes (Fig. 34). The clay indicates circular patterns which may indicate production via a wheel. The rim has three chipped marks next to each other on the left side of the rim. Smaller chips can also be seen at the upper section of the rim in the image. The lower right section has a small chip on the interior and a flat section on the exterior.

Figure 34: Lagynos Vessel Bottom. Documentation of damage to the bottom of the vessel.

Around the edge of the body, there is a cluster of chipped paint at the edge. Smaller chips can be seen near the wreath itself. An additional chip is visible near the handle in the top right corner of the image. A large chip is visible near the wreath with very deep edges at the top of the shape. The paint of the wreath in the image also shows flaking and fading (Fig. 35A). Additional chipping is visible to the side of the lagynos decoration. The paint of the decoration itself is fading and flaking in places. The wreath to the left of the lagynos also has large spots where the paint has faded and flaked (Fig. 35B). The wreath visible in the image has several spots where the paint has faded and chipped. There are several small, chipped sections around the shape of the wreath as well (Fig. 29C). The lower section of the handle is more preserved than other sections of the ceramic. It has minimal chipping although the paint is becoming faded in several spots. The inside of the lower part of the handle has several large chips in the paint which extend up the length of the handle (Fig. 29D).

Figure 35 (A-D): Lagynos Vessel Damage. Documented damage and deterioration of the vessel body.

As the damage to the paint and exterior of the vessel is extensive, it was unadvised that chemical analysis of any kind is performed in order to preserve the structure and integrity of the vessel and decorations. With this in mind, the lagynos vessel itself was handled as little as possible during the documentation period.

Chapter 4. Methods

In order to verify the presence and determine the identity of the liquid from inside of the lagynos vessel, the soil fragments and reference samples were examined using several different methodologies. Photographic documentation of the samples was first carried out, followed by observation with LED optical microscopy in order to classify the fragments. Then, a Scanning Electron Microscope coupled with an Energy Dispersive Spectrometer was used to determine the elemental composition of the different fragments (Palamara, et al., 2016, p. 139). Raman spectroscopy was then attempted in order to identify the presence of organic compounds (Palamara, et al., 2016, p. 139). This presence was further verified using Fourier-Transform Infrared Spectroscopy (Koupadi, et al., 2021, p. 3613). Additional FTIR protocols were implemented to identify the organic compounds present in the different sample and reference groups (McGovern, et al., 2017); (McGovern & Hall, 2015).

3.1 Documentation & Classification

Photo documentation of the samples collected from the Archaeological Museum of Messenia were taken in natural lighting on a white background using the Laboratory of Archaeometry's Canon EOS 600D camera. A rough classification of the sample group was performed based on the visual characteristics of the samples.

3.2 LED Optical Microscopy

Following the macroscopic rough classification, the characteristics of the soil clusters were determined using a portable Light Emitting Diode Microscope and the Munsell Soil Color Chart. The examination focused on color, frequency of inclusions, size and shape of inclusions, coarseness, and porosity in order to determine the homogeneity of the overall sample group. From this information, the Sample Group was further refined as previously mentioned to create the Refined Analysis Group (3.4). The Reference Group was also examined using the same protocol.

3.3 SEM/EDS

The chemical composition of the Refined Analysis Group and the Reference Group was determined by a Scanning Electron Microscope (SEM) by JEOL (JSM-6510LV) coupled with EDS (Oxford Systems) from the Archaeometry Lab of the University of the Peloponnese. The analytical data were obtained by INCA software. The analyses were conducted at 20 kV accelerating voltage with a count time of 120 s. Multiple positions of the smooth side of the samples were examined via SEM and images were taken using 30x, 100x, 150x, and 200x magnification. The EDS spectra were recorded at 200x magnification at 5-10 different locations on the smooth side of each sample, depending on its homogeneity. The rough side of the samples were then analyzed which resulted in approximately 5 EDS spectra for each of the samples; however, it should be noted that the amount of spectra recorded depended on the physical surface of the rough side of each of the samples.

3.4 RAMAN

Two of the Refined Analysis Group Samples, A1 and B1, - selected for their flat surfaces- were analyzed by a Bruker BRAVO Handheld RAMAN spectrometer using OPUS spectroscopy software. An area on the flattest part of the smooth side of the sample was examined with an analysis time of 40-50s; this process was repeated on the rough side. When possible, additional spots were examined on both sides of the samples depending on the physical characteristics of the sample itself.

3.5 FTIR

Powder samples from the Refined Analysis Group and the Reference Group were compressed into KBr discs using the unadulterated methodology below and analyzed using the Bruker Alpha II FTIR Spectrometer using OPUS spectroscopy software at the University of West Attica to the Department of Conservation of Antiquities and Works of Art (*CAWA*) Laboratory (Koupadi, et al., 2021, p. 3613).

Following the initial FTIR analysis, the four samples (A1S, A1, B1, & REF_E1) with indications of organic remains were extracted using methanol and dichloromethane (DCM) and, accordingly, dripped on to KBr disc as detailed in the respective methodology below; this process was done in order to remove the inorganic interference provided from the powdered soil samples (McGovern, et al., 2017); (McGovern & Hall, 2015). In each extraction, different classes of organic materials were expected to be recorded according to their solubility in the two solvents; in particular, polar components are extracted with

methanol while nonpolar components are extracted with dichloromethane (Koupadi, et al., 2021, p. 3613).

Unadulterated KBr Disc Analysis

A section of the sample was scraped with a scalpel to remove a small amount of material from the smooth side of the sample. This material was ground using a mortar and pestle with approximately 10x the same amount of potassium bromide (KBr); the components were ground until homogeneous in appearance. The mixture was then transferred to the disc mold apparatus in an even layer. A die was added on top of the layer and pressed into place using a manual hydraulic press to apply 10 tons of pressure for 1 minute. The sample was then repositioned in the press to allow for the removal of the die and extraction of the KBr disc; the disk was then collected and labeled. This process was repeated for each of the samples- A1, B1, B3, B4, B6, B7, C3, and E1 respectively- and reference soils- REF_A1, REF_B1, REF_C1, REF_D1, and REF_E1- for a total of 13 discs. The discs were analyzed using the FTIR Spectrometer with a scan rate of 15. Before each analysis, no disc was placed in the instrument to create an atmospheric blank was used to calibrate the FTIR Spectrometer; this methodology was repeated for each analyses.

Dichloromethane Analysis

A scalpel was used to collect additional material from a single location on the samples; this small amount of material was collected in a labeled glass vial. This process was repeated for each of the samples and the reference soil, REF_E1; in addition to the primary samples, a second additional sample was taken from the rough side of A1 in order

to compare the smooth and rough sides of the sample. A total of 10 sample vials were created.

Approximately 0.25mL of dichloromethane, also called DCM (CH_2Cl_2), was pipetted into each of the sample vials. The vials were placed in a DI water bath to sonicate for 15 minutes; the DI water bath was allowed to cool for several minutes before sonication was repeated for an additional 15 minutes; this resulted in a total sonication time of 30 minutes. The vials were removed from the ultrasonic bath and set aside for 10 minutes to allow the suspension to settle. Once the supernatant and sediment had separated, a pipet was used to transfer 9 drops of the supernatant onto a blank KBr disc. This process was repeated for each of the vials and the discs were allowed to dry for 3 minutes. Once dry, discs were analyzed using the FTIR Spectrometer using the same methodology as before.

Methanol Analysis

The same section of the smooth side of the sample was scraped with a scalpel to remove a small amount of material which was collected in a labeled glass vial. This process was repeated for each of the samples and the reference soil, REF_E1, which includes the two samples which were extracted from A1 for side comparison which resulted in a total of 10 sample vials.

Approximately 0.25mL of methanol (MeOH) was pipetted into each of the vials. The vials were placed in a DI water bath to sonicate for 15 minutes; the DI water bath was allowed to cool for several minutes before sonication was repeated for an additional 15 minutes; this resulted in a total sonication time of 30 minutes. The vials were removed from the ultrasonic bath and set aside for 10 minutes to allow the suspension to settle. Once

the supernatant and sediment had separated, a pipet was used to transfer 4 drops of the supernatant onto a blank KBr disc. This process was repeated for each of the vials and the discs were allowed to dry for 10 minutes. Once dry, discs were analyzed using the Bruker Alpha II FTIR Spectrometer.

Following their initial analysis, an additional 4 drops of supernatant were added to each of the discs respectively and were allowed to dry for 10 minutes; once dry, the discs were analyzed again. This additional depositional process was repeated a second time for a total of 3 depositional events. This resulted in a total of 3 FTIR spectra for each of the samples.

3.6 Refined FTIR

Based on the results of the previous methodology, four samples (A1, B1, REF_D1, & REF_E1) with indications of the presence of organic material were selected for further analysis. The previous MeOH and DCM methodology was modified and refined as detailed below. In addition to the previous methodology, an additional extraction utilizing methanol and chloroform - which form a monophasic solvent system to extract and dissolve lipids - was also performed (McGovern, et al., 2017); (McGovern & Hall, 2015). These extractions were performed using elemental silicon wafers instead of KBr discs; the elemental silicon wafers were cleaned with acetone and dried using a nitrogen stream.

Refined Sample Preparation

Under examination of the Opticak Stereoscope, a scalpel was used to remove a portion of the sample which was then weighed using a mass balance. The samples were

then placed in a glass vial and labeled. A standardized volume of each solvent was added to the respective samples in order to refine the results of the previous methodology.

Methanol Analysis

1ml of methanol was pipetted into the vials labeled A1S_M, B1S_M, REF_D1_M, and REF_E1_M. The vials were placed in a DI water bath to sonicate for 15 minutes; the DI water bath was allowed to cool for several minutes before sonication was repeated for an additional 15 minutes; this resulted in a total sonication time of 30 minutes. The vials were removed from the ultrasonic bath and set aside for 10 minutes to allow the suspension to settle. 0.5 mL of the A1S_M suspension was pipetted into an Eppendorf tube; this process was repeated for each of the samples. A control sample of 0.5 mL of methanol was also prepared. The tubes were then centrifuged for 5 minutes at 4,000 rpm.

A silicon wafer was placed on a hot plate at 64.7 °C and A1S_M supernatant was dripped onto one side of the wafer until a film was visible. The wafer was allowed to dry for one minute. The blank side of the wafer was analyzed using the FTIR as a control. After this, the treated side of the wafer was analyzed. In both cases, the wafers were analyzed using FTIR Spectrometer with a scan rate of 50. Before each analysis, no wafer was placed in the instrument to create an atmospheric blank was used to calibrate the FTIR Spectrometer. This process was repeated for each of the methanol samples and the methanol control.

A second amount (0.25ml) of supernatant was deposited onto each of the respective elemental silicon wafers using the same method as before. The FTIR analysis method was

also repeated. This process was repeated resulting in the 3rd addition of supernatant and resulting FTIR examination.

Dichloromethane Analysis

1ml of DCM was pipetted into the vials labeled A1S_D, B1S_D, REF_D1_D, and REF_E1_D. The vials were placed in a DI water bath to sonicate for 15 minutes; the DI water bath was allowed to cool for several minutes before sonication was repeated for an additional 15 minutes; this resulted in a total sonication time of 30 minutes. The vials were removed from the ultrasonic bath and set aside for 10 minutes to allow the suspension to settle.

A silicon wafer was placed on a hot plate at 39.6 °C and A1S_D supernatant was dripped onto one side of the wafer until a film was visible. The wafer was allowed to dry for one minute. The blank side of the wafer was analyzed using FTIR as a control. After this, the treated side of the wafer was analyzed. In both cases, the wafers were analyzed using the FTIR Spectrometer with a scan rate of 50. Before each analysis, no wafer was placed in the instrument to create an atmospheric blank was used to calibrate the FTIR Spectrometer. This process was repeated for each of the DCM samples and a control sample of DCM.

Following this analysis, an additional 1mL of solvent was added to the DCM sample vials and 1 round of sonication was performed for 15 minutes. A second amount (0.25ml) of supernatant was deposited onto each of the respective elemental silicon wafers using the same method as before. The FTIR analysis method was also repeated.

Following this, the DCM sample vials were sonicated for an additional 15 minutes. A third amount (0.25ml) of supernatant was deposited onto each of the respective elemental silicon wafers using the same method as before. The FTIR analysis method was also repeated.

A third amount (0.25ml) of supernatant was deposited onto each of the respective elemental silicon wafers of the A1S and B1S samples using the same method as before. The FTIR analysis method was also repeated.

Following this, an additional amount of supernatant was deposited onto the A1S and B1S wafers for a total of four times. The FTIR analysis method was also repeated.

Methanol-Chloroform Analysis

1 ml of a 1:1 ratio of methanol (MeOH) and chloroform ($CHCl_3$) was pipetted into the vials labeled A1S_X, B1S_X, REF_D1_X, and REF_E1_X. The vials were placed in a DI water bath to sonicate for 15 minutes; the DI water bath was allowed to cool for several minutes before sonication was repeated for an additional 15 minutes; this resulted in a total sonication time of 30 minutes. The vials were removed from the ultrasonic bath and set aside for 10 minutes to allow the suspension to settle.

A silicon wafer was placed on a hot plate at 60 °C and A1S_X supernatant was dripped onto one side of the wafer until a film was visible. The wafer was allowed to dry for one minute. The blank side of the wafer was analyzed using FTIR as a control. After this, the treated side of the wafer was analyzed. In both cases, the wafers were analyzed using the FTIR Spectrometer with a scan rate of 50. Before each analysis, no wafer was

placed in the instrument to create an atmospheric blank was used to calibrate the FTIR Spectrometer. This process was repeated for each of the mixed MeOH-$CHCl_3$ samples and a control sample of the MeOH-$CHCl_3$ mixture.

Following this analysis, an additional 1mL of solvent was added to the MeOH-$CHCl_3$ sample vials and 1 round of sonication was performed for 15 minutes. A second amount (0.25ml) of supernatant was deposited onto each of the respective elemental silicon wafers using the same method as before. The FTIR analysis method was also repeated.

A third amount (0.25ml) of supernatant was deposited onto each of the respective elemental silicon wafers of the A1S and B1S samples using the same method as before. The FTIR analysis method was also repeated.

Following this, an additional amount of supernatant was deposited onto the A1S and B1S wafers for a total of four times. The FTIR analysis method was also repeated.

Chapter 5. Results

4.1 Documentation & Classification

The collected samples were preliminarily separated into groups of their assumed position within the vessel by the observed basic physical characteristics (Appendix B). Defining characteristics of the smooth side included the angle, curvature, and general evenness; the rough side was determined by particle size and texture (Fig. 31). The color of each sample was also recorded. Fragments without a discernable smooth or rough side were considered loose soil.

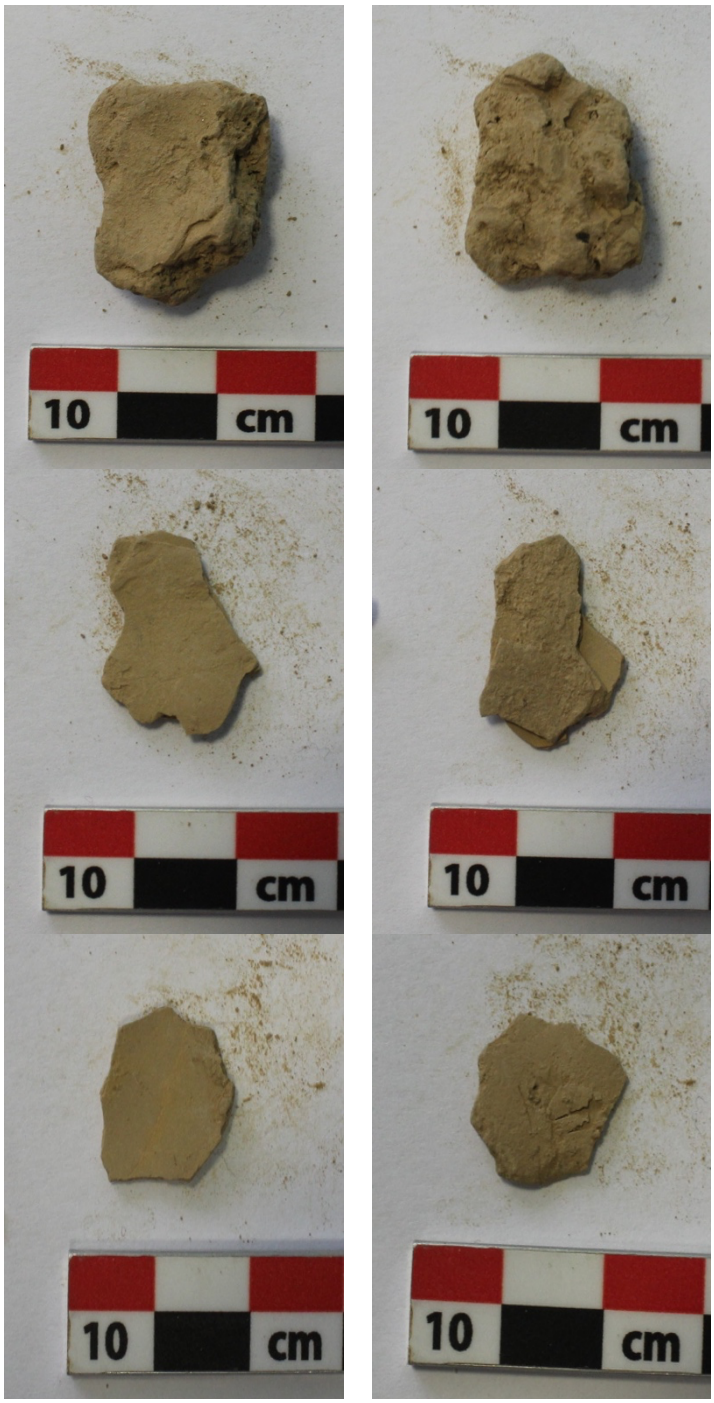
10 cm
10 cm
10 cm
10 cm
10 cm
10 cm

Figure 31: Sample Side Comparison. Comparison of the smooth (left) and rough (right) sides of the Refined Analysis group. (From top to bottom: A1, B1, B4, B6, B7, & C3[6]).

4.2 LED Optical Microscopy

Using optical microscopy, the colors of fragments were determined with the assistance of the Munsell Color Chart by means of visual color comparison (Munsell Color Company, 1975). An image of the fragment's representative fabric was taken at 50x magnification. Through examination of this image, the frequency of inclusions, shape and size of inclusions, coarseness, and porosity of the sample group were determined (Appendix C). Based on these characteristics and the physical appearance of the samples, the sample group was further refined to include only 7 samples; this group will be referred to as the "Refined Analysis Group" from this point forward (Table 1). Only samples with smooth, flat surfaces were selected. The evaluation of characteristics was also repeated for the reference samples also known as the Reference Group to determine which samples shared characteristics with the Refined Analysis Group (Table 2).

[6] Sample E1 was excluded for lack of discernable smooth and rough sides for documentation.

Table 1: LED and Munsell of the Refined Analysis Group. A macroscopic analysis of Samples A1 - E1.

Sample	*LED Photo (X50)*	*Munsell Soil Color Chart*	*Frequency of Inclusions*	*Size & Shape of Inclusions*	*Coarseness*	*Porosity*
A1		2.5Y 6/3 Light yellowish-brown	60%	small inclusions; granular, angular, subangular; fine to coarse	coarse	5%
B1		2.5Y 6/3 Light yellowish-brown	70%	small inclusions; granular, angular, subangular; fine to coarse	coarse	10%
B4		2.5Y 6/3 Light yellowish-brown	10%	small inclusions; granular; fine	fine	0%
B6		2.5Y 6/3 Light yellowish-brown	10%	very few small inclusions; granular; fine	fine	0%
B7		2.5Y 6/3 Light yellowish-brown	5%	very few small inclusions; granular; fine	fine	0%
C3		2.5Y 6/4 Light yellowish-brown	30%	small inclusions; granular, subangular; fine to coarse	fine	10%
E1		2.5Y 6/3 Light yellowish-brown	10%	small inclusions; granular, angular, subangular; fine to coarse	fine	40%

Table 2: LED and Munsell analysis of the Reference Group. A macroscopic analysis of Samples REF_A1 - REF_E1.

Sample	*LED Photo (X50)*	*Munsell Soil Color Chart*	*Frequency of Inclusions*	*Size & Shape of Inclusions*	*Coarseness*	*Porosity*
REF_A1		10YR 5/3 Brown	50%	medium and small inclusions; granular, angular, subangular; fine to coarse	coarse	5%
REF_B1	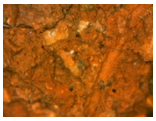	7.5YR 5/4 Brown	80%	large, medium, and small inclusions; platy, angular, subangular; fine to coarse	coarse	10%
REF_C1		2.5Y 6/4 Light yellowish-brown	70%	small inclusions; granular, angular, subangular; fine to coarse	coarse	0%
REF_D1		2.5Y 6/4 Light yellowish-brown	80%	small inclusions; granular, angular, subangular; fine to coarse	coarse	0%
REF_E1		2.5Y 6/3 Light yellowish-brown	60%	small inclusions; granular, angular, subangular; fine to coarse	coarse	15%

4.3 SEM

The smooth and rough sides of the Refined Analysis Group were analyzed using different magnifications of SEM (Appendix D). Multiple images were recorded of different locations on the samples with a preference for visible inclusions and surface texture. The samples were analyzed in an unpolished state. The rough and smooth sides of samples were observed at different magnifications in Secondary Electron Imagining (SEI) mode (Table 3).

Table 3: Sample Side Comparison. A comparison of rough and smooth side of sample A1 & B1.

Sample	*30x Magnification*	*200x Magnification*
A1 S	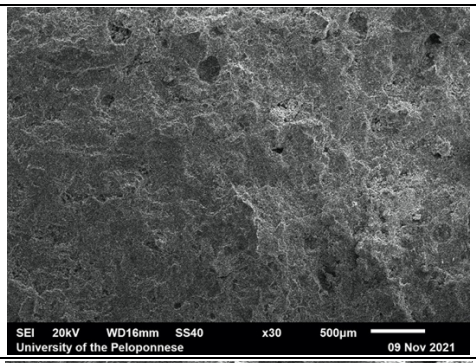	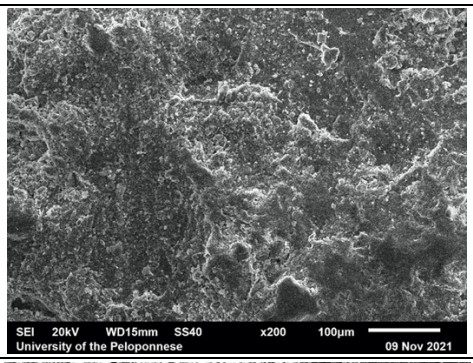
A1 R	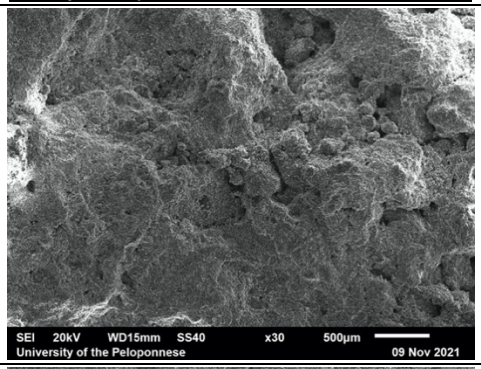	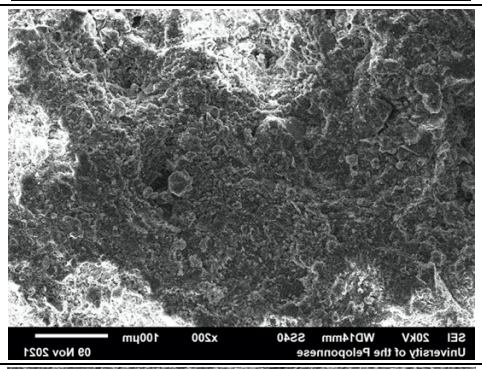
B1 S	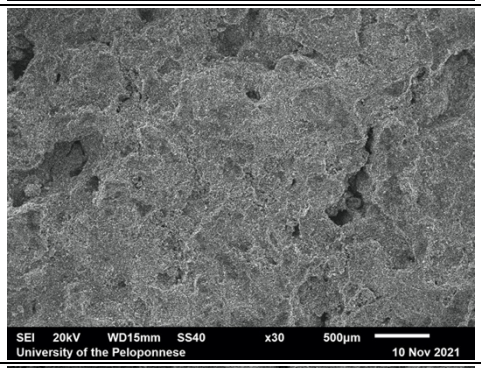	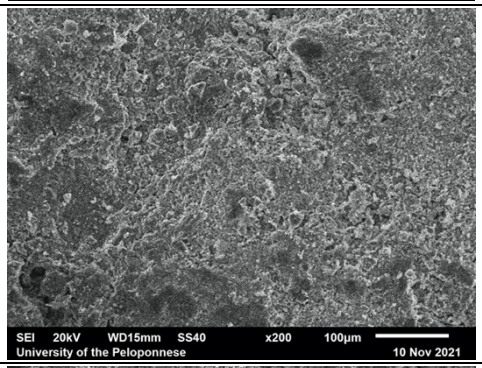
B1 R	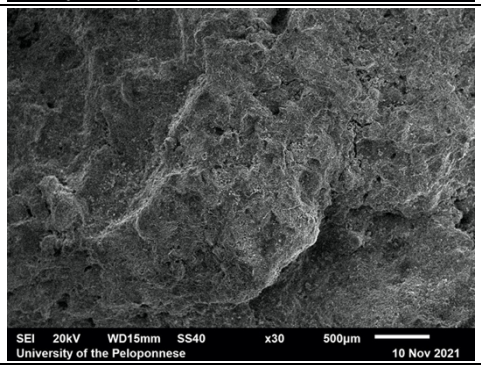	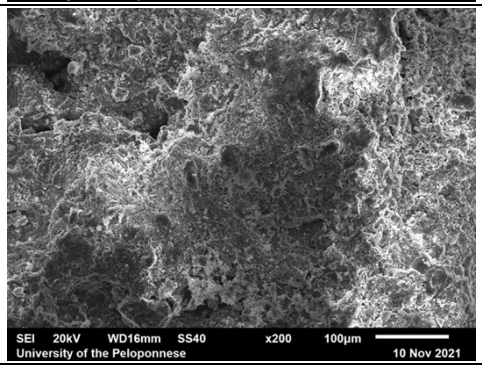

In addition to comparing the sides of the same sample, samples from Group A and Group B were also compared at different magnifications (Table 4).

Table 4: Group Magnification Comparison. SEM images from the smooth sides of samples from Group A and Group B.

Sample	***30x Magnification***	***200x Magnification***
A1	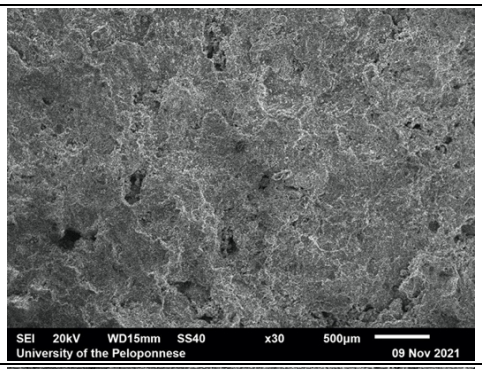	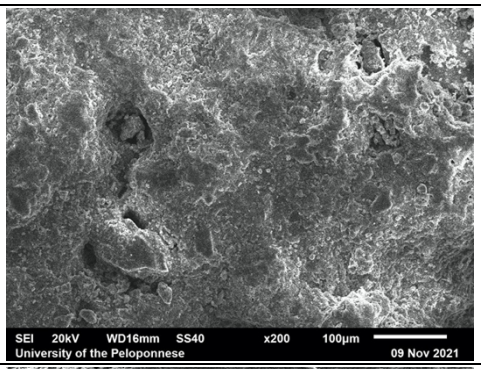
B1	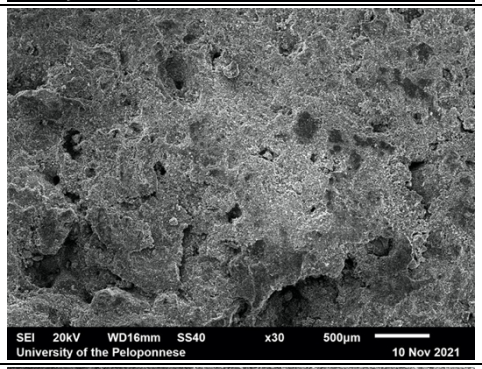	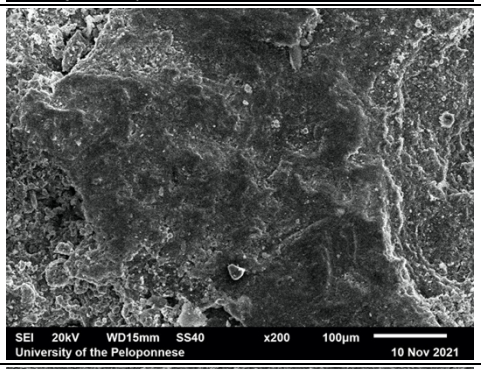
B4	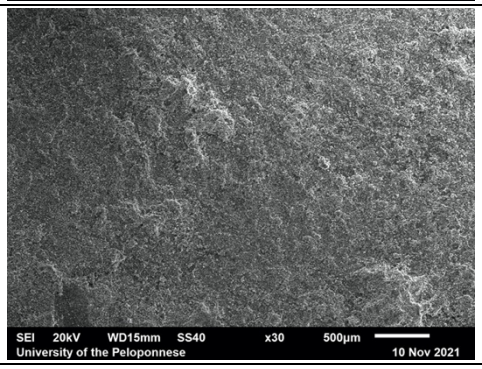	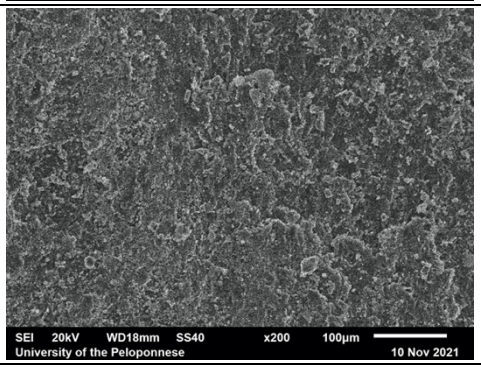

B6	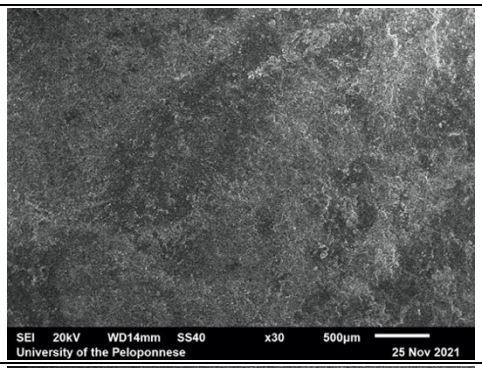	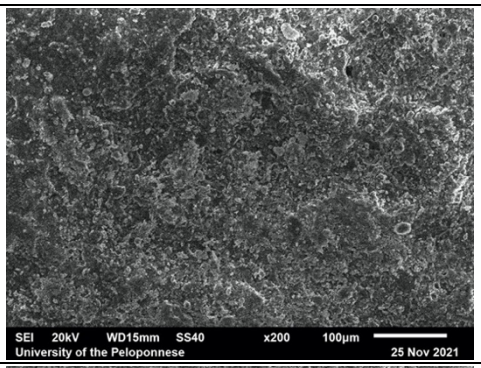
B7	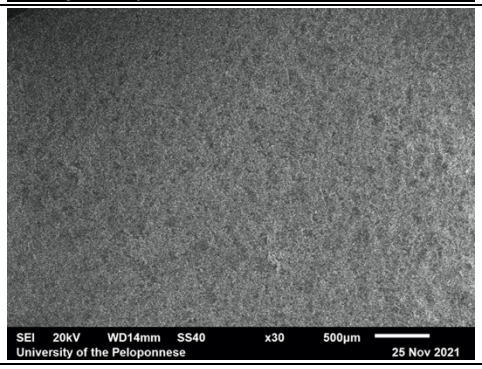	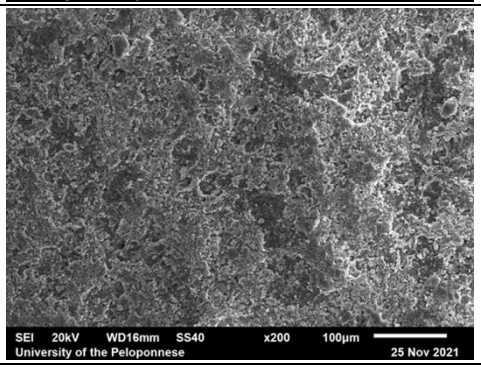

4.4 EDS

EDS analysis was performed on both the rough and smooth sides of the samples. The data of the most representative elemental spectra for each sample in the Refined Analysis Group was compiled (Table 5). This was repeated for the Reference Group (Table 6). The total elemental bulk elemental data for each sample was also recorded (Appendix E).

Table 5: EDS Representative Data of the Refined Analysis Group. The group values are given as compound% (normalized to 100%).

Sample	***Side***	***Spectrum Number***	***MgO***	***Al_2O_3***	***SiO_2***	***K_2O***	***CaO***	***FeO***	***Na_2O***
A1	S	4	2.95	14.64	54.77	3.92	18.56	5.16	0.00
	R	7	2.16	13.59	57.25	3.06	18.36	5.58	0.00
B1	S	4	2.46	14.63	52.03	3.80	19.65	7.43	0.00
	R	3	3.50	16.82	50.14	4.32	18.17	7.04	0.00
B4	S	7	4.64	17.29	48.90	3.63	21.33	4.22	0.00
	R	3	3.57	17.88	48.10	5.44	17.25	7.77	0.00

B6	S	3	2.46	14.68	49.74	3.70	22.41	5.89	1.11
	R	1	1.93	15.95	50.40	4.15	21.81	5.77	0.00
B7	S	4	3.10	16.93	45.80	4.41	20.64	9.12	0.00
	R	3	3.02	17.51	48.47	4.08	18.57	6.63	1.72
C3	R	2	3.92	15.04	51.10	2.37	19.12	8.45	0.00
E1	R	5	3.70	15.53	51.20	3.62	20.52	5.43	0.00

Table 6: EDS Representative Data of the Reference Group. The group values are given as compound% (normalized to 100%).

Sample	***Spectrum Number***	***MgO***	***Al_2O_3***	***SiO_2***	***K_2O***	***CaO***	***FeO***	***Na_2O***
REF_A1	1	1.83	15.61	63.53	2.47	10.10	6.47	0.00
REF_B1	2	2.87	17.23	57.59	3.18	12.27	6.86	0.00
REF_C1	7	2.26	20.04	62.18	3.45	2.63	9.45	0.00
REF_D1	5	1.48	18.72	61.04	2.62	8.75	7.39	0.00
REF_E1	3	3.47	15.89	57.83	1.03	13.93	7.85	0.00

4.5 RAMAN

Two samples from the Refined Analysis Group were analyzed using portable Raman spectroscopy. The smooth side of the samples are referred to as Side 1. The rough side of the samples are called Side 2. Two sharp peaks are detected in most samples at 1086 nm and 465 cm^{-1} both corresponding to calcium carbonate, indicate the v_1 (symmetric stretch) and v_2 (symmetric bend) of the carbonate ion (CO_3^{2-}) respectively (Figs. 36 & 37).

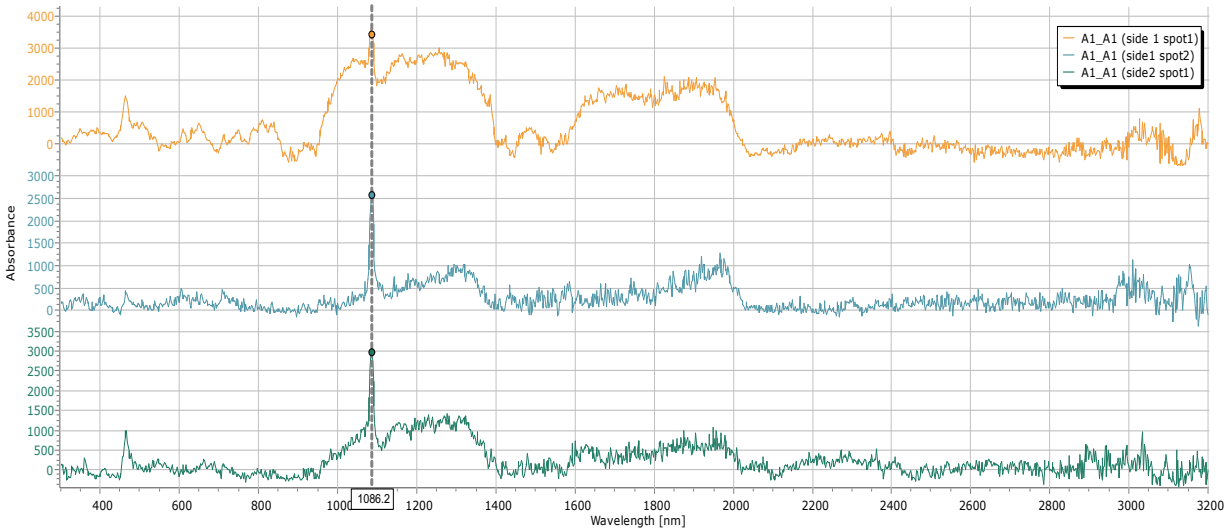

Figure 36: A1 Raman Spectra. Raman spectrum of the A1 fragment on the smooth (side 1) and rough (side 2) sides of the fragment.

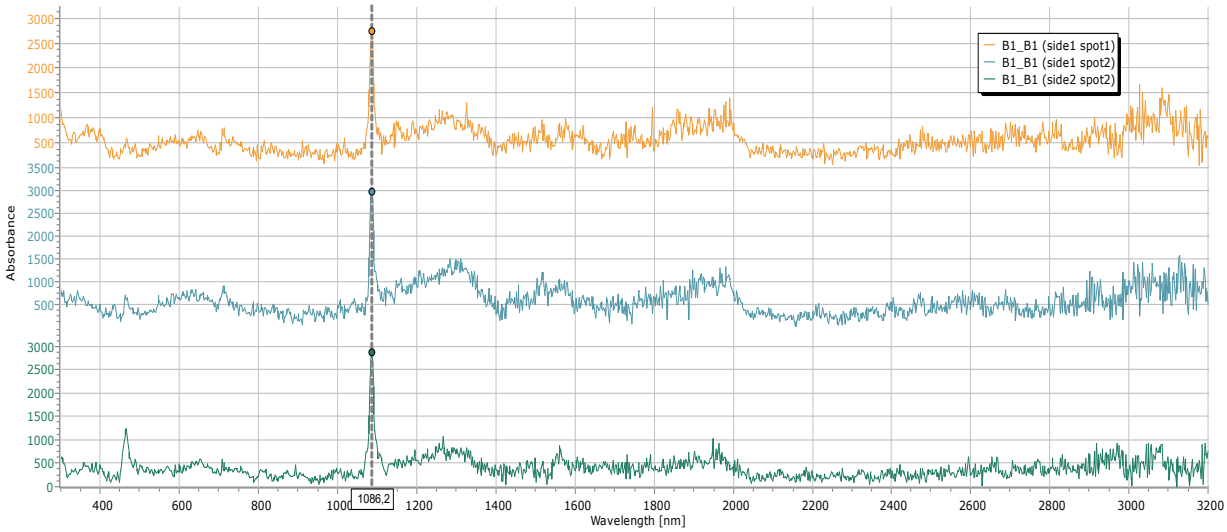

Figure 37: B1 Raman Spectra. Raman spectrum of the B1 fragment on the smooth side of the fragment.

4.6 FTIR

Powder samples from the Refined Analysis Group and the Reference Group were analyzed using FTIR spectroscopy. The spectra of each of the Refined Analysis Group samples and Reference Group of the compressed KBr disc methodology were overlayed

on a graph (Fig. 38); a select region of the spectra was expanded for further analysis and discussion (Fig. 39).

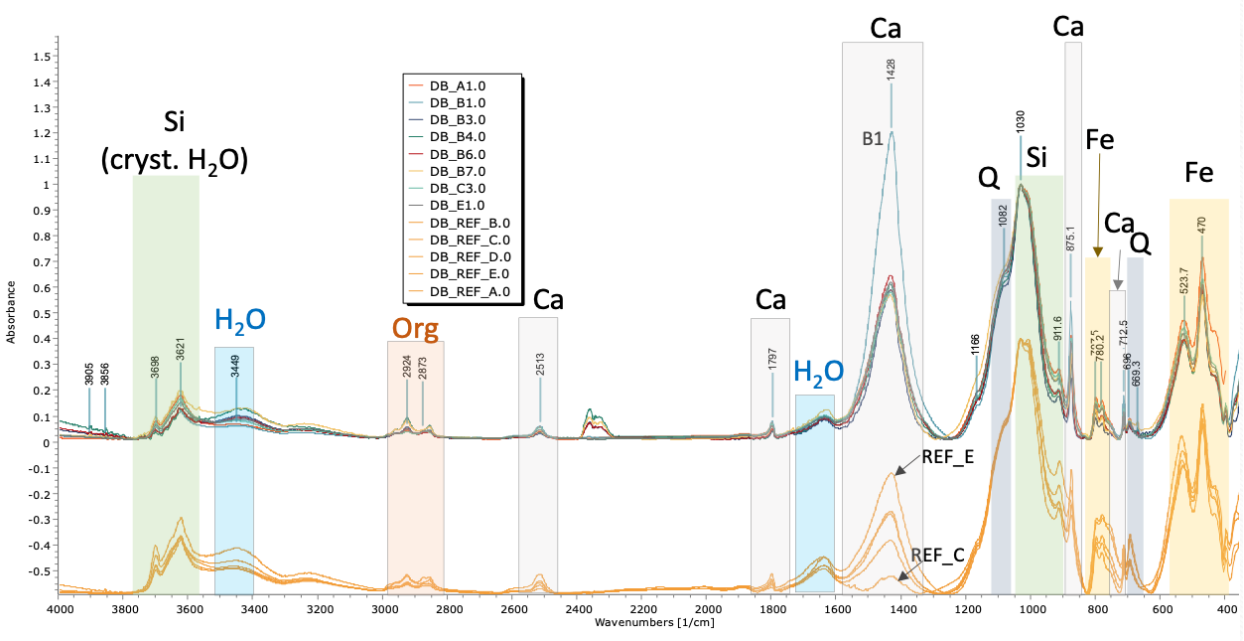

Figure 38: KBr Spectra. Spectra from the Reference and Refined Analysis group samples pressed into KBr discs were overlayed onto a graph. Legend: Si: silicates (mainly clay); H2O: crystalline water; Org: organics; Ca: calcium carbonate, the calcite polymorph ($CaCO_3$); Fe: iron oxides and hydroxy oxides; Q: quartz.

The KBr discs of the analytical grouping produced several clear and prominent absorbance peaks; of these peaks, many are associated with the soil composition itself which is to be expected as the KBr discs are composed of ground soil samples. The IR absorbance bands of soil samples associated with characteristic soil attributes can typically be divided into three regions: 4000-2000 cm^{-1}, 2000-1400 cm^{-1}, and 1200-500 cm^{-1} which correspond to the hydrogen-bond region, the organic matter region, and the inorganic soil matrix, respectively (Krivoshein, et al., 2020, p. 8). Among all the samples, a broadband can be observed in the 3700-2700 cm^{-1} region which is indicative of O-H stretching vibrations from adsorbed water (Krivoshein, et al., 2020, p. 9). Additionally, the sharp

bands at 3730-3650 cm^{-1} can be attributed to silica-bonded O-H in clay minerals (Krivoshein, et al., 2020, p. 8). These peaks were consistently observed in each of the sample spectra which is to be expected as each sample contains soil fragments. In addition, large peaks can be observed around 2380 cm^{-1} which correspond to carbon dioxide as a result of improper background subtraction (Filopoulou, et al., 2021, p. 6).

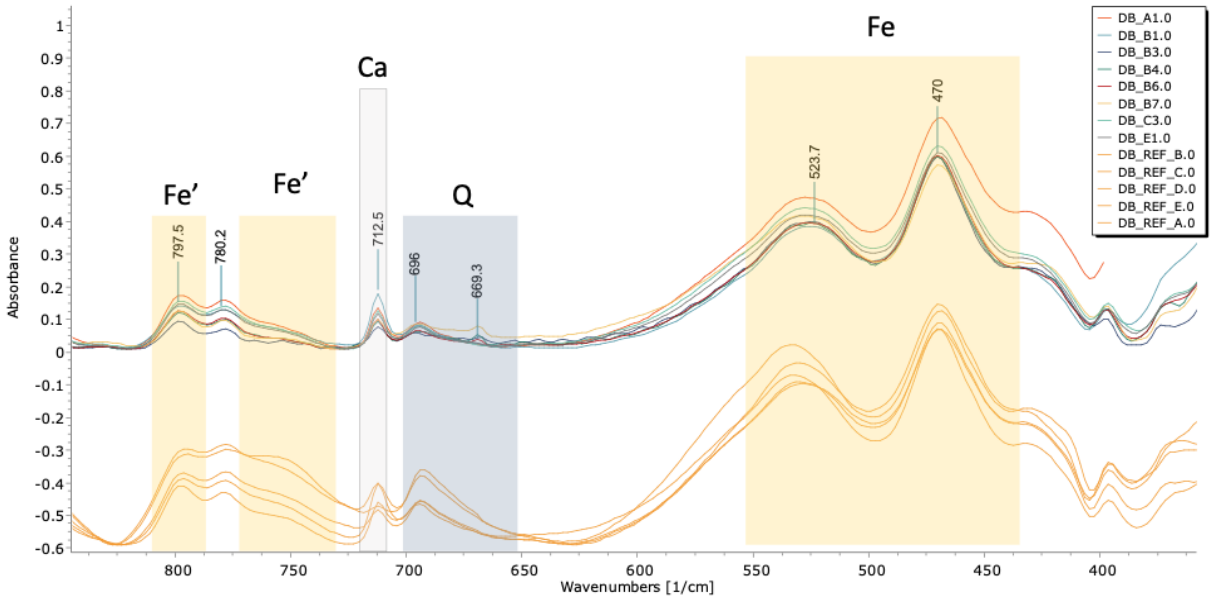

Figure 39: Zoomed KBr Spectra. Zoom in the region 900-450 cm^{-1} of spectra from the Reference and Refined Analysis group samples pressed into KBr discs were overlayed onto a graph. Legend: Si: silicates, mainly clay; Ca: calcium carbonate, the calcite polymorph ($CaCO_3$); Fe: iron oxides; Fe´ iron hydroxy oxides; Q: Quartz.

The spectra shown are normalized with respect to the silicate (Si) clay peaks which have the strongest absorbance in the spectrum (Figs. 38 & 39). Based on the spectra, the peaks appear to have similar features corresponding to the earthen nature of the material in the samples; this includes such classes as silicate material (clay and quartz sand), iron oxide (hematite, α-Fe_2O_3) and hydroxy oxides (mainly goethite, α-FeOOH) which correlate to specific absorbance maxima (Table 1) (Koupadi, et al., 2021, p. 3618). Of the spectra

observed, only four samples (A1S, A1, B1, & REF_E1) showed the greatest indications of organic materials which warranted additional analysis.

Table 7: FTIR Regions. FTIR maxima and assignments from KBr spectra of powder samples.

FTIR maximum (cm^{-1})	***Assignment***
3698, 3621	Si (cryst. H_2O): Hydroxides or crystalline H_2O associated with clay
3449, 1633	H_2O: Absorbed water in clay
2924, 2873	Org: Organic materials ($v_{as}CH_2$ and v_sCH_2)
2513, 1797, 1428, 875, 712	Ca: calcite ($CaCO_3$)
1082, 696, 669	Q: Quartz crystals vSi–O and v_{as}Si–O–Si (doublet), respectively
1030, 911	Si: Silicates in clay such as clay ($_v$Si–O)
797, 523, 470	Fe & Fe′: Iron oxides and hydroxy oxides

Following the initial FTIR analysis, the samples were extracted using methanol and dichloromethane (DCM). In each extraction, different classes of organic materials – methanol is utilized in the extraction of polar components such as lower fatty acids, alcohols, and most types of organic salts while dichloromethane is used to extract relatively nonpolar components such as higher fatty acids and carbonyl compounds - were expected to be recorded according to their solubility in the two solvents (Koupadi, et al., 2021, p. 3613). The spectra of the samples from each step of the solvent methodology were further refined and the baseline of the spectra of selected samples were corrected which can be seen both overlayed and stacked on graphs (Figs. 40-43).

The analytical group for the extraction methodology was refined to only include the A1 samples, A1S samples, B1 samples, and reference sample REF_E1. (Figs. 40-43);

these samples were selected based on the indications of organic materials present during the aforementioned unadulterated KBr analysis. The spectra of these samples are shown as *non-normalized* as they reflect the relative quantities of organics extracted from comparable amounts of powder samples with similar solvent volumes. In the stacked spectra- which is positioned as the lower spectra in each figure- specifically, the relative absorbances of each spectrum can be separately seen along the y-axis – which signifies absorbance- in different colors, thus providing a rough estimate of the relative quantities. Based on the consistent increase in absorbance observed, only the peaks from the final depositional event for all elution methods (2M) will be identified for all samples from this point on; it should be noted that the presence of sedimentary contamination in the 1200-500 cm^{-1} range also increased for all samples with the increase in depositional events which was to be expected.

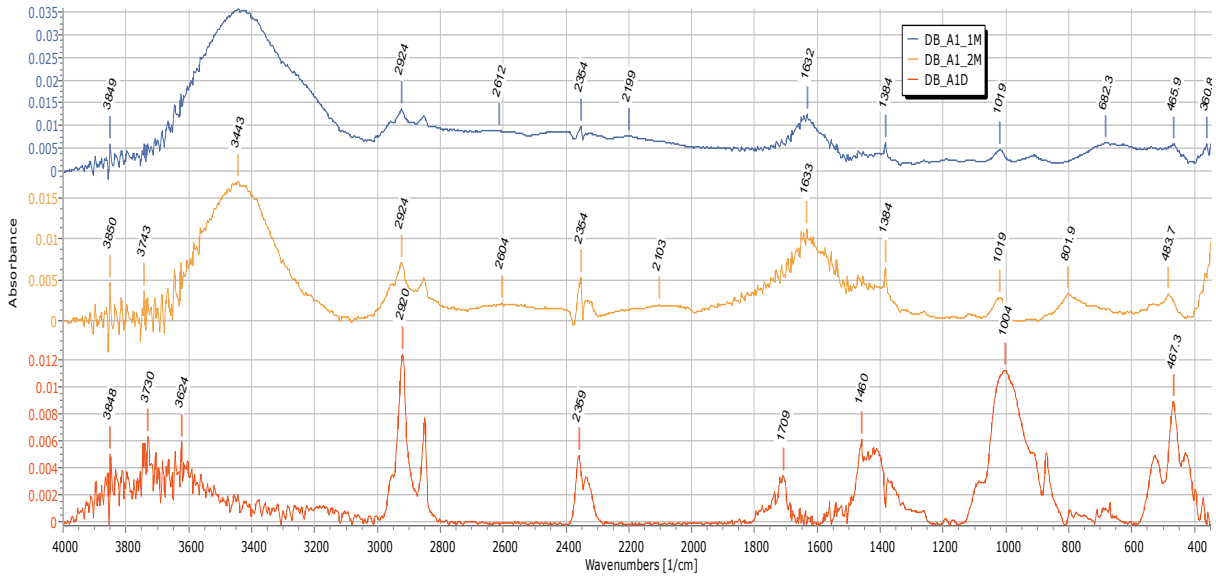

Figure 40: A1 Spectra. Spectra from the A1 sample using the first depositional methodology (1M), second depositional methodology (2M), and DCM methodology (D) on the KBr disc.

Based on the spectra (Fig. 40), the methanol extractions of sample A1- which was sampled from the rough side of the fragment- indicated the presence of organic materials. The spectra show peaks with maxima at 2924 cm^{-1}($v_{as}CH_2$), 2854 cm^{-1} (v_sCH_2), 1580 cm^{-1} ($v_{as}COO^-$), and 1409 cm^{-1} (v_sCOO^-) which may be indicative of an organic salt; this could be in the form of a carboxylate or the reaction product of a carboxylic acid with a metal ion (most likely calcium, magnesium, or iron of geogenic or other origins) in a basic environment (Koupadi, et al., 2021, p. 3618). In addition, low traces of inorganic material present at ~1020 cm^{-1} (vSi–O) and 1384 cm^{-1} (a biomarker of activity from nitrifying bacteria), can also be detected (Shillito, et al., 2009, p. 123); (Volkov, et al., 2021, pp. 6-11).

In addition, a clear indication of organic material was investigated in spectra recorded from the DCM extract for the A1 sample. Peaks with a maxima at 2920 cm^{-1} ($v_{as}CH_2$), 2857 cm^{-1} (v_sCH_2), 1709 cm^{-1} (acidic vC=O), and 1460 cm^{-1} (δC-H) were observed; this could possibly correspond with an organic acid (Filopoulou, et al., 2021, p. 4). Similarly to the methanol spectra, additional inorganic peaks with a maxima at 1004 cm^{-1}, 527 cm^{-1}, and 467 cm^{-1} corresponding to clay mineral silicates were observed (Shillito, et al., 2009, p. 123). Additionally, ~1430 cm^{-1}, 871 cm^{-1}, and 710 cm^{-1} peaks are commonly associated with calcite ($CaCO_3$) (Shillito, et al., 2009, p. 123).

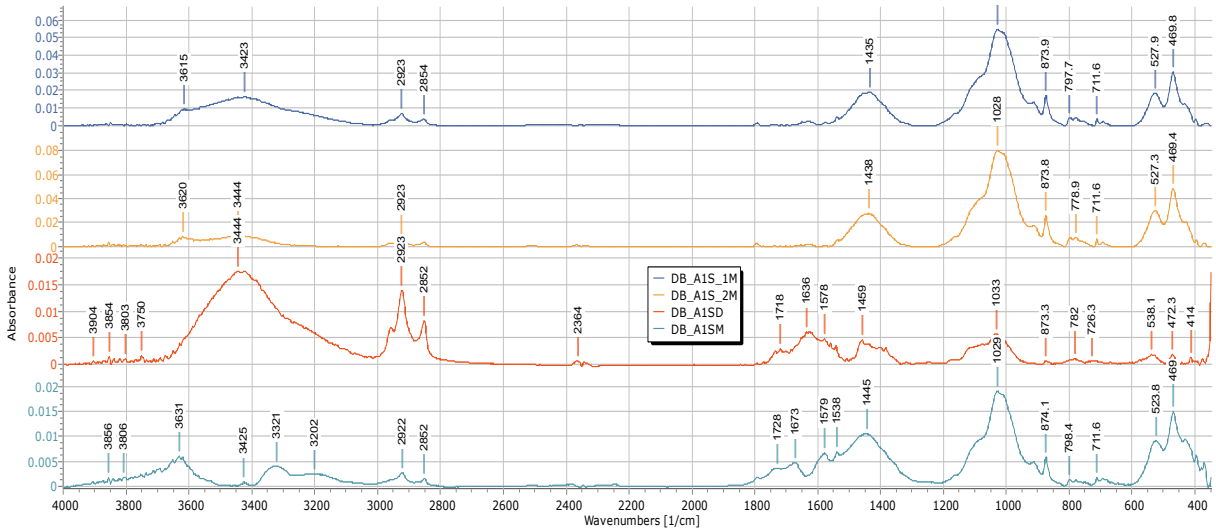

Figure 41: A1S Spectra. Spectra from the A1S sample using the first depositional event (M), second depositional event (1M), third depositional event (2M), and DCM methodology (D) on the KBr disc stacked on a graph.

Upon examination of the methanol extractions of sample A1S -which was sampled from the smooth side of the fragment- indicated the presence of organic materials. The spectra (Fig. 41) show peaks with maxima at 2923 cm^{-1} ($v_{as}CH_2$) which may be indicative of an organic salt; a small peak at 2852 cm^{-1} (v_sCH_2) can also be observed (Koupadi, et al., 2021, p. 3618). In addition, low traces of inorganic material present at ~1028 cm^{-1} ($_v$Si–O) and 1438 cm^{-1} ($CaCO_3$) can also be detected (Shillito, et al., 2009, p. 123); while a sharp peak at 3621 cm^{-1} is due to crystalline water.

Alternatively, a clear indication of organic material was investigated in spectra recorded from the DCM extract for the A1S sample. The spectra show peaks with maxima at 2923 cm^{-1} ($v_{as}CH_2$), 2852 cm^{-1} (v_sCH_2), 1718 cm^{-1} (acidic vC=O), and 1459 cm^{-1} (δC-H) which may be indicative of an organic acid (Filopoulou, et al., 2021, p. 4). Similarly to the methanol spectra, additional inorganic peaks with maxima at 1033 cm^{-1}, 538 cm^{-1}, and 472 cm^{-1} corresponding to clay mineral silicates were observed (Shillito, et al., 2009, p.

123); additionally, ~1459 cm^{-1}, 873 cm^{-1}, and 726 cm^{-1} peaks are commonly associated with calcite ($CaCO_3$) (Shillito, et al., 2009, p. 123) A broad band at 3444 cm^{-1} and a peak at 1625 cm^{-1} can be indicative of adsorbed water which could imply that the solvent did not fully evaporate before the spectrum was collected (Krivoshein, et al., 2020, p. 9); (Shillito, et al., 2009, p. 123).

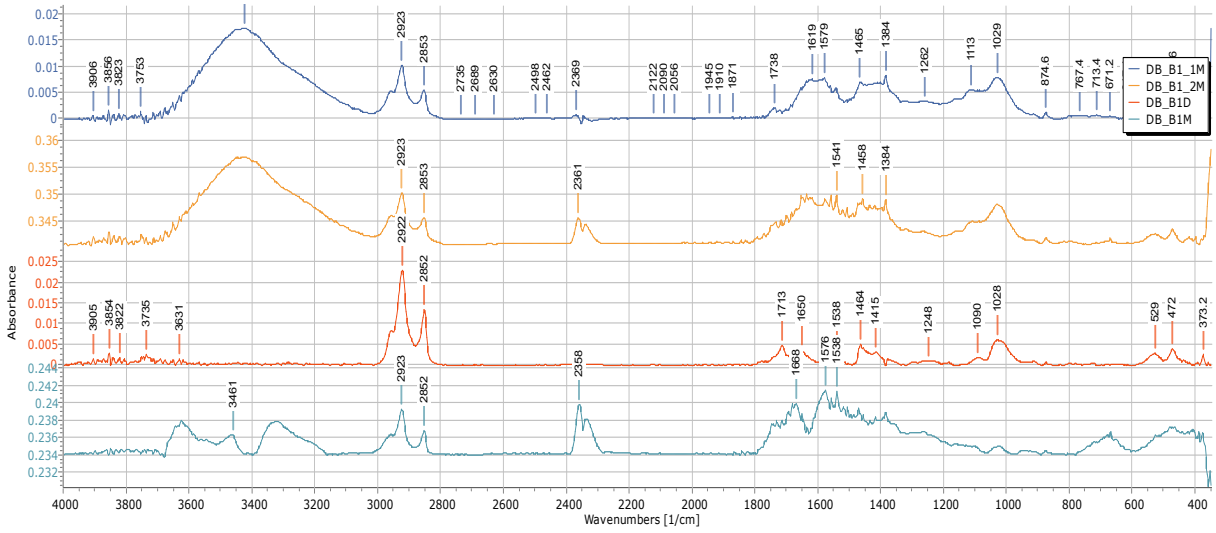

Figure 42: B1 Spectra. Spectra from the B1 sample using the first depositional event (M), second depositional event (1M), third depositional event (2M), and DCM methodology (D) on the KBr disc overlayed (upper) and stacked (lower) on a graph.

Based on the spectra, the methanol extractions of sample B1 indicated the presence of organic materials. The spectra (Fig. 42) show peaks with maxima at 2923 cm^{-1} ($_{vas}CH_2$), 2853 cm^{-1} (v_sCH_2), 1579 cm^{-1} ($v_{as}COO^-$), and 1384 cm^{-1} (v_sCOO^-) indicating an organic salt (Koupadi, et al., 2021, p. 3618); (Filopoulou, et al., 2021, p. 4). In addition, low traces of inorganic material present at ~1029 cm^{-1} can also be detected (Shillito, et al., 2009, p. 123).

Also, a clear indication of organic material was investigated in spectra recorded from the DCM extract for the B1 sample. Peaks with maxima at 2923 cm^{-1} ($v_{as}CH_2$), 2853 cm^{-1} (v_sCH_2), and 1458 cm^{-1} (δC-H) were observed; this could possibly correspond with an organic acid (Filopoulou, et al., 2021, p. 4). Similarly to the methanol spectra, additional inorganic peaks with maxima at 1028 cm^{-1}, 529 cm^{-1}, and 472 cm^{-1} corresponding to clay mineral silicates were observed (Shillito, et al., 2009, p. 123). A peak at 3631 cm^{-1} could be indicative of crystalline water (Shillito, et al., 2009, p. 123).

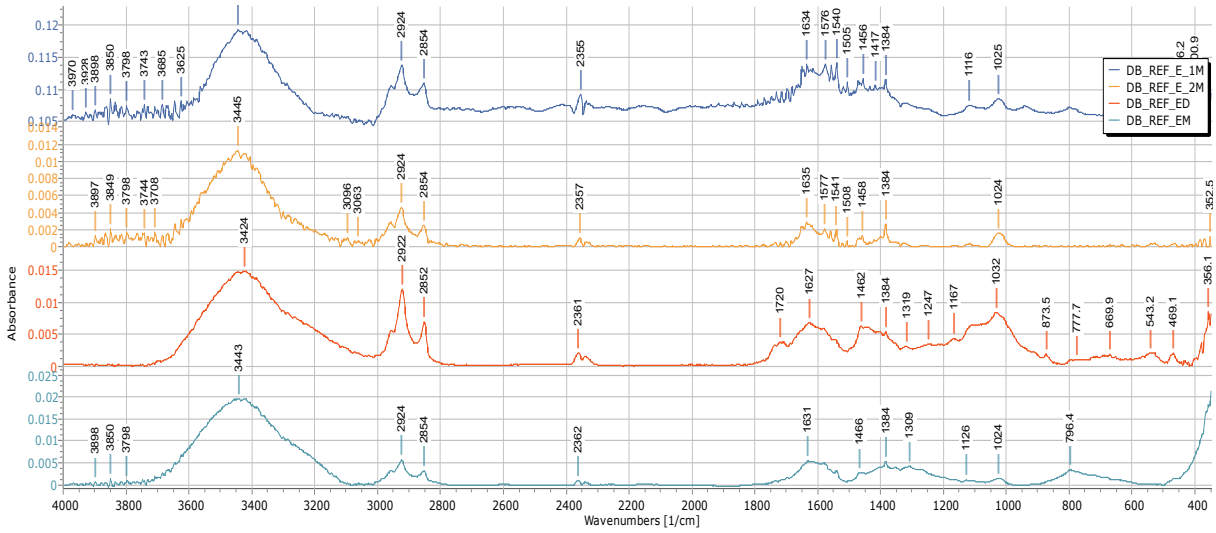

Figure 43: REF_E1 Spectra. Spectra from the REF_E1 sample using the first depositional event (M), second depositional event (1M), third depositional event (2M), and DCM methodology (D) on the KBr disc overlayed (upper) and stacked (lower) on a graph.

Based on the spectra, the methanol extractions of the reference, REF_E1, also indicated the presence of organic materials. The spectra (Fig. 43) show peaks with maxima at 2924 cm^{-1} ($v_{as}CH_2$) and 2854 cm^{-1} (v_sCH_2), indicative of an organic salt (Koupadi, et al.,

2021, p. 3618). In addition, low traces of silicate material present at ~1024 cm^{-1} can also be detected (Shillito, et al., 2009, p. 123); (Volkov, et al., 2021, pp. 6-11).

In addition, a clear indication of organic material was investigated in spectra recorded from the DCM extract for the REF_E1 sample. Peaks with a maxima at 2922 cm^{-1} ($\nu_{as}CH_2$), 2852 cm^{-1} (ν_sCH_2), and 1720 cm^{-1} ($\nu C{=}O$) were observed; this could possibly correspond with an organic ester (Filopoulou, et al., 2021, p. 4). Similarly to the methanol spectra, additional inorganic peaks with a maxima at 1032 cm^{-1}, 543 cm^{-1}, and 469 cm^{-1} corresponding to clay mineral silicates were observed (Shillito, et al., 2009, p. 123); additionally, ~1462 cm^{-1}, 873 cm^{-1}, and 777 cm^{-1} peaks are commonly associated with calcite ($CaCO_3$) (Shillito, et al., 2009, p. 123). A broad band at 3424 cm^{-1} and a peak at 1627 cm^{-1} can be indicative of absorbed or structural water which could imply that the solvent did not fully evaporate before the spectrum was collected (Krivoshein, et al., 2020, p. 9); (Shillito, et al., 2009, p. 123).

4.7 Refined FTIR

The FTIR methodology was modified and refined to optimize the results from the previous experiment. In order to standardize the methodology, each of the samples were weighed and separated into categories based on solvent; such standardization allowed for more consistent results across the different samples and between methodologies. The masses of the cut samples were recorded, and the identities of the samples were assigned (Table 12). Of the samples prepared, the analytical group was further refined to only include the A1 samples (Fig. 44-46), B1 samples (Fig. 47-49), and reference samples

REF_D1 & REF_E1 (Fig. 50-55). These samples underwent extraction using CHCl3+MeOH DCM, and MeOH. In each extraction, different classes of organic materials were expected to be recorded according to their solubility in the three solvents (Koupadi, et al., 2021, p. 3613). Unlike the previously mentioned solvents, methanol and chloroform are used in conjunction to form a monophasic solvent system to extract and dissolve lipids – such as carbonyl compounds and fatty acids (McGovern, et al., 2017, p. 2). As mentioned previously (4.6), the extractions were recorded on a Si wafer. The spectra of the samples from each step of the solvent methodology were further refined and the baseline of the spectra of selected samples were corrected which can be seen both individually and overlayed on graphs (Figs. 44-55).

Table 8: Mass and identity of the different samples. The masses of the samples are given in grams (g).

Sample	Classification	Mass (g)
A1S	A1S_D	0.0507
	A1S_M	0.0506
	A1S_X	0.0505
A1R	A1R_D	0.0501
	A1R_M	0.0509
	A1R_X	0.0508
B1S	B1S_D	0.0507
	B1S_M	0.0506
	B1S_X	0.0505
B1R	B1R_D	0.0506
	B1R_M	0.0509
	B1R_X	0.0508
B3	B3_D	0.0505
	B3_M	0.0502
	B3_X	0.0503
B4	B4_D	0.0508
	B4_M	0.0501
	B4_X	0.0504

B6	B6_D	0.0508
	B6_M	0.0508
	B6_X	0.0501
B7	B7_D	0.0506
	B7_M	0.0509
	B7_X	0.0500
C3	C3_D	0.0505
	C3_M	0.0501
	C3_X	0.0508
E1	E1_D	0.0508
	E1_M	0.0500
	E1_X	0.0508

Based on the consistent increase in absorbance observed, only the peaks from the final depositional event for all elution methods will be identified for all samples from this point on; it should be noted that the presence of sedimentary contamination in the 1200-500 cm^{-1} range also increased for all samples with the increase in depositional events which was to be expected.

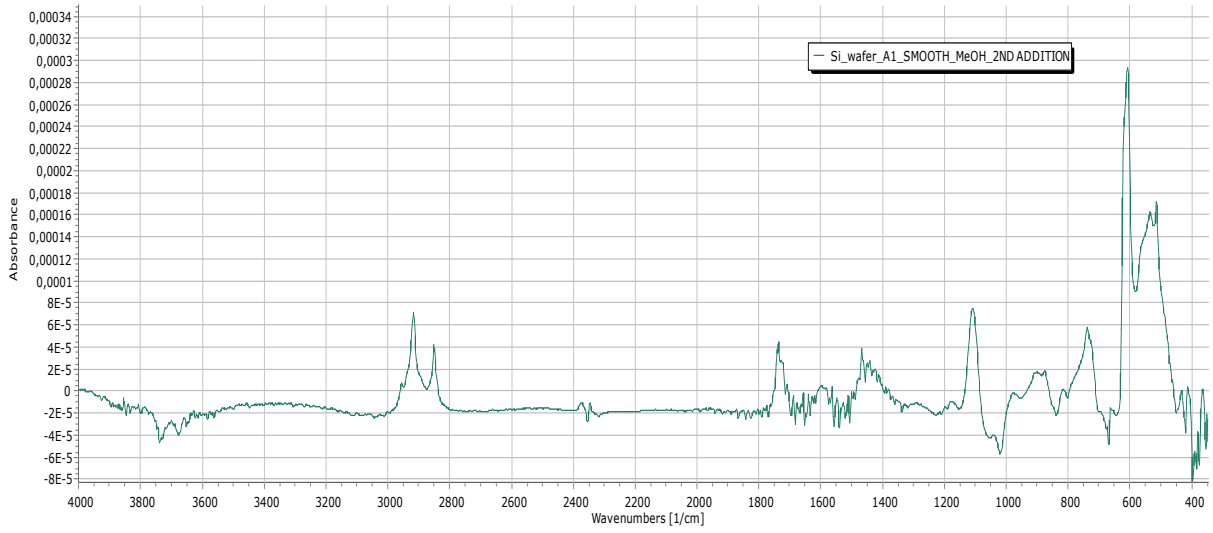

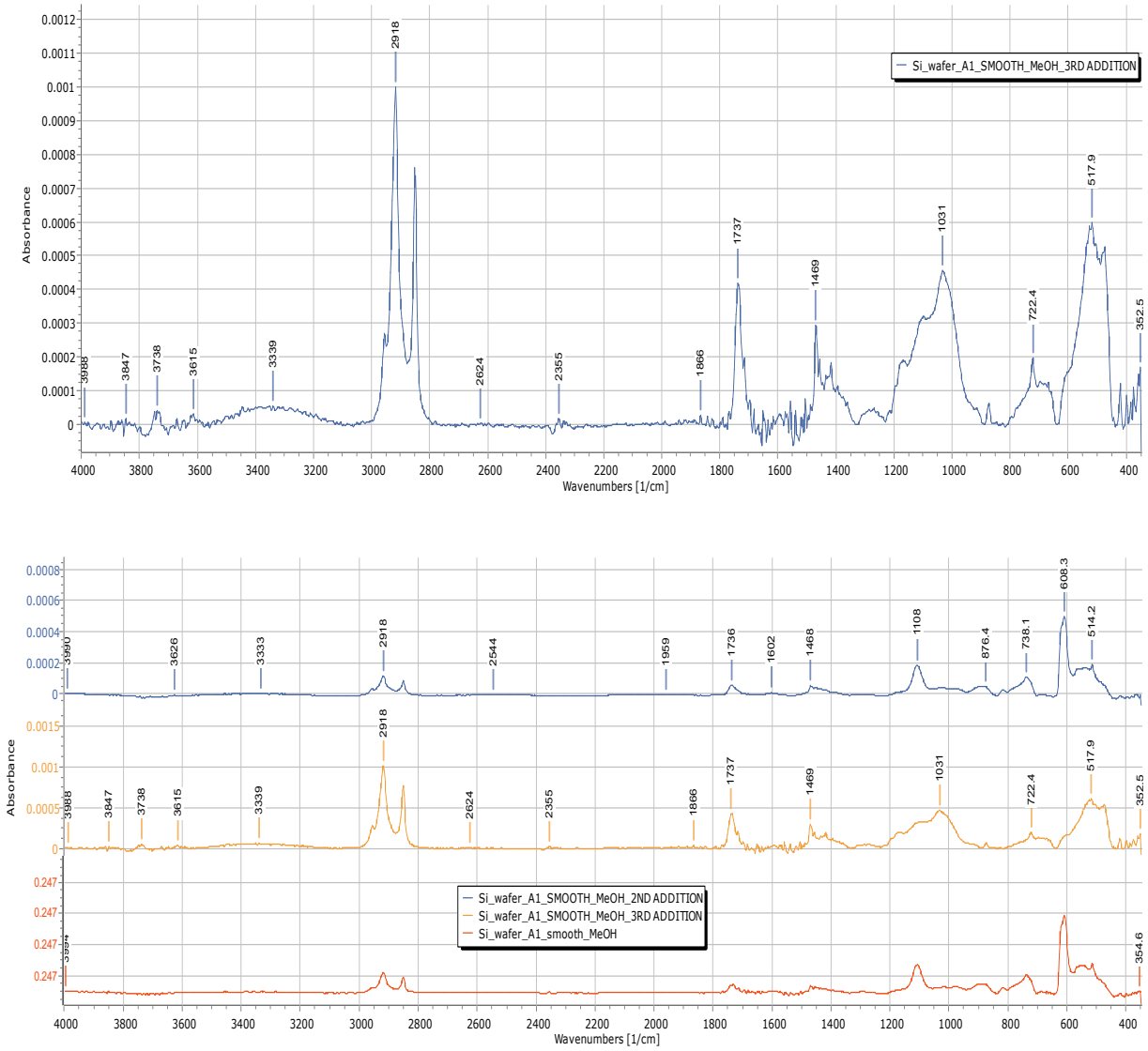

Figure 44: A1 MeOH Spectra. Spectra from the Si_wafer_A1 samples in MeOH from the first depositional event (MeOH), the second deposition event (MeOH_2ND ADDITION), and the third deposition event (MeOH_3RD ADDITION).

Based on the spectra, the methanol extractions of sample A1 indicated the presence of organic materials. The spectra (Fig. 44) show two peaks with maxima at 2918 cm^{-1} ($v_{as}CH2$) and ~2853 cm^{-1} (v_sCH_2) (Koupadi, et al., 2021, p. 3618); (Filopoulou, et al., 2021, p. 4). The strong peak at 1737 cm^{-1} ($_vC=O$) is assumed to be associated with ester C=O stretching which is indicative of the presence of fatty substances (Filopoulou, et al., 2021,

p. 4). A broad band at 3339 cm^{-1} ($_{v}OH$) could be indicative of adsorbed water or a carboxyl group in a free fatty acid as this region is associated with O-H stretching from hydrogen-boding (Krivoshein, et al., 2020, p. 9). Clay mineral peaks associated with silicates at 1030 cm^{-1} & 518 cm^{-1} and calcium carbonate at 722 cm^{-1} can also be observed (Shillito, et al., 2009, p. 123). The peak at 1469 cm^{-1} may be associated with calcium carbonate ($CaCO_3$) or with CH_2 vibrations in the organic fraction (Hermans & Helwig, 2022, pp. 1-2); (Shillito, et al., 2009, p. 123).

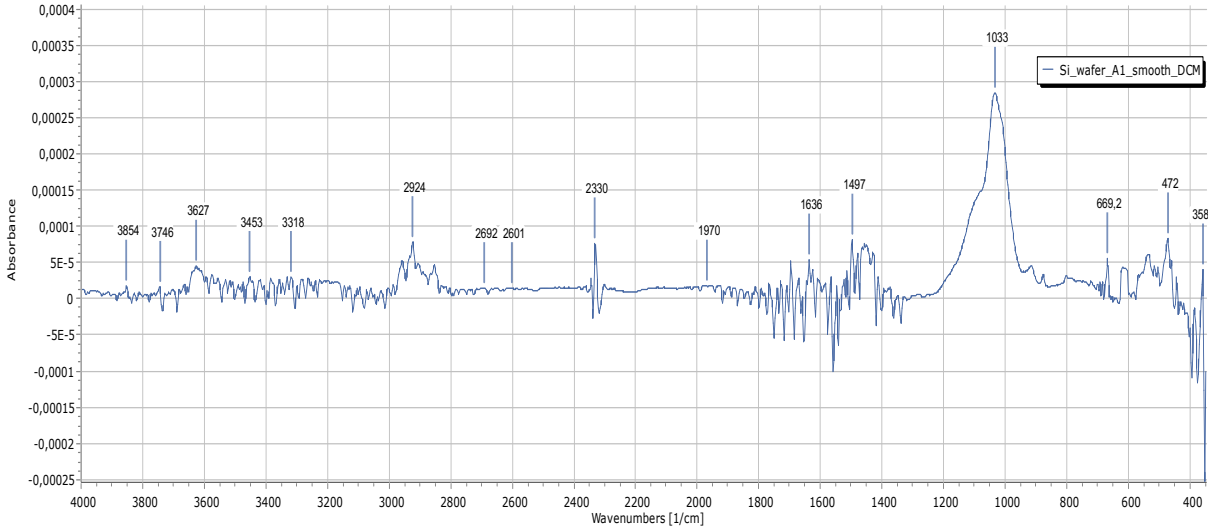

Figure 45: A1 DCM Spectra. Spectra from the Si_wafer_A1 sample in DCM.

In addition, the DCM spectrum of A1 also indicates the presence of organics. The spectra (Fig. 45) show peaks with a maxima at 2924 cm^{-1} ($v_{as}CH_2$), ~2862 cm^{-1} ($v_{s}CH_2$), and 1636 cm^{-1} ($_{v}OH$) were observed which could correspond with an organic salt (Filopoulou, et al., 2021, p. 4); (Hermans & Helwig, 2022, p. 6). Possible progression bands from 1350-1200 cm^{-1} ($_{\tau}CH_2$) are also observed (Hermans & Helwig, 2022, pp. 1-2); (Filopoulou, et al., 2021, p. 4). Similarly to the methanol spectra, additional inorganic peaks with a maxima at 1004 cm^{-1}, 527 cm^{-1}, and 467 cm^{-1} corresponding to clay mineral

silicates were observed (Shillito, et al., 2009, p. 123); additionally, peaks at 1497 cm^{-1}, 871 cm^{-1}, and 710 cm^{-1} are commonly associated with calcite ($CaCO_3$) (Shillito, et al., 2009, p. 123).

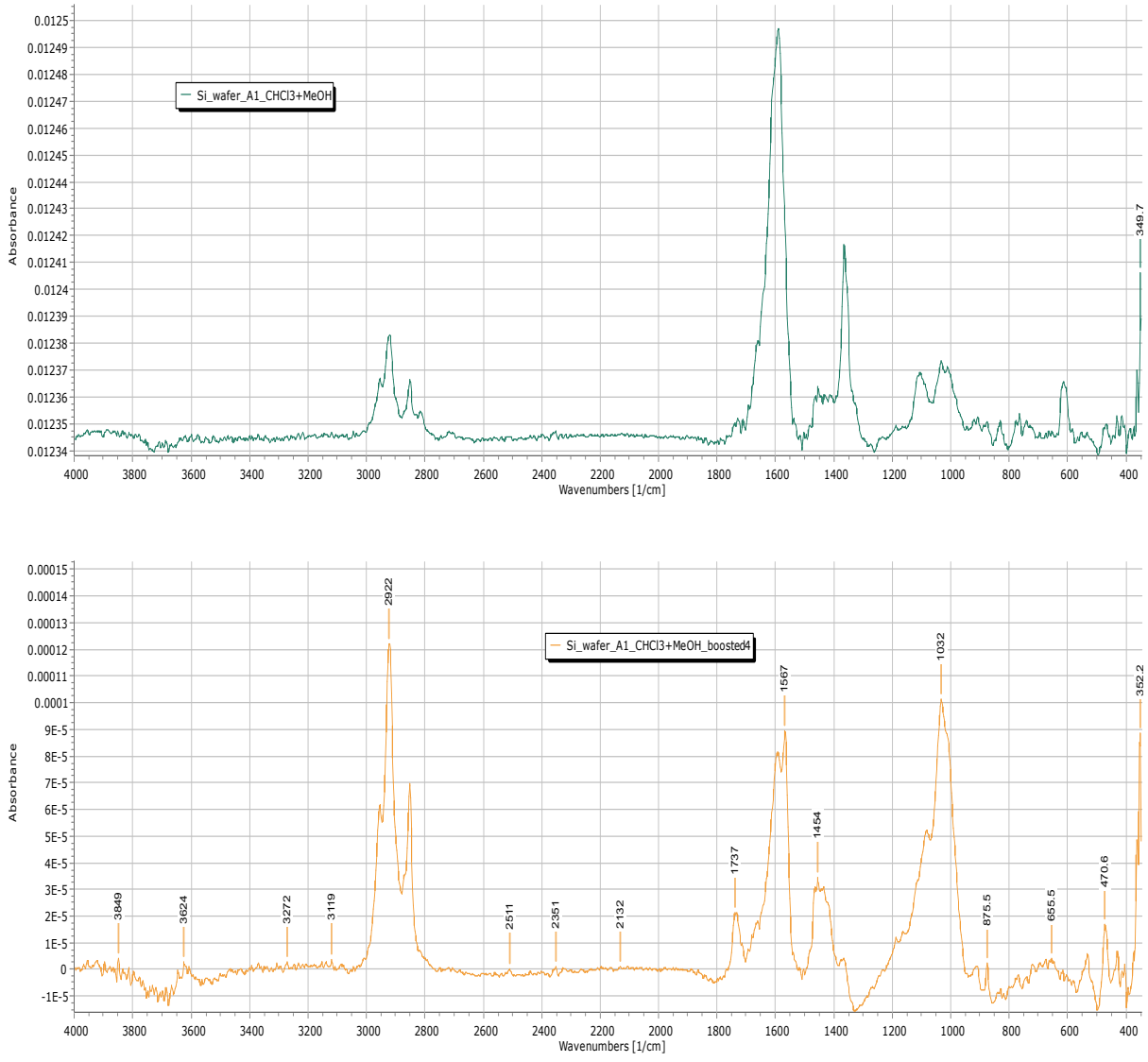

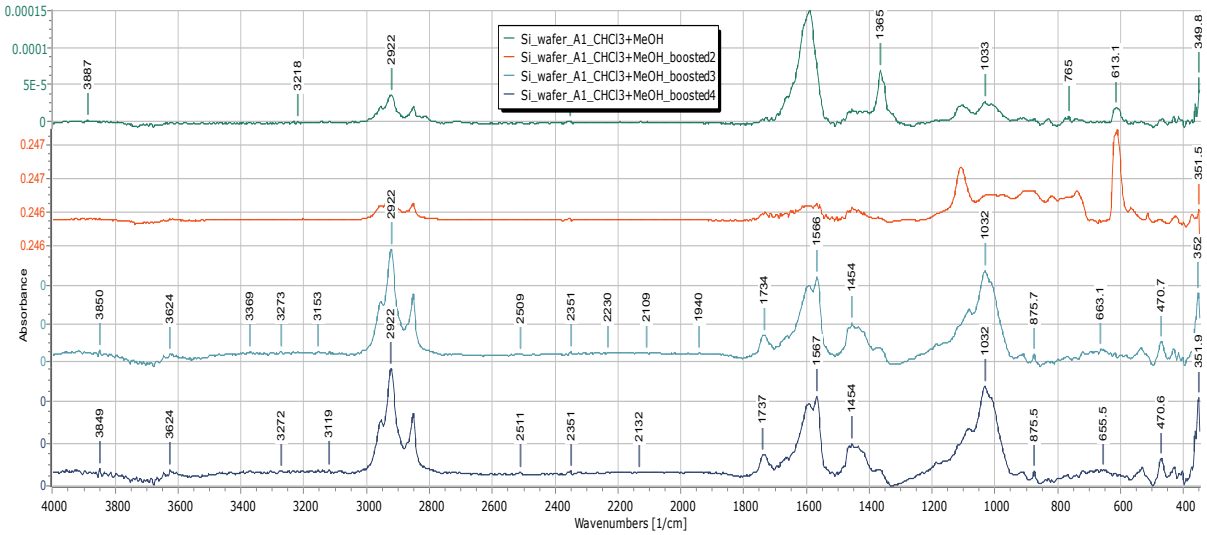

Figure 46: A1 $CHCl_3$+MeOH Spectra. Spectra from the Si_wafer_A1 samples in $CHCl_3$+MeOH from the first depositional event ($CHCl_3$+MeOH), the second deposition event ($CHCl_3$+MeOH_boosted2), the third deposition event ($CHCl_3$+MeOH_boosted3), and the fourth depositional event ($CHCl_3$+MeOH_boosted4).

In addition to the methanol and DCM extractions, sample A1 underwent extraction using chloroform-methanol ($CHCl_3$+MeOH). The spectra (Fig. 46) show peaks with maxima at 2918 cm^{-1} ($\nu_{as}CH_2$), and ~2864 cm^{-1} (ν_sCH_2). Strong peaks indicate fatty esters, at 1738 cm^{-1} ($_\nu C{=}O$); this is further supported by the presence of a main ester peak, 1922 cm^{-1}, and a shoulder peak of the salt at 1917 cm^{-1} (Volkov, et al., 2021, pp. 6-11). A double peak at 1597 cm^{-1} and 1567 cm^{-1} ($\nu_{as}COO^-$) which is indicative of carboxylate ion can also be observed (Koupadi, et al., 2021, p. 3618); (Filopoulou, et al., 2021, p. 4). This is further supported by a peak at 1378 cm^{-1} (ν_sCOO^-) which is related to the carboxylate ion symmetric stretch (Filopoulou, et al., 2021, p. 10). Similarly to the methanol spectra, inorganic peaks with a maxima at 1032 cm^{-1}, 537 cm^{-1}, and 470 cm^{-1} corresponding to clay mineral silicates were observed (Shillito, et al., 2009, p. 123); additionally, peaks at ~1430 cm^{-1} and 875 cm^{-1} are commonly associated with calcite ($CaCO_3$) (Shillito, et al., 2009, p. 123).

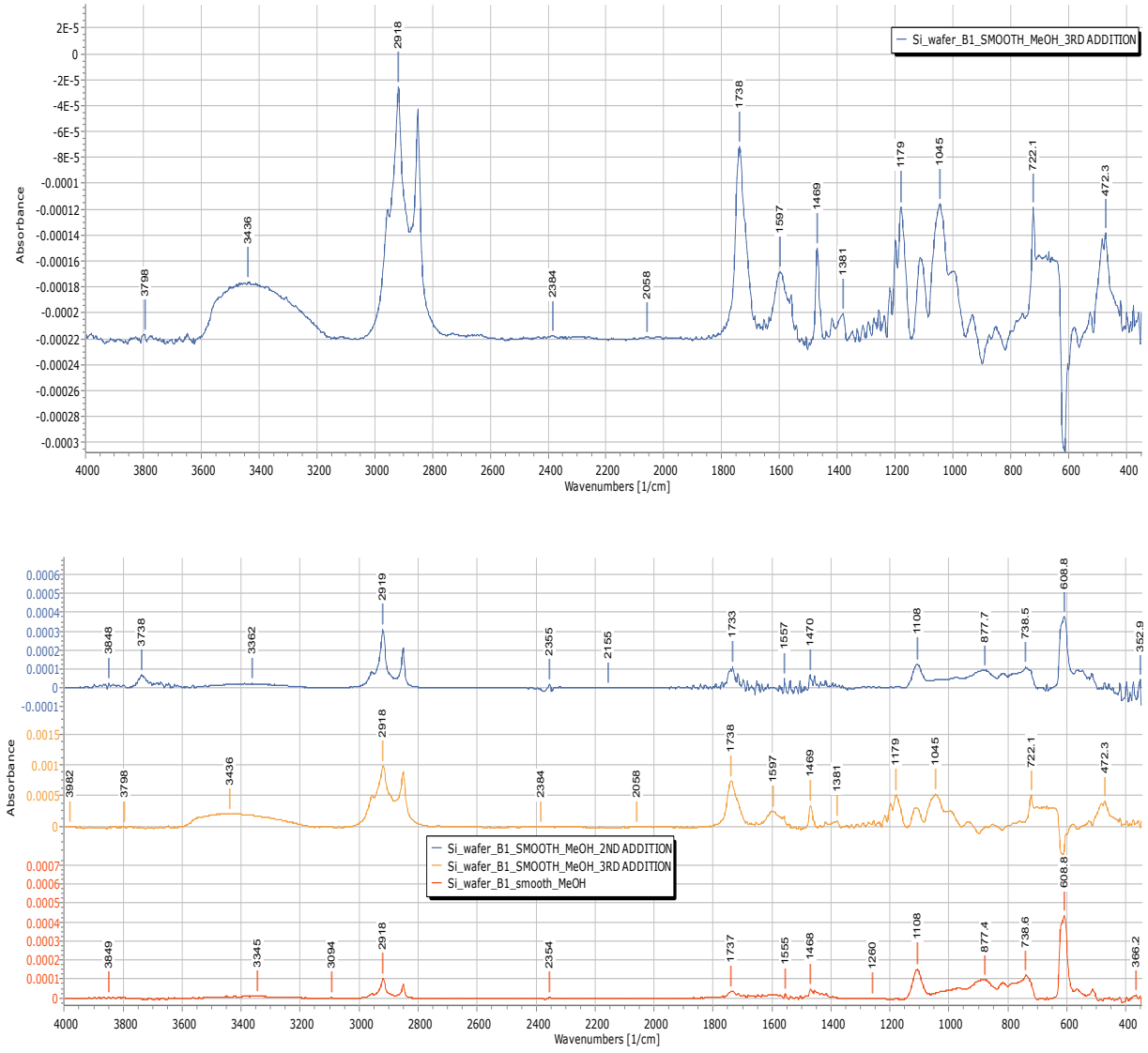

Figure 47: B1 MeOH Spectra. Spectra from the Si_wafer_B1 samples in MeOH from the first depositional event (MeOH), the second deposition event (MeOH_2nd ADDITION), and the third deposition event (MeOH_3rd ADDITION).

Based on the spectra, the methanol extractions of sample B1 indicated the presence of organic materials. The spectra (Fig. 47) show peaks with maxima at 2918 cm^{-1} ($v_{as}CH_2$), ~2864 cm^{-1} (v_sCH_2), and 1738 cm^{-1} (vC=O) which are indicative of an ester; this is further supported by an ester triad at 1179 cm^{-1}, 1100 cm^{-1}, and 1045 cm^{-1} (vC-O) (Koupadi, et al., 2021, p. 3618); (Filopoulou, et al., 2021, p. 4). It should be noted that spectra show a

baseline over-correction in the 1200-1000 region which has influenced the appearance of the peaks. In addition, carboxylate ions can be observed at 1597 cm^{-1} ($v_{as}COO^-$) and 1381 cm^{-1} (v_sCOO^-) (Koupadi, et al., 2021, p. 3618); (Filopoulou, et al., 2021, p. 4). A possible progression band from 1350-1200 cm^{-1} ($_\tau CH_2$) can also be seen (Hermans & Helwig, 2022, pp. 1-2); (Filopoulou, et al., 2021, p. 4). A broad band at 3436 cm^{-1} ($_vOH$) could be indicative of adsorbed water or a carboxyl group in a free fatty acid (Krivoshein, et al., 2020, p. 9). In addition, low traces of inorganic material are present at ~1045 cm^{-1} and 472 cm^{-1} which indicate clay mineral silicates; additional peaks at 1429 cm^{-1} and 722 cm^{-1} (CaCO3), which correspond to calcite, can also be detected (Shillito, et al., 2009, p. 123).

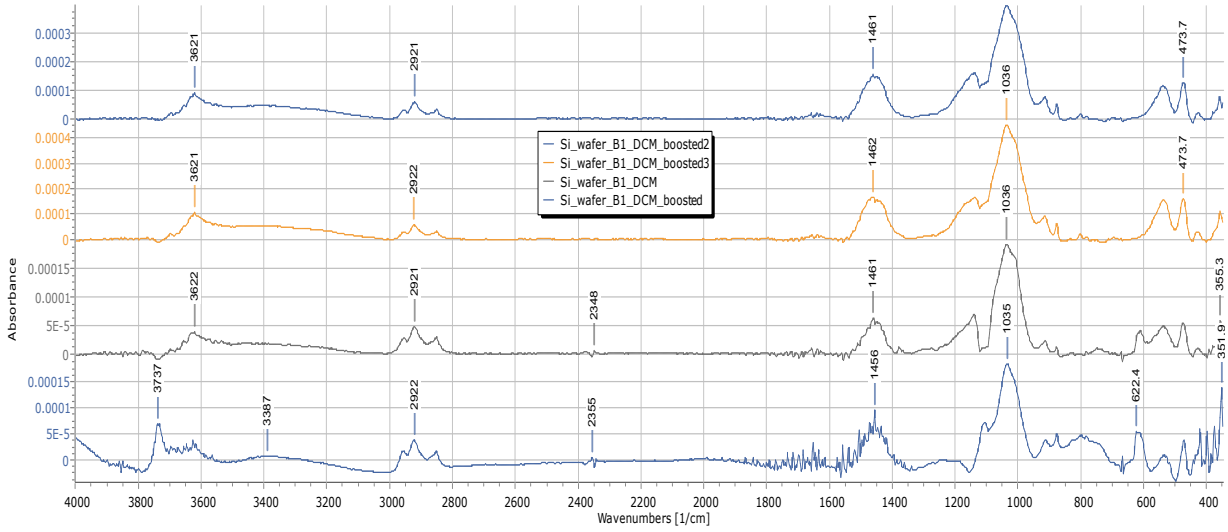

Figure 48: B1 DCM Spectra. Spectra from the Si_wafer_B1 samples in DCM from the first depositional event (DCM), the second deposition event (DCM_boosted), the third deposition event (DCM_boosted2), and the fourth depositional event (DCM_boosted3).

In addition, the DCM spectrum of B1 also indicates the presence of organics (Fig. 48). Peaks with a maxima at 2922 cm^{-1} ($v_{as}CH_2$), ~2857 cm^{-1} (v_sCH_2), and 1656 cm^{-1} ($_vOH$) were observed which could correspond to adsorbed water (Hermans & Helwig, 2022, p. 6). In addition, inorganic peaks with a maxima at 1036 cm^{-1}, ~535 cm^{-1}, and 473 cm^{-1}

corresponding to clay mineral silicates were observed (Shillito, et al., 2009, p. 123). Peaks at 1462 cm^{-1} and 876 cm^{-1} indicate calcium carbonate (CCO_3) (Shillito, et al., 2009, p. 123).

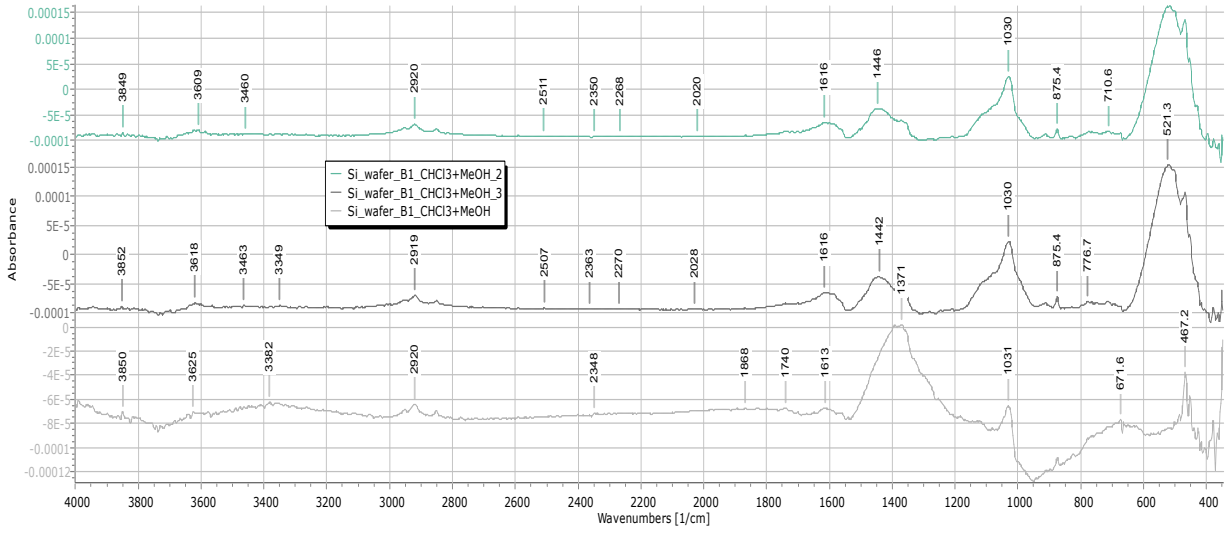

Figure 49: B1 $CHCl_3$+MeOH Spectra. Spectra from the Si_wafer_B1 samples in $CHCl_3$+MeOH from the first depositional event ($CHCl_3$+MeOH), the second deposition event ($CHCl_3$+MeOH_2), and the third deposition event ($CHCl_3$+MeOH_3).

In conjunction with the methanol and DCM extractions, sample B1 experienced extraction using chloroform-methanol ($CHCl_3$+MeOH). The spectra (Fig. 49) show peaks with maxima at 2919 cm^{-1} ($v_{as}CH_2$), 2868 cm^{-1} (v_sCH_2), and 1616 cm^{-1} ($_v$OH) which may be indicative of traces of an organic salt (Koupadi, et al., 2021, p. 3618); (Hermans & Helwig, 2022, p. 6). Similarly to the other spectra, inorganic peaks with a maxima at 1030 cm^{-1} and 521 cm^{-1} corresponding to clay mineral silicates were observed (Shillito, et al., 2009, p. 123); additionally, peaks at 1497 cm^{-1}, 875 cm^{-1}, and 776 cm^{-1} are commonly associated with calcite ($CaCO_3$) (Shillito, et al., 2009, p. 123).

Figure 50: REF_D1 MeOH Spectra. Spectra from the Si_wafer_REF_D1 samples in MeOH from the first depositional event (MeOH), the second deposition event (MeOH_2nd ADDITION), and the third deposition event (MeOH_3rd ADDITION).

Based on the spectra, the methanol extractions of sample REF_D1 also indicated the presence of organic materials. The spectra (Fig. 50) show peaks with maxima at 2918 cm^{-1} ($\nu_{as}CH_2$), ~2862 cm^{-1} ($\nu_{s}CH_2$), and 1737 cm^{-1} ($_{\nu}C{=}O$) which may be indicative of the presence of an ester (Koupadi, et al., 2021, p. 3618); (Filopoulou, et al., 2021, p. 4). In

addition, low traces of inorganic material present at 1468 cm^{-1}, 1032 cm^{-1}, and 772 cm^{-1} can be detected (Shillito, et al., 2009, p. 123).

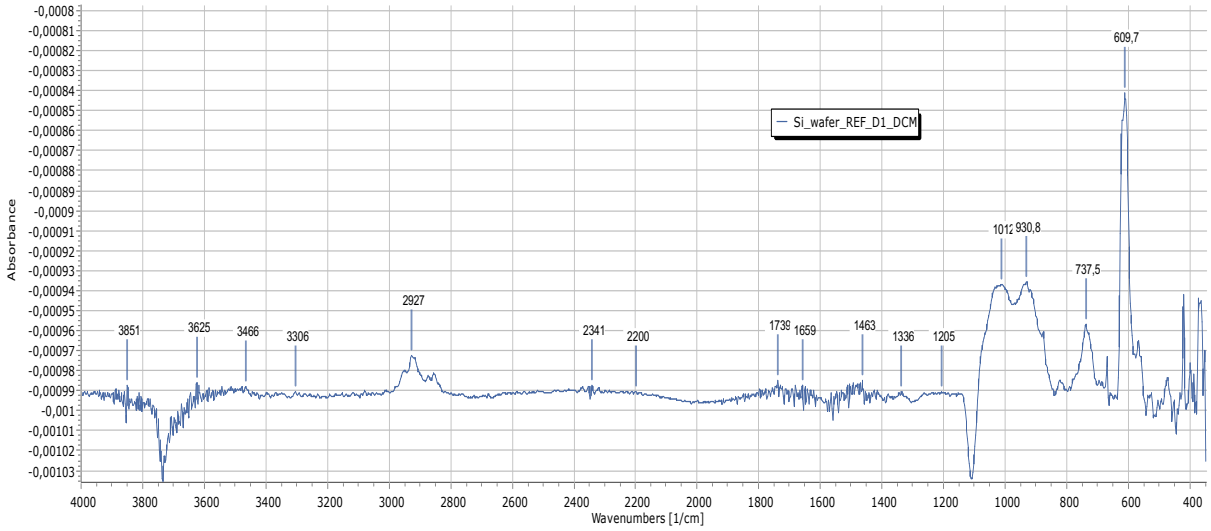

Figure 51: REF_D1 DCM Spectra. Spectra from the Si_wafer_REF_D1 sample in DCM.

In addition, the DCM spectrum of REF_D1 does not indicate organic materials. The spectra (Fig. 51) show peaks with a maxima at 2927 cm^{-1} ($v_{as}CH_2$) and ~2872 cm^{-1} (v_sCH_2) were observed (Filopoulou, et al., 2021, p. 4); (Hermans & Helwig, 2022, p. 6). Similarly to the methanol spectra, additional inorganic peaks with a maxima at 1012 $cm^{-1}$and 930 cm^{-1} corresponding to clay mineral silicates were observed (Shillito, et al., 2009, p. 123); additionally, peaks at 1463 cm^{-1} and 735 cm^{-1} are commonly associated with calcite ($CaCO_3$) (Shillito, et al., 2009, p. 123). The spectrum shows two negative peaks at 3700 cm^{-1} and 1100 cm^{-1} are a result of the subtraction of the blank area from the background of the spectrum.

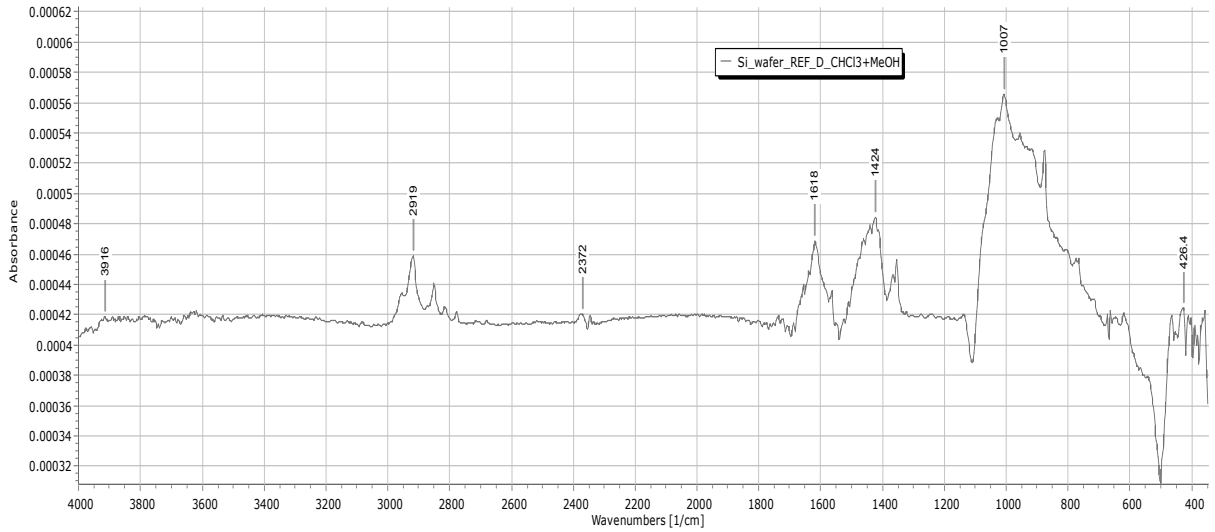

Figure 52: REF_D1 $CHCl_3$+MeOH Spectra. Spectra from the Si_wafer_REF_D1 sample in $CHCl_3$+MeOH.

In order to supplement the methanol and DCM extractions, sample REF_D1 underwent extraction using chloroform-methanol ($CHCl_3$+MeOH). The spectra (Fig. 52) show peaks with maxima at 2919 cm^{-1} ($\nu_{as}CH_2$), ~2876 cm^{-1} (ν_sCH_2), and 1618 cm^{-1} ($_\nu$OH) which may be indicative of a crystalized organic salt (Koupadi, et al., 2021, p. 3618); (Hermans & Helwig, 2022, p. 6). Also, inorganic peaks with a maxima at 1424 cm^{-1}, 1007 cm^{-1}, and 425 cm^{-1} corresponding to clay mineral silicates were observed (Shillito, et al., 2009, p. 123).

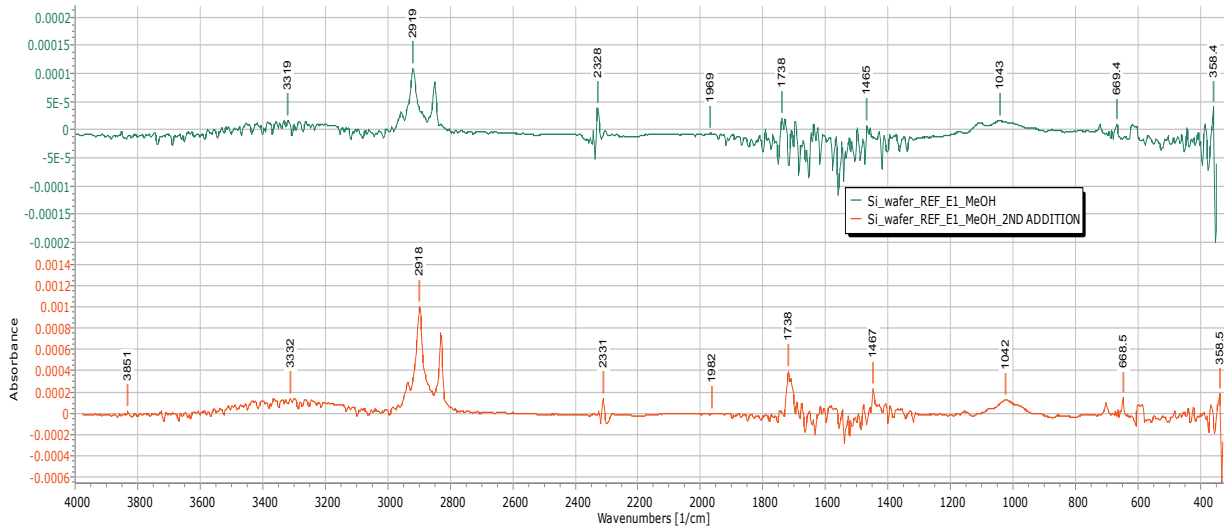

Figure 53: REF_E1 MeOH Spectra. Spectra from the Si_wafer_REF_E1 samples in MeOH from the first depositional event (MeOH) and the second deposition event (MeOH_2ND ADDITION).

Based on the spectra, the methanol extractions of sample REF_E1 indicated the presence of possible organic materials. The spectra (Fig. 53) show peaks with maxima at 2918 cm^{-1} ($\nu_{as}CH_2$), ~2862 cm^{-1} (ν_sCH_2), and 1738 cm^{-1} ($_\nu C{=}O$) which may be indicative of an organic salt (Koupadi, et al., 2021, p. 3618); (Filopoulou, et al., 2021, p. 4). In addition, low traces of inorganic material present at 1467 cm^{-1} and 1042 cm^{-1} can also be detected (Shillito, et al., 2009, p. 123).

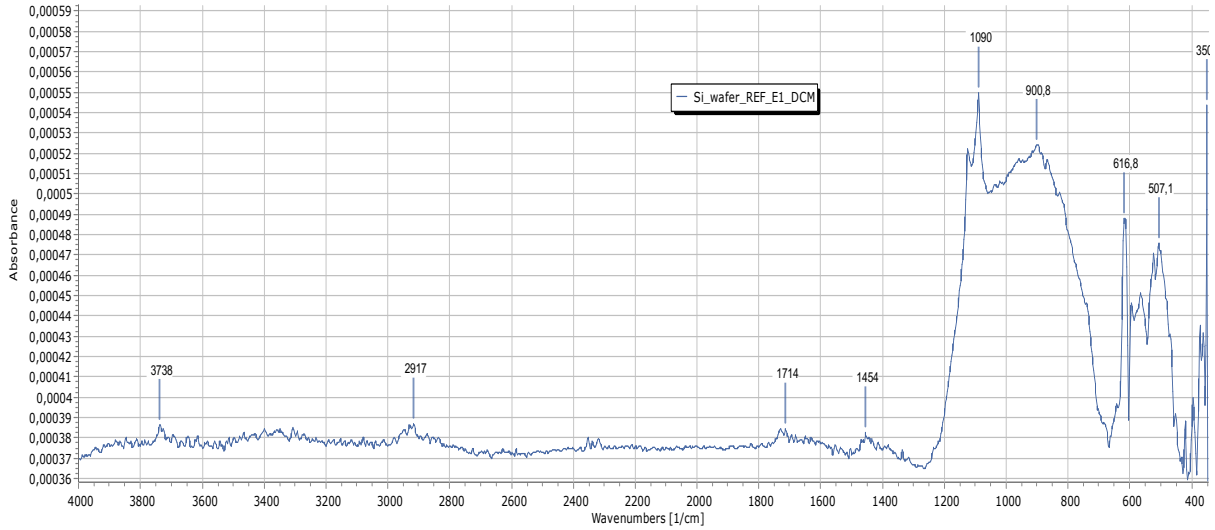

Figure 54: REF_E1 DCM Spectra. Spectra from the Si_wafer_REF_E1 sample in DCM.

However, the DCM spectrum of REF_E1 does not indicate the presence of organics. The spectra (Fig. 54) show inorganic peaks with a maxima at 1090 cm^{-1} and 507 cm^{-1} corresponding to clay mineral silicates were observed (Shillito, et al., 2009, p. 123). In addition, major peaks at 900 cm^{-1} and 616 cm^{-1} are indicative of calcium carbonate (CCO_3) (Shillito, et al., 2009, p. 123).

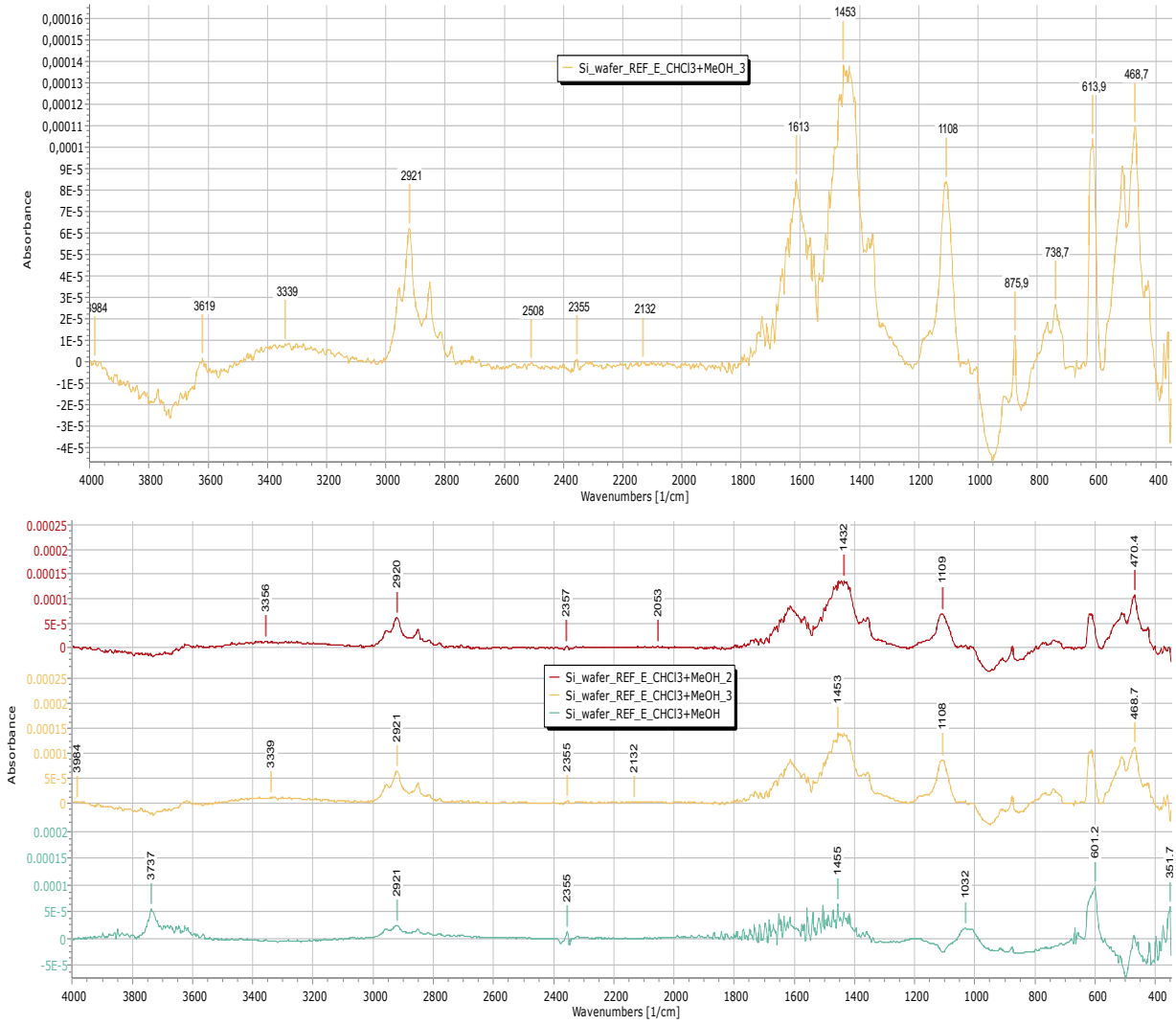

Figure 55: REF_E1 $CHCl_3$+MeOH Spectra. Spectra from the Si_wafer_REF_E1 samples in $CHCl_3$+MeOH from the first depositional event ($CHCl_3$+MeOH), the second deposition event ($CHCl_3$+MeOH_2), and the third deposition event ($CHCl_3$+MeOH_3).

In addition to the methanol and DCM extractions, sample REF_E1 underwent extraction using chloroform-methanol ($CHCl_3$+MeOH). The spectra (Fig. 55) show peaks with maxima at 2921 cm^{-1} ($\nu_{as}CH_2$), ~2882 cm^{-1} (ν_sCH_2), and 1613 cm^{-1} ($_\nu$OH) which may be indicative of an organic salt (Koupadi, et al., 2021, p. 3618); (Hermans & Helwig, 2022, p. 6). Also, inorganic peaks with a maxima at 1108 cm^{-1} and 468 cm^{-1} corresponding to clay mineral silicates were observed (Shillito, et al., 2009, p. 123). The peaks at ~1434 cm^{-}

^{1}, 874 cm^{-1}, and 738 cm^{-1} are commonly associated with calcite ($CaCO_3$) (Shillito, et al., 2009, p. 123).

Chapter 6. Discussion

6.1 Documentation & Classification

The majority of samples were selected based on their size and visible surface texture. It is assumed that the smooth parts of the fragments are due to a position pressed against the wall of the vessel which resulted in a characteristically flat surface (McGovern & Hall, 2015, p. 594). Samples that lacked this smooth surface are considered to be from the interior of the vessel without contact with the vessel walls. During photo documentation, it was determined that each of the samples had a "smooth side" and a "rough side" (Fig. 35). In many cases, a sample has the same characteristic surface texture on both sides in which case the side that fit the designation "smooth" the most was selected. Thus, each sample was assigned a smooth or rough side for analysis (Appendix B).

Through visual examination and documentation, the sample fragments were rudimentarily classified by their characteristics. As the majority of the samples were selected for their smooth or flat surface, this was the primary characteristic for classification. On the flat side of the sample, referred to as the smooth side hereto forth, the curvature and angle of the surface were analyzed; samples were considered concave, convex, flat, or, if no smooth surface was identified, friable. The concave fragments had a smooth side that curved inward around the vessel's angles like that of where the neck connects to the body (Fig. 56). The convex fragments had a smooth side that curved outward around the vessel's angles like that of the rounded body (Fig. 57). The flat fragments displayed no visible curvature despite their smooth surfaces. The friable surfaces had no smooth surfaces but instead consisted of slightly crumbly soil clusters.

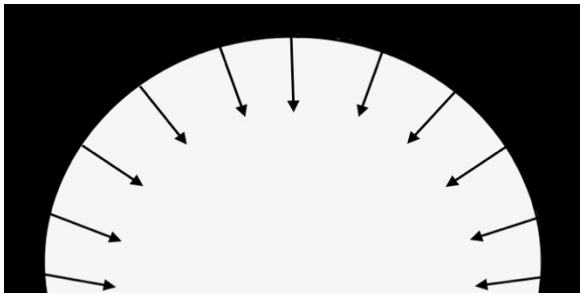

Figure 56: Soil Fragment Curvature. Example of Concave inward curve in which the white is the vessel and the black is the soil.

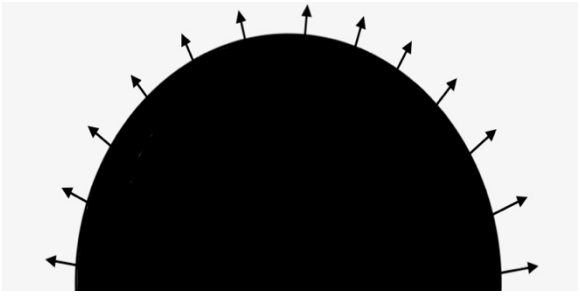

Figure 57: Soil Fragment Curvature. Example of convex outward curve in which the white is the vessel and the black is the soil.

Additional classification criteria included the visible particle size, texture, and color. The color was based on a rough visual analysis; although no visible differences in color were observed, this could be an indicator that the soil of the vessel came from one or more locations (Vranová, et al., 2015, pp. 1418-1419). The particle size was determined based on the visibility of large grains or clusters within the soil fabric and their resulting distribution throughout the samples. Based on the differences in particle size between the smooth and rough sides of the samples, the textures of the fragments were determined. As there were no extreme differences in particle size, texture, or color, it can be assumed that

the soil is from similar geographic layers although it is not yet possible to assess how many different events resulted in soil being added to the vessel (Goffer, 2007, pp. 210-219).

The visible analysis of the soil also supports the assumption that the vessel once contained liquid. This is supported by Stokes law which relates to the velocity at which particles settle through a liquid based on their diameter and the viscosity of the liquid. Based on this law, the largest particles settle out first and the smallest settle out last (Wesley, 2009, pp. 29-31). This can be observed in the soil fragments as the flat fragments assumed to be from the bottom of the vessel containing the largest particles. On the other hand, the fragments assumed to be from the neck of the vessel have a fine fabric which aligns with the fact that the smallest particles settle last in a suspension. There is little distribution of large particles throughout the soil fragments, assumed to be from the middle and upper positions, which could be indicative that the vessel was not moved once the soil was added. If the vessel had been moved or additional soil added after the liquid inside of the vessel dried, this would be evident in the distribution of larger particles throughout the fragments (Wesley, 2009, p. 30).

Based on these factors, fragments assumed to be from the bottom of the vessel were classified as Group A (Fig. 58). Fragments assumed to be from the upper section of the ceramic body were classified as Group B (Fig. 59). Fragments from the neck and lip were classified as Group C (Fig. 60); fragments whose position could not be determined were also included in this grouping. The shell fragments were separated from the main loose soil body and classified as Group D. The loose soil fragments and loose dirt were classified as

Group E. Upon reassessment, sample A4 should have been classified in Group B and sample B1 should have been classified in Group A[7].

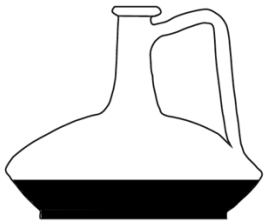

Figure 58: Soil Fragment Position. Visual representation of Group A's assumed location in the vessel.

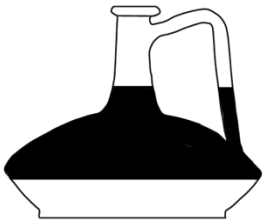

Figure 59: Soil Fragment Position. Visual representation of Group B's assumed location in the vessel.

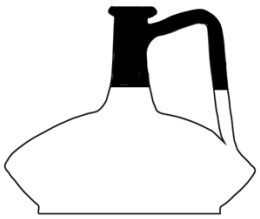

Figure 60: Soil Fragment Position. Visual representation of Group C's assumed location in the vessel.

6.2 LED

Using LED optical microscopy, the fabrics of the soil fragments were examined. Through magnification, it was possible to see the characteristics of the soil of the individual fragments. Based on this information and that of the rough classification, the sample group was refined to include the most representative samples from each grouping to create the Refined Analysis Group. This process was also performed on the Reference Group which were collected from different areas around the vessel's discovery site.

[7] The author acknowledges this correction but for the sake of clarity the samples A4 and B1 were not reclassified.

The colors of the soils were analyzed using the Munsell Color Chart. This was done in order to evaluate if the soil displayed variety in color from sample to sample. If the soil color was different, this might be an indicator against the initial assessment that the soil is from a single or similar geological layer (Vranová, et al., 2015, pp. 1418-1419). However, very little variation was observed using the Munsell classifications (Table 1). This was not the case for the reference samples (Table 2) which displayed a greater variety in coloring between the different soil fabrics which is supported by the fact that they were collected from different stratigraphic layers. Of the reference samples, REF_C1, REF_D1, and REF_E1 displayed the closest visual similarities to that of the Analysis Group.

The frequency, shape, and size of the inclusions of the samples were analyzed. This was done to determine the different components of the fabric in addition to the soil. The shapes of the inclusions were classified as granular, angular, and subangular. The sizes of the inclusions were considered fine to coarse and small to large (Edmonds, et al., 1998, p. 8). The fragments from the Refined Analysis Group displayed inclusions of consistently small sizes and relatively similar shapes (Table 1). Alternatively, the Reference Group had a variety of inclusion shapes and sizes (Table 2). This is to be expected as the fragments from the Refined Analysis Group have been compacted during the depositional process while the fragments of the Reference Group were taken directly from the soil bed.

The fragment's fabric was evaluated for coarseness and porosity (Edmonds, et al., 1998, p. 25). This was done in order to evaluate the morphology of the soils. The differences in coarseness and porosity of the sample and reference groups can also be attributed to their source materials as the fragments from the Reference Group were rough soil clumps and thus would not be expected to be fine. Alternatively, the fact that the

samples assumed to be from the bottom of the vessel have a higher coarseness and porosity than the samples assumed to be from the upper vessel is further supported by Stokes Law; this law asserts that the larger soil particles settle to the bottom of a container (Wesley, 2009, pp. 29-31). In addition, although most porous soil clusters can be considered crumbly, there are some which can be classified as compact and firm. This strong, porous structure is often a result of entrapped liquids during the compaction process (Wesley, 2009, p. 36). This is supported by samples A1 and B1 which are assumed to be from the bottom of the vessel as they are firm, tightly packed fragments with visible porosity (Table 1); these characteristics are not shared by any of the other fragments in the grouping. The other samples that display porosity are the coarse soil fragments of C3 and E1 (Table 1) and the coarse soil reference samples REF_A1, REF_B1, and REF_E1 (Table 2).

6.3 SEM

Having eliminated unsuitable samples which lacked smooth surfaces to create the Refined Analysis Group through the use of OM, SEM was performed on the new group. This was done in order to examine the surface topography, morphology, and microstructure of the samples at different magnifications. It should be noted that as the samples were in their rough and unpolished state, this resulted in limited flat, even spaces on the samples to take clear and focused images. As such, the majority of images were recorded from the smooth sides of the samples. Even though the sides of the samples are smooth, the images were recorded in Secondary Electron Imaging (SEI) mode due to the still rough and unpolished nature of the fragments.

An assumption is made that the smooth sides will have different characteristics than the rough sides due to their position against the vessel walls. This is supported by the differences in the soil fabric that can be observed on the rough and smooth sides of the samples from Group A (Table 3). The smooth side of A1 has a much flatter topography under magnification and there are fewer morphological features visible while the rough side of A1 has large clusters of morphological features and uneven topography. A similar observation was made for the smooth and rough sides of B1 which exhibit the same characteristics. Further confirmation for this assumption is given by EDS and FTIR analysis which will be discussed in later sections.

Based on the SEM images from the two samples from Group A and the three samples from Group B, there is a clear difference in the texture and porosity of the samples (Table 4). The samples from Group A have a more porous structure under 30x magnification and larger morphological features under 200x magnification. Group B's samples display a smoother surface structure under 30x magnification and 200x magnification. The smoothness of the topography of the Group B samples is supported by the fine texture of the samples observed with optical microscopy (Table 1). Overall, the SEM images indicate that the samples from Group A have a notable dissimilarity in topography and morphology to that of Group B. This further support's the classification of the Group A samples as lower vessel soil fragments as previously determined based on sedimentary particle distribution (Wesley, 2009, pp. 29-31). Although the Reference Group was analyzed using the SEM, the results were considered inconclusive as the samples contained loose soil which did not allow for the same standard of comparison as that of the Reference Group.

6.4 EDS

EDS analysis locations were determined on both the smooth and rough sides of these smooth spaces indicated in the SEM images. As the samples were in their raw, unpolished state as previously mentioned, this limited the number of observation locations for the rough sides of the samples as the sample sites were selected to correspond to the SEM locations; as such, only the elemental compositions of these locations were recorded. Thus, the majority of spectra recorded were taken from the smooth sides of the samples. It should be noted that through examination of the SEM and LED imaging, some of the spectra were removed for having very uneven surfaces, bad working distances, or large visible inclusions that would influence the bulk spectrum's accuracy. The outlying data has also been removed to allow for a better bulk understanding (Appendix D). The remaining spectra were re-evaluated, and the most representative spectrum for each sample has been selected; the spectra have been classified by their sample identity and side of analysis (Table 5). This process was repeated for the reference samples (Table 6).

Based on this data, there are patterns between the rough and smooth sides of each sample with a high similarity between the two sides. However, these patterns are not replicable from sample to sample. These differences are comparable with the variations in elemental data that can be observed for individual samples from a single soil layer (Panagiotidis, et al., 2019, pp. 262-265). This is further supported by the comparison of elemental data of the Refined Analysis Group against those of the Reference Group. Although soil is predominately composed of major elements such as silicon, aluminum, carbon, calcium, iron, sodium, and magnesium (Goffer, 2007, p. 221), elemental quantities

vary depending on the soil's origin. It is imperative to also consider that many of the white-ground lagynoi are assumed to have originated in Asia Minor and thus the soil inside of the vessels may share similar origins (Vogeikoff-Brogan, 2000, p. 302). As such, it is important to measure and compare these values for the Refined Analysis Samples individually and against reference values like those of the Reference Group.

As aluminum and silicon are found in proportional quantities in soil, this is an important indicator of general soil provenance. In addition, calcium values indicate if the soil is calcareous or non-calcareous. Through comparison of this data, it is possible to evaluate if the soil samples are from a similar geological area to each other and the reference samples (Goffer, 2007, pp. 227-228). Thus, the oxides of aluminum, silicon, and calcium - as detected through EDS analysis - were compared (Fig. 61). Based on these values, the samples of the Reference Group and Refined Analysis Group have a similar concentration of silicon and aluminum; it should be noted that grain size greatly influences the quantities of these materials as finer soils will be more enriched in Al and coarser soils in Si (Goffer, 2007, pp. 223-224). As the variation in concentration among the samples is minimal, it can be assumed that the reference and analysis groups are from a similar or the same geological area. This is supported by other soil studies performed in the region which display similar variations (Panagiotidis, et al., 2019, pp. 262-265) As such, this supports the assertation that the lagynos vessel was filled with soil from the tomb where it was discovered.

However, the calcium values of the samples vary greatly between the Refined Analysis Group and the Reference Group. Although this could be an indicator that the Refined Analysis Group originated from an area with calcareous soil, this does not mean

that the soil came from somewhere outside of the Thouria Area. Instead, it might be an indicator that the soil in the Thouria Area has changed calcium concentrations over time; this is further supported by the study by Panagiotidis, et al. which shows differences in calcium concentrations among individual stratigraphic layers (2019, pp. 262-265). In addition, the variation in the Refined Analysis Group itself is further supported by the fact that shell fragments were visible in the loose soil (Group D) and other samples not chosen for the Refined Analysis Group (Appendix A), this could influence the quantity of calcium oxide observed in the bulk elemental analysis of the samples. These shells were not visually observed in the loose reference soils or the samples of the Reference Group. As such, this will impact the overall calcium oxide composition observed. That being said, the Refined Analysis Group indicates an overall homogenous elemental concentration.

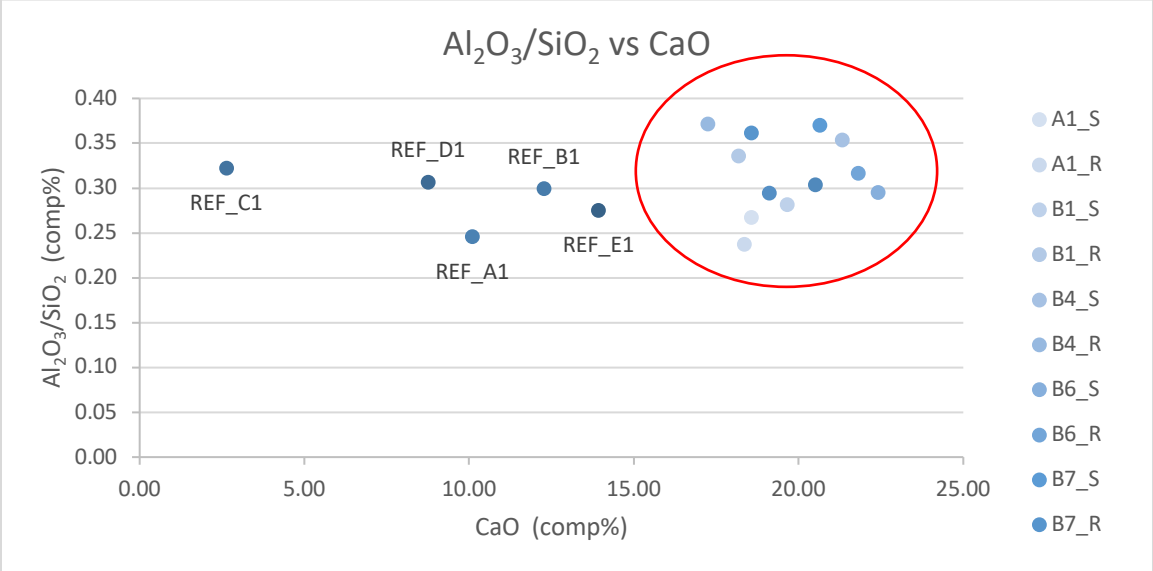

Figure 61: Biplot of Al_2O_3/SiO_2 and CaO. Plot of the Refined Analysis Group and Reference Group.

In addition to calcium, aluminum, and silicon, iron is also a major component of soil elemental compositions. Elemental oxides of iron and calcium of the Reference and Refined Analysis Groups were compared (Fig. 62). The variations in iron concentration can be attributed to the fact that iron is found in lower quantities in calcareous soils; this is because calcareous soils have a higher quantity of calcium carbonate which produce hydroxyl ions which result in an alkaline soil pH (Goffer, 2007, pp. 223-224). At a high pH, iron forms insoluble compounds which produce an iron deficiency in the soil (Incitec Pivot Limited, 2017). That being said, the amount of iron variation among the sample is consistent with iron variations among stratigraphic layers in the region (Panagiotidis, et al., 2019, pp. 262-265).

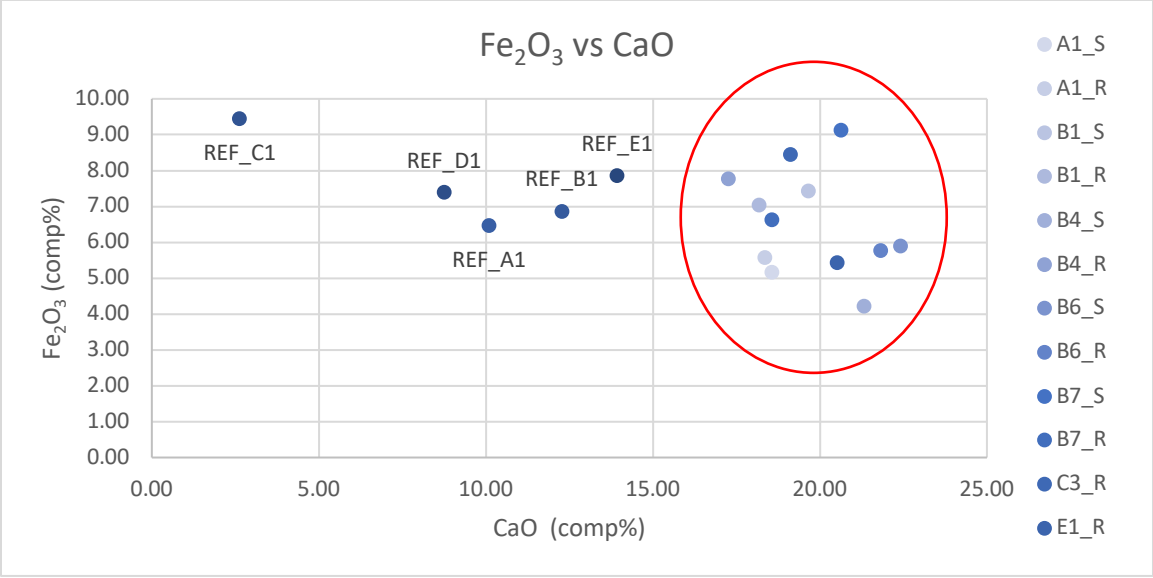

Figure 62: Bipolot of CaO and Fe_2O_3. Plot of the Refined Analysis Group and Reference Group.

Based on the elemental, morphological, and physical data, it can be assumed that the samples of the Refined Analysis Group are from the same stratigraphic layer and

depositional event. Variations in elemental quantities can be attributed to different elemental distributions during sedimentary settlement following deposition into the vessel. These variations can be observed in the comparison of elemental concentrations of magnesium oxide and potassium oxide (Fig. 63). Variations in trace elements like potassium and magnesium can be indicators of human habitation and organic materials (Goffer, 2007, pp. 227-228). Although there is an observable variation in elemental quantities between samples, these variations can also be observed between the sides of the samples. The smooth side of the samples seems to have a lower concentration of potassium than the rough counterparts. Alternatively, the smooth side of the samples seems to trend towards having a higher concentration of magnesium. This supports the fact that there are visually observable and chemical differences between the rough and smooth sides of the samples which could be attributed to elemental leaching from the ceramic vessel into the soil; this aligns with the assertation that the smooth sides of the samples can be attributed to a position against the wall of the lagynos vessel (Golitko, et al., 2021, p. 450).

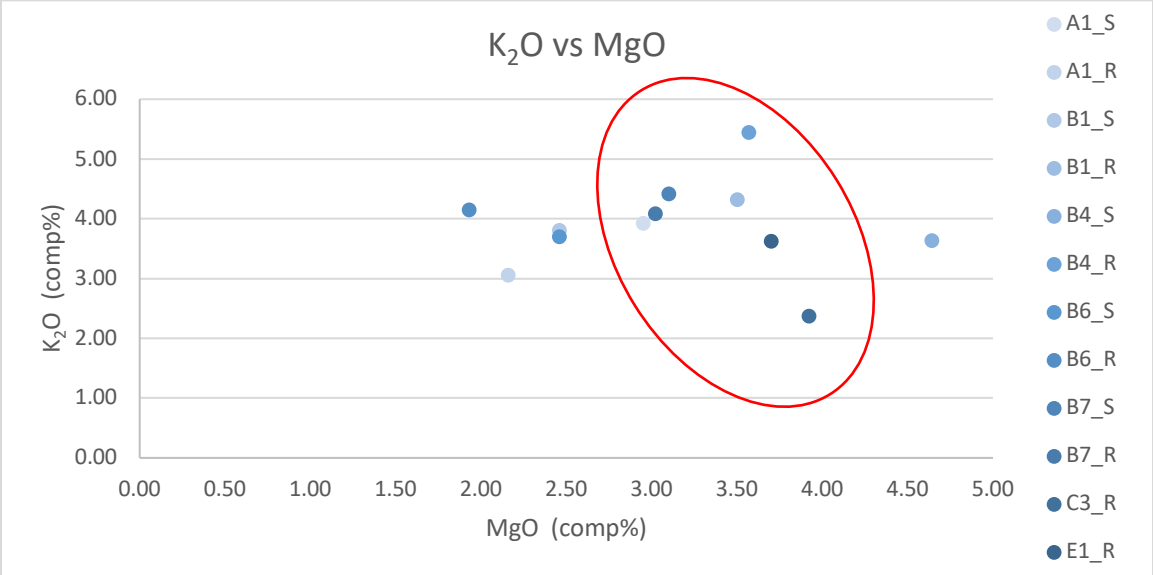

Figure 63: Bipolot of MgO and K_2O. Plot of the Refined Analysis Group.

It should be noted that although not present in any other samples, two of the assumed upper body samples (B6 & B7) contain significant traces of sodium oxide (NaO_2). This could be indicative of salts that formed during the evaporation of the liquid and condensed at the upper body of the vessel, near the neck; however, further analysis of upper neck fragments is necessary before any conclusions can be made (Style, 2007, p. 204).

6.5 Raman

Raman analysis was performed on the A1 and B1 samples which underwent no preparation. As this was performed on unpolished samples, there were few locations flat enough for analysis. For each fragment, two spectra were taken from the smooth side and only one spectrum from the rough side. Both samples displayed a significant peak at 1086.2 nm. This peak corresponds with symmetric stretching vibration ν_1 of carbonate (CO_3^{2-}). A secondary peak was observed at 465 nm which corresponds to the symmetric bend ν_2 of carbonate (Xi, et al., 2019, p. 762). Calcium carbonate is a key component of calcareous soils and can also be found in the shells of marine organisms (Goffer, 2007, p. 214). This is supported by the visual identification of white shell fragments within the soil samples. Fluorescence interference made all other peaks illegible and indeterminate. As such, further analysis was required on prepared samples in order to differentiate between the actual peaks and the interference.

Raman and infrared spectroscopy (FTIR) are both categorized as vibrational spectroscopy techniques since they are providing information on bond vibrations of

molecules in the samples, although they are working based on different principles: Raman spectroscopy is based on the 'Raman scattering' phenomenon of infrared radiation, while FTIR is based on the absorption of infrared radiation. As such, although both techniques operate based on the same principle, the peaks of the resulting spectra will provide different information. Thus, FTIR was conducted following the Raman analysis in order to determine if additional information regarding organic materials could be obtained.

6.6 FTIR

In addition to evaluating the presence of organic residues within the Refined Analysis Group, it is also important to consider what *type* of residue may have been present inside of the Thouria lagynos vessel. As previously discussed (1.3), based on the physical and typological characteristics of the vessel it is hypothesized that the white-ground style lagynoi contained either oil or wine (Walters, et al., 1925, p. 513); (Richter, 1953, p. 130); (Leroux, 1913, p. 39). As both wine and oil are associated with funerary rights during this time period, the contents of the white-ground lagynos cannot be definitively stated based on the vessel's appearance or situational context (Garland, 1985, p. 37). As such, in addition to determining the presence of organic residue, this analysis will evaluate the hypothesized identity of organic residue through comparison to known wine and fatty substance residue biomarkers.

The Refined Analysis Group was examined in conjunction with the Reference Group of the compressed KBr disc methodology; the spectra of these samples were overlayed (Fig. 38) and a select region of the spectra was expanded for further analysis and

discussion (Fig. 39). This was performed in order to determine which reference samples, if any, were most similar to that of the Refined Analysis group in order to provide a baseline for comparisons. In confirmation of the aforementioned SEM-EDS results, there appears to be a pattern discerning the Refined Analysis group samples from the Reference Analysis group samples; generally, higher iron oxides, hydroxy-oxides, and calcium carbonate amounts are detected in the latter group over the former. That being said, it is to be expected that the Reference Analysis group, which was present inside of the lagynos vessel, would have been affected by the surrounding material to a moderate degree. Based on this data, the REF_E1 sample was evaluated to be the most similar to that of the Refined Analysis Group. This is further supported by the fact that the soil sample was collected from the location closest to the tomb where the lagynos vessel was uncovered and the additional analysis performed earlier in this study. From this point, the Reference Group is refined to only include REF_E1. In all instances, it is difficult to discern clear and distinct peaks using the KBr disc of the ground samples as the weaker peaks - especially those associated with organics - were obscured by the peaks due to inorganics; this is particularly true for the soil samples. In order to refine the peaks due to organics in KBr spectra, the powdered samples were extracted in two solvents of opposite polarities, methanol and dichloromethane (DCM).

The solvents were selected based on their polarity and volatility (Koupadi, et al., 2021, p. 3613). In order to increase the absorbance of the samples, the methanol solvent was deposited onto the KBr disc multiple times after successive extraction events; as a result, increased absorbances across all of the samples from the first depositional event to the third depositional event (Fig. 40) were observed which were particularly distinct in

samples DB_B1. Based on the consistent increase in absorbance, only the final depositional event (2M) will be discussed for all samples from this point on; it should be noted that the presence of sedimentary contamination in the 1200-500 cm^{-1} range also increased for all samples with the increase in depositional events which was to be expected. The DCM extraction was only deposited once on the KBr disc due to the identification of already distinct peaks (Fig. 41). Following the examination of the sample group as a whole, the peaks from samples A1, A1S, and B1 were isolated for further analysis as they showed the most distinct and clear peaks within the organic material region. Sample REF_E1 was also selected for examination as a reference as a standard for comparison of unadulterated soil.

The spectra from samples A1 and A1S were examined in conjunction as they represent two sides of the same soil sample; the spectra of DB_A1M was removed from the analysis due to a lack of discernable data. Based on the absorbance spectra, there is little difference between the smooth and rough sides of the sample; however, it should be noted that the absorbances from the A1S sample were clearer than that of the A1 sample. This most likely is a result of increased interference from additional sediment which was deposited on the A1 sample. This is supported by greater absorbance peaks in the inorganic soil matrix region. Although these peaks are visible in both spectra, they are clearer in that of A1 which supports the assumption that there was an increase in sediment during the depositional events. In both samples, broad bands at 3425 cm^{-1} and 1625 cm^{-1} can be observed which are indicative of absorbed water; this implies that the solvent did not fully evaporate before the spectrum was collected (Krivoshein, et al., 2020, p. 9). However, the peaks in the 1633 cm^{-1} region could be indicative of structural water (Koupadi, et al., 2021).

In order to determine if this was due to environmental water or structural, refined analytical methods are required in order to increase the quality of the spectra.

In addition to the A1 and A1S samples, sample B1 also shows indications of organic materials. As both samples originate from the bottom of the vessel, this is not unexpected.

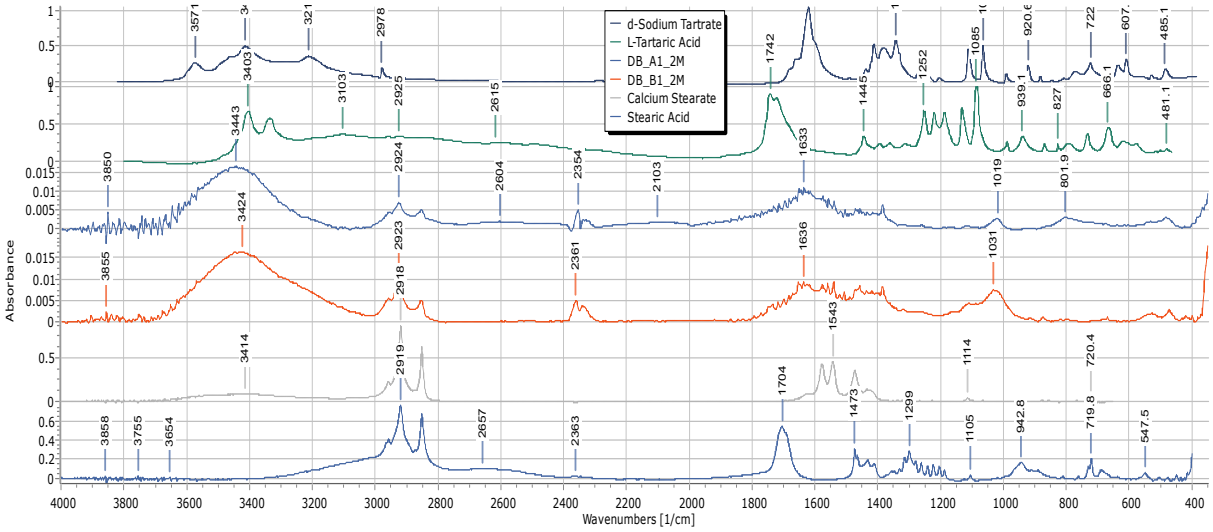

Figure 64: A1 & B1 Comparison Spectra. Comparison of the final depositional event of the A1 and B1 samples against (a) two known biomarkers for ancient wines, D-sodium tartrate and L-tartaric acid and (b) two typical fatty substance residues, stearic acid and calcium stearate.

In order to evaluate the *wine marker* and the *fatty substance* hypotheses, these results were compared to known biomarkers for (a) ancient wine residues – i.e. tartaric acid and tartrate salts (McGovern & Hall, 2015, p. 601) (McGovern, et al., 2017, p. 5) - and (b) typical fatty substance residues – i.e. stearic acid and stearate salts (Koupadi, et al., 2021, p. 3613) - in an attempt to take the analysis a step further and identify the contents of the vessel (Fig. 64); as organic salt (i.e. carboxylate) peaks were observed in the spectra - based on peaks due to antisymmetric and often symmetric vibrations -, it stands that there is a

possibility that the organic salt could correspond with either tartrate or with fatty acid salts, such as calcium stearate. That being said, although the spectra share some peaks in the 1700-1400 cm^{-1} range, nothing can be clearly or conclusively identified. In addition, when compared to the Refined Analysis Samples, the reference sample, REF_E1, spectrum results are inconclusive as peaks due to organics were also detected in conjunction with those due to inorganics in the soil region. The presence of these peaks could be attributed to the methodology as it dictated that the soil was not processed following collection in order to preserve the integrity of the chemical profile; this means that the soil may still contain organic materials like roots or plant materials - as well as humic acids - which have not degraded yet but should not be considered as characteristic for the overall soil profile (Volkov, Rogova, & Proskurnin, 2021, p. 3). With this and the inconclusive results of the spectra of the other samples, an additional methodology is needed in order to further refine the spectrum results.

6.7 Refined FTIR

The FTIR methodology was refined to optimize the results from the previous experiment. In order to standardize the methodology, each of the samples were weighed and separated into categories based on the solvent (Table 12); such standardization allowed for more consistent results across the different samples and between methodologies. So as to optimize the visible results, the background silicon discs were removed from the spectra using the *Spectragryph* program (v1.2.16) (Fig. 65); it should be noted that the blank area displays peaks associated with the silicon wafer around the 1110-900 cm^{-1} region, which correspond with the absorption by Si-O vibrations of the ultra-thin silicon oxide coating in

the wafer's surface, and the peaks in the 600-500 cm^{-1} region, which are associated with the absorption of the lattice phonons of the silicon wafer (Hava, Ivri, & Auslender, 2001). As these peaks are lacking from the B1_DCM sample, it can be determined that the subtraction methodology implemented with the *Spectagryph* program is effective.

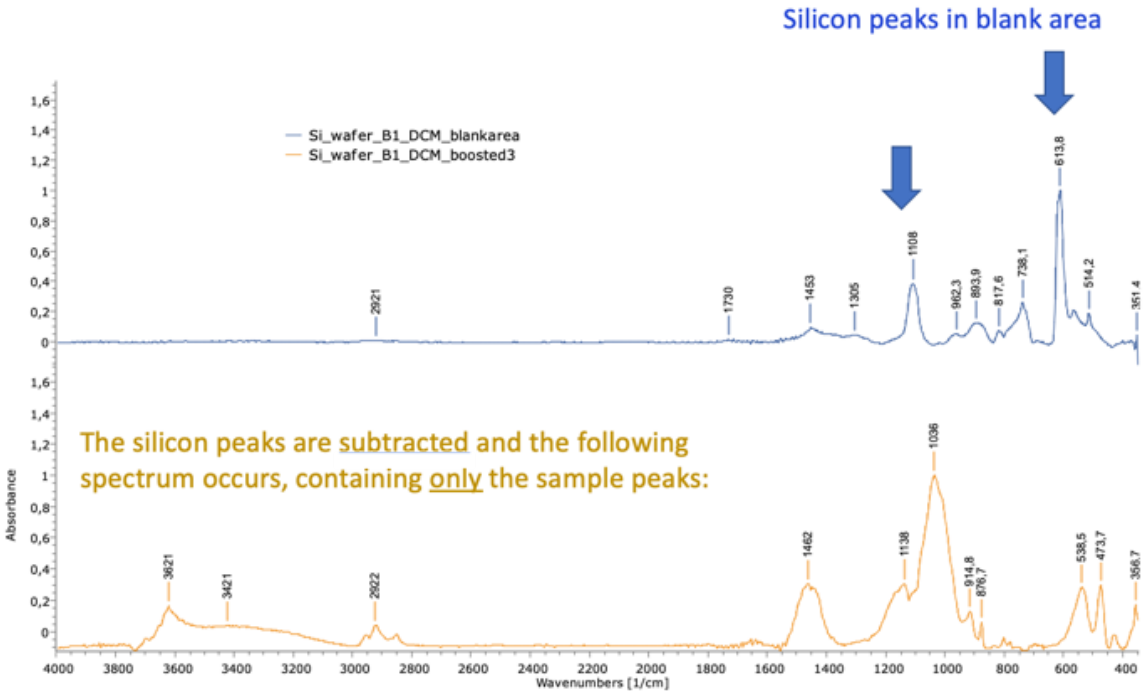

Figure 65: Peak Subtraction Example. B1 DCM spectra displaying the spectrum of the blank area (ie. the silicon wafer) and the B1_DCM_boosted3 spectrum with the blank area extracted.

In addition, in order to increase the absorbance of the organic components in the samples, the samples eluted in $CHCl_3$+MeOH and MeOH were deposited on the silicon disc multiple times; this resulted in a clear increase in the concentration of absorbance frequencies visible on the spectra following each depositional event. Based on this, only the final depositional event of each sample will be discussed from this point forward. Of the samples prepared, only the samples from the previous analysis which showed

indications of organic material were analyzed; this grouping includes samples A1S, B1S, REF_D1, and REF_E1. As only the A1S and B1S samples are being examined, the samples will be referred to as A1 and B1 for convenience. In addition, the reference group was expanded upon re-evaluation of the previous results for organic indications; this reassessment fits with the previous analysis as the REF_D1 sample contains similar elemental and physical characteristics to sample REF_E1 and the analysis grouping. This is further supported by the fact that REF_D1 originates from a very similar location to that of REF_E1.

A1 Spectra

The A1 samples were eluted into MeOH (Fig. 44), DCM (Fig. 45), and $CHCl_3$+MeOH (Fig. 46); in order to include all molecular events, the peaks produced in these solvents will be discussed as a whole. The MeOH extraction of A1 shows significant indicators of organic materials. The 3rd depositional event (Fig. 65) displays indicators of esters ($_{\nu}C=O$) which support the presence of fatty substances.

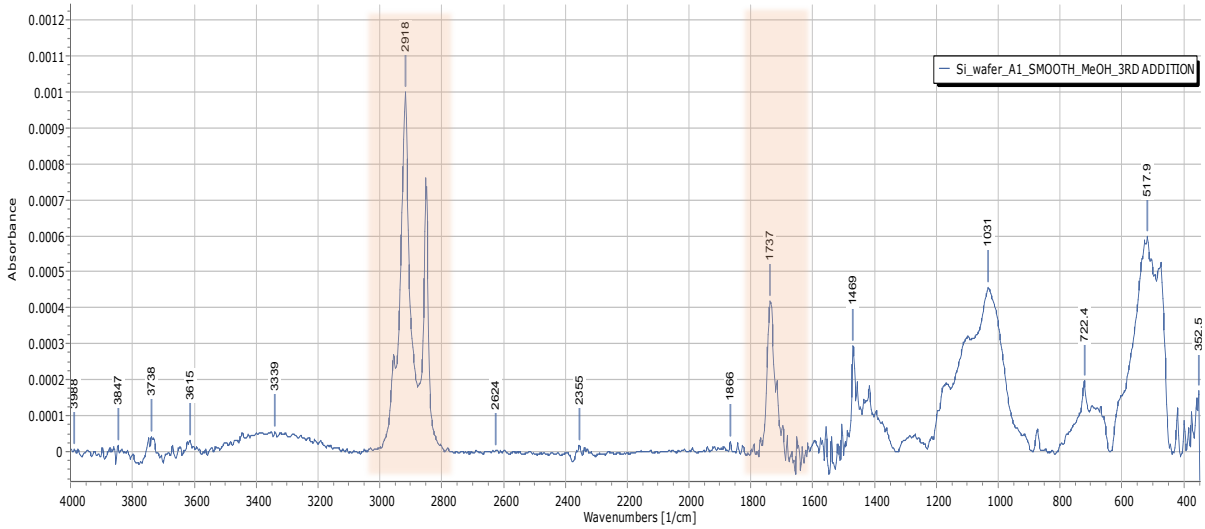

Figure 66: Organic Indicators in A1 MeOH Spectra. Spectra of the third depositional event of A1_ MeOH indicate the presence of esters and organic salts.

The $CHCl_3$+MeOH extraction of A1 shows significant indicators of organic materials. The first depositional event spectra (Fig. 67) display significant peaks indicating crystalized organic salts ($v_{as}COO^-$ and v_sCOO^-). This is further supported by the fourth depositional event spectra (Fig. 68) which displays clear indicators of fatty esters ($_vC=O$) and carboxylates ($v_{as}COO^-$ and v_sCOO^-).

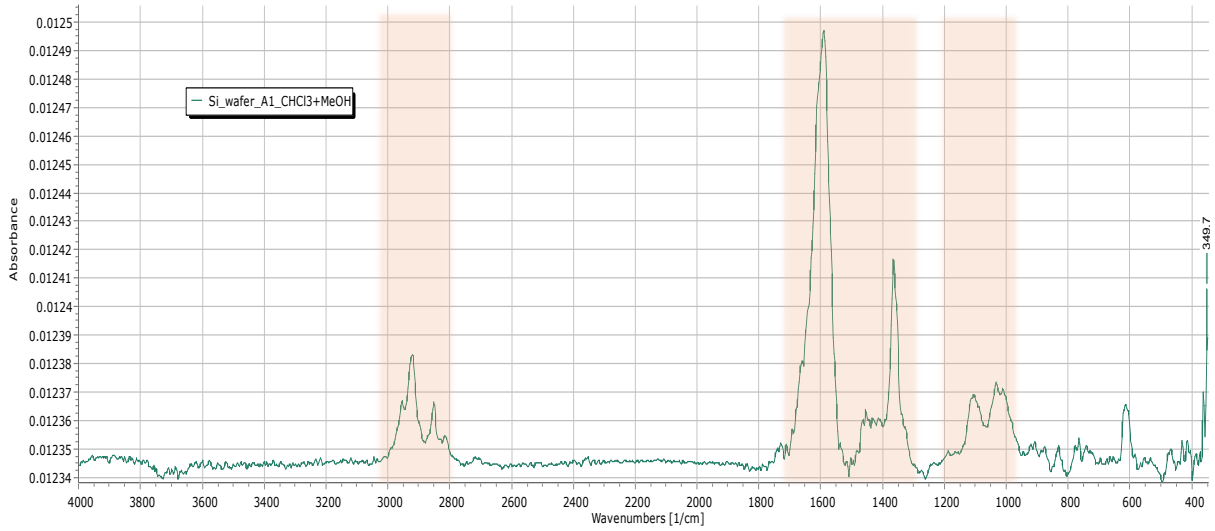

Figure 67: Organic Indicators in A1 $CHCl_3$+MeOH Spectra. Spectra of the first depositional event of A1_$CHCl_3$+MeOH indicating strong carboxylate ion peaks and weak organic salts.

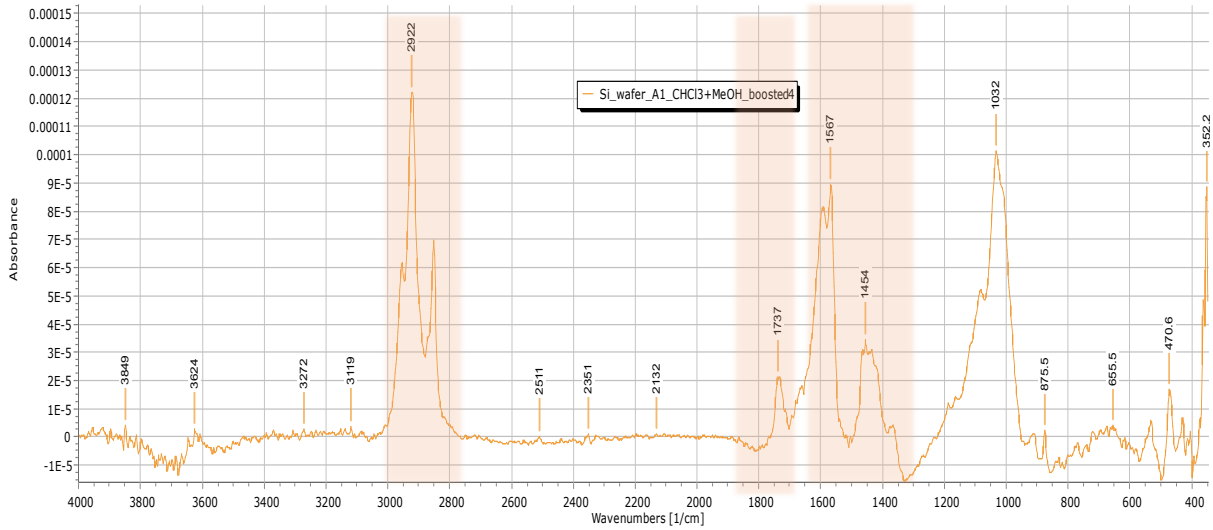

Figure 68: Organic Indicators in A1 $CHCl_3$+MeOH Spectra. Spectra of the fourth depositional event of A1_$CHCl_3$+MeOH which displays clear indicators of fatty esters, and carboxylates or organic salts.

Overall, the presence of these indicators implies that the A1 sample contained residues of carboxylate salts and fatty esters.

B1 Spectra

As the B1 sample is from a similar area of the vessel as the A1 sample, it can be assumed that the spectra will show similar peaks. Similar to the A1 sample, the B1 samples were eluted into MeOH (Fig. 47), DCM (Fig. 48), and CHCl3+MeOH (Fig. 49); in order to include all molecular events, the peaks produced in these solvents will be discussed as a whole. The MeOH extraction of B1 shows significant indicators of organic materials. The 3rd depositional event (Fig. 69) displays indicators of esters ($_{v}$C=O) and ester triads (vC-O) which supports the presence of fatty substances. In addition, significant carboxylate peaks

($v_{as}COO^-$ and v_sCOO^-) can be observed. Based on this, the presence of these indicators implies that the B1 sample contained residues of carboxylate salts and fatty esters.

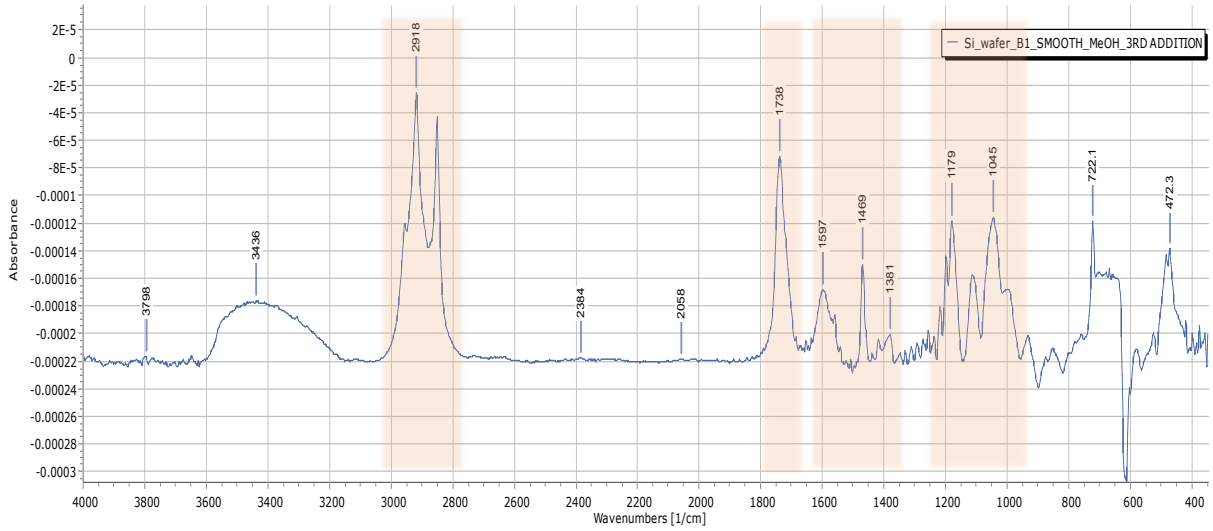

Figure 69: Organic Indicators in B1 MeOH Spectra. Spectra of the third depositional event of B1_ MeOH indicate the presence of esters, and carboxylates or organic salts.

Reference Spectra

The A1 and B1 spectra were compared against the REF_D1 and REF_E1 samples. Of the two reference samples, the REF_D1 showed the strongest indicators of organic materials. The 3rd depositional event (Fig. 70) displays indicators of esters ($_vC=O$); however, their quantities are significantly lower than the ones detected in sample A1 after the corresponding workup.

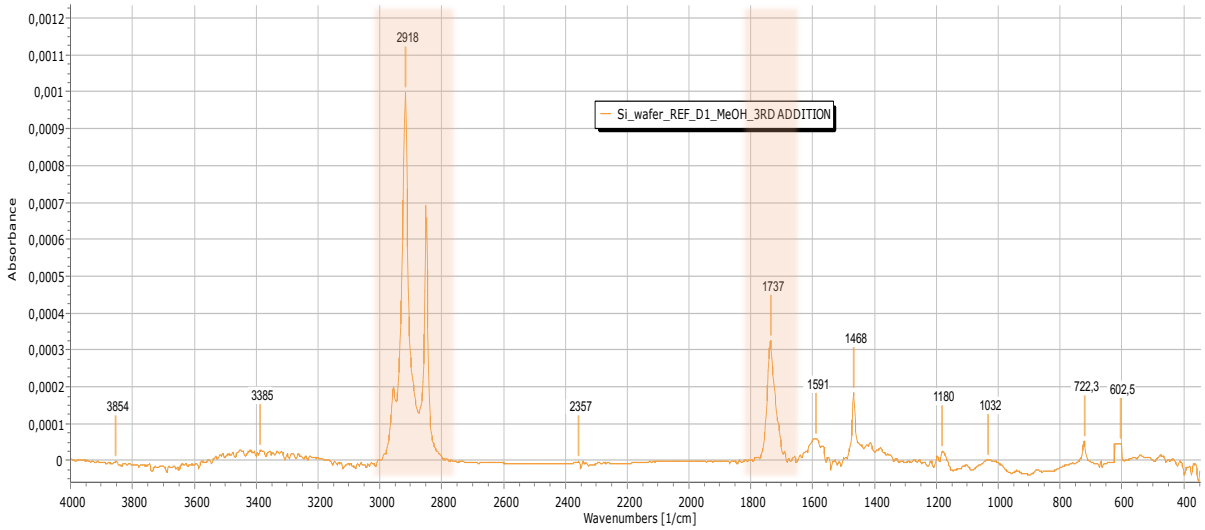

Figure 70: Organic Indicators in REF_D1 MeOH Spectra. Spectra of the third depositional event of REF_D1 MeOH indicate the presence of esters and organic salts.

In addition, the $CHCl_3$+MeOH extraction of REF_D1 shows indicators of poorly crystallized organic salts (Fig. 71). Similar poorly crystallized organic salts can also be observed in the REF_E1 spectra of the same solvent (Fig. 72).

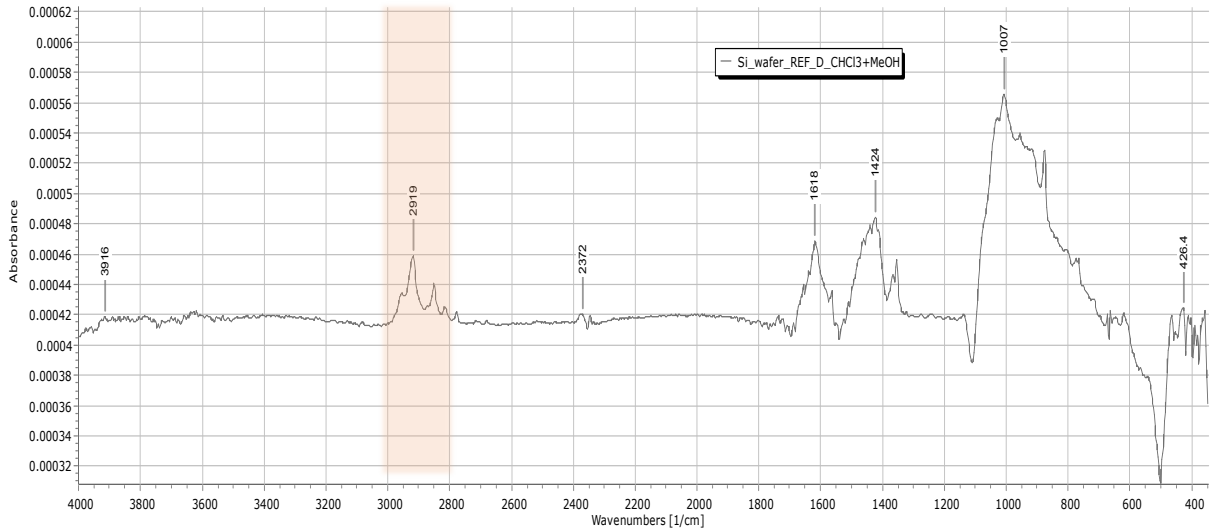

Figure 71: Organic Indicators in REF_D1 $CHCl_3$+MeOH Spectra. Spectra of REF_D1 $CHCl_3$+MeOH indicate the presence of poorly crystalized (i.e. broad peak lineshapes for the sym- and asym- peaks) organic salts.

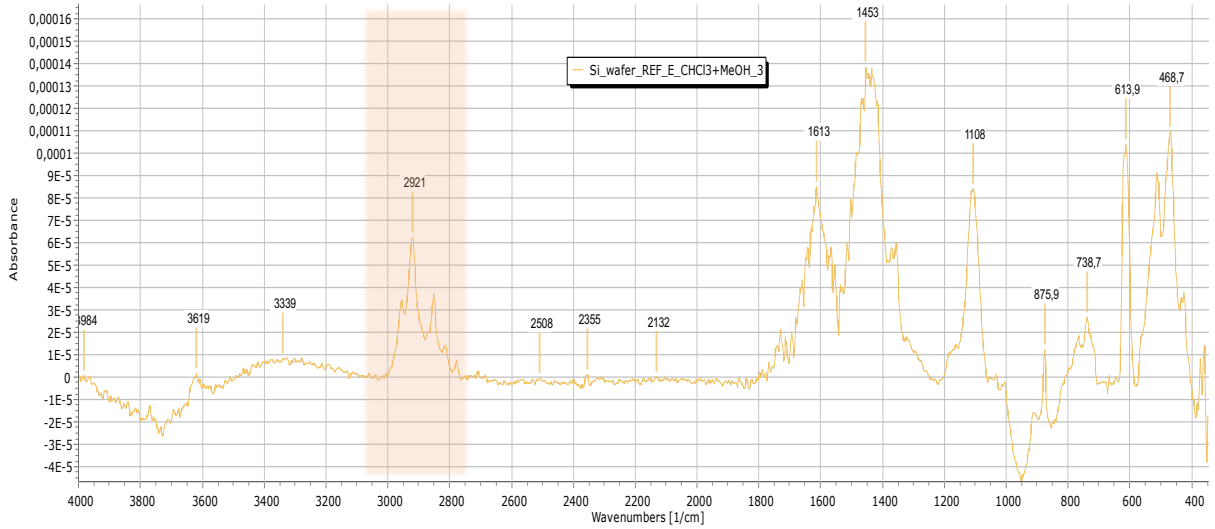

Figure 72: Organic Indicators in REF_E1 $CHCl_3$+MeOH Spectra. Spectra of the third depositional event of REF_E1_ $CHCl_3$+MeOH indicate the presence of poorly crystalized organic salts.

Although the REF_D1 sample does contain indicators of esters, it lacks the significant peaks associated with fatty esters. In addition, the reference samples do contain indicators of organic salts but lack the significant peaks associated with carboxylates. Overall, based on this it can be assumed that the organic materials present in the reference samples are not the same organic material present in the A1 and B1 samples. Additional analysis is required - on the basis of the present results – to determine if the organic material present within the Thouria lagynos vessel is better associated with an oily or oil-based substance in alignment with and supporting the second part of the initial hypothesis.

With this in mind, it can be concluded that organic material inside of the Thouria lagynos vessel has been detected through the use of archaeological soils. In addition, the organic remains from inside of the vessel have been determined to be different than that of the reference samples which were collected from soils outside of the vessel. This conclusion supports the overall goal of the analysis which was to determine if the proposed non-destructive and non-invasive analytical methodology can be utilized for the identification of archaeological organic residues.

Chapter 7. Conclusions

A lagynos vessel ascribed at Hellenistic Times from the Ancient Thouria archaeological site was found undamaged in a tomb that was uncovered during a rescue excavation in 2018 (Malapani, 2021, p. 44). As discussed in this study, based on the vessel type and appearance it was hypothesized to have contained wine or oils which were presumably used in a funerary context (Oakley, 2004). However, as the vessel was discovered in a rescue excavation, it is difficult to determine the context of the vessel in addition to its contents. Thus, in order to verify the identity of the vessel's possible organic residue, the aforementioned archaeometric analysis was required. Based on the results of the analyses performed in this study, several conclusions can be made.

Vessel Analysis

The white-ground lagynos was constructed and eventually deposited in the grave as a funerary or ritual object; it was not intended for use outside of a funerary context. The preservation state of the vessel also supports this conclusion. As a funerary object, the vessel is assumed to have contained an unknown liquid; this is further supported by the typological characteristics of the vessel such as a small mouth and a long neck.

Following its deposition in the tomb, the vessel was filled with soil. The liquid was still present inside of the vessel which was absorbed by the soil following the single depositional event; this implies that the vessel was filled with soil soon after burial. This is supported by the analysis of sedimentary deposition amongst the soil fragments. In

addition, this supports that the vessel was unmoved post-deposition in the tomb until its rediscovery in 2018.

Method Evaluation

It was proposed that due to the delicate and unique state of the lagynos, the archaeological soil inside of the vessel could be analyzed for evidence of organic residue in order to prevent damage to the vessel itself. The study was conducted through the use of minimally invasive optical microscopy, SEM-EDS, RAMAN spectroscopy, and FTIR spectroscopy. In order to evaluate the results, the archaeological soil was compared against reference soils collected from the Thouria area at various distances from the tomb. Based on the results of the analysis, it has been determined that there are organic remains inside of the vessel; organic biomarkers were preserved within the soil in the vessel which were not present in the soil outside of the vessel. The results of this analysis support the goal of the study which was to determine if archaeological soils could be utilized in the examination of initially liquid organic residue without the destruction of intact ceramic bodies or potsherds fragments (Roffet-Salque, et al., 2017, pp. 627-628).

Organic Residue Identification

As previously discussed, the organic biomarkers preserved within the soil of the vessel were not present in the reference soil from the archaeological site of Thouria. These markers were then compared to known biomarkers of initially liquid archaeological organic residues. As previously mentioned, it is hypothesized that the lagynos vessel contained residue of either wine or fatty substances based on the context of the vessel itself. Based on the results of the FTIR analyses, it was determined that the samples contained peaks

related to fatty esters and carboxylates - in addition to esters and organic salts - which are indicators of fatty substances and oily products. Additional research is required in order to determine the specific identity of the fatty substance (i.e. walnut oil, olive oil, perfume, etc.).

Further Analysis

Although it was beyond the goals of this analysis – which was to determine the efficacy of using archaeological soils for organic residue analysis -, the organic liquid within the Thouria lagynos was identified to be an oil-based product. As previously discussed, oils are also called lipids which are composed of carboxylic acids and glycerol. The length of the carboxylic acid chain influences the identity of the ester. In order to determine the identity of the fatty acids, additional examinations which is sensitive enough to verify the length of the carboxylic acid chains are required. This can be done through the use of chromatographic techniques, typically GC-MS (Koupadi, et al., 2021). As such, further analysis will be performed at a later date in order to effectively identify the oil product within the vessel.

That being said, the conclusions drawn from this analysis have met the goals of this study; although the specific oil product within the vessel cannot be fully identified with the present forms of analyses, the fact that the biomarkers of a lipid were detected within the archaeological soil supports the objective of this study which was to determine if archaeological soils can theoretically also be utilized in the examination of previously-liquid organic residue *without* the destruction of intact ceramic bodies or potsherds fragments (Roffet-Salque, et al., 2017, pp. 627-628).

It is the goal of this author to continue the archaeometric analysis of the Thouria lagynos through the use of archaeological soils in order to identify the oil product contained within this vessel. In addition, the presence of sodium (NaO_2) on the unexamined rim samples warrants further investigation as that could provide additional clues to the identity of the oil product and the liquid evaporation process (Hendy, et al., 2018). This information will provide additional context to the vessel and close debate over the contents of the lagynos as a funerary vessel.

Bibliography

Αραπογιάννη, Ξ. (2017). *Ancient Thouria: the Asklepieion*. Athens: Archive Publications.

Αραπογιάννη, Ξ. (2018). Αποκαλύπτοντας ένα άγνωστο θέατρο: Στην Αρχαία Θουρία Μεσσηνίας. *Περιοδικό Αρχαιολογία & Τέχνες,* 126, 47-57.

Alexandrescu, C. G. (2019). Images of Music and Musicians as Indicators of Status, Wealth and Political Power on Roman Funerary Monuments. In R. Eichmann, M. Howell, & G. Lawson, *Music and Politics in the Ancient World: Exploring Identity, Agency, Stability and Change through the Records of Music Archaeology* (pp. 183-200). Berlin.

Ancient Thouria Excavation Website. (2016). *History*. Retrieved January 2022, from https://ancientthouriaexcavation.gr/en/history/

Arnold, D. E., Neff, H., & Bishop, R. L. (1991). Compositional Analysis and "Sources" of Pottery: An Ethnoarcheological Approach. *American Anthropologist*, 93(1), 70-90.

Barnard, H., Ambrose, S. H., Beehr, D. E., Forster, M. D., Lanehard, R. E., Malainey, M. E., Yohe II, R. M. (2007). Mixed results of seven methods for organic residue analysis applied to one vessel with the residue of a known foodstuff. *Journal of Archaeological Science,* 34, 28-37.

Beazley, J. D. (1938). *Attic White Lekythoi* (19th ed.). Oxford: Oxford University Press.

Bennet, J. (2005). *Τα αρχεια με πινακίδες Γραμμικής Β και το βασίλειο του Νέστορα, Πύλος η Αμμουδερή.* (J. L. Davis, Ed.) Athens: Παπαδημα.

Berthold, C., Zimmer, K. B., Scharf, O., Koch-Brinkmann, U., & Bente, K. (2016). Nondestructive, optical and X-ray analytics with high local resolution on attic white-ground lekythoi. *Journal of Archaeological Science*: Reports, 1-8.

Blázovics, A., Horváth, B. Z., & Győry, H. (2019). Blessing or Curse: The consumption of Wine in Ancient Egypt. *Aegyptus et Pannonia VI* (pp. 113-166). Budapest: Archeobooks.

Carter, C. B. (2007). *Ceramic Materials: Science and Engineering*. Springer.

Chiriu, D. P. (2020). Application of Raman Spectroscopy to Ancient Materials: Model and Results from Archaeometric Analyses. *Materials*, 13(11), 2456 (1-17).

Drieu, L., Horgnies, M., Binder, D., Pétrequin, P., Pétrequin, A. M., Peche-Quilichini, K., Regert, M. (2019). Influence of Porosity on Lipid Preservation in the Wall of Archaeological Pottery. *Archaeometry*, 61(5), 1081-1096.

Drieu, L., Rageot, M., Wales, N., Stern, B., Lundy, J., Zerrer, M., Craig, O. E. (2021). Is it possible to identify ancient wine production using biomolecular approaches? *STAR: Science & Technology of Archaeological Research*, 6(1), 16-29.

Edmonds, W. J., Thomas, P. J., Simpson, T. W., & Baker, J. C. (1998). Land Judging and Soil Evaluation. *Virginia Polytechnic Institute and State University Department of Crop and Soil Environmental Sciences*, 1-26.

Eliasson, C. W. (2020). *Artefacts in funerary scenes on Athenian white-ground lekythoi: A comparison between iconography and text.* Uppsala: Uppsala Universitet.

Evershed, R. P. (2008). Organic Residue Analysis in Archaeology: The Archaeological Biomarker Revolution. *Archaeometry*, 6, 895-924.

Evershed, R. P., & Heron, C. (1993). The Analysis of Organic Residues and the Study of Pottery Use. *Journal of Archaeological Method and Theory*, 5, 247-284.

Filopoulou, A., Vlachou, S., & Boyatzis, S. C. (2021). Fatty Acids and Their Metal Salts: A Review of Their Infrared Spectra in Light of Their Presence in Cultural Heritage. *Molecules*, 26(6005), 1-27.

Garland, R. (1985). *The Greek Way of Death*. Ithaca: Cornel University Press.

Goffer, Z. (2007). Sediments and Soils. In *Archaeological Chemistry* (pp. 209-229). Hoboken: John Wiley & Sons, Inc.

Golitko, M., McGrath, A., Kreiter, A., Lightcap, I. V., Duffy, P. R., Parditka, G. M., & Giblin, J. I. (2021). Down to the Crust: Chemical and Mineralogical Analysis of Ceramic Surface Encrustations on Bronze Age Ceramics from Békés 103, Eastern Hungary. *Minerals,* 11, 436-454.

Gosselain, O. P. (2018). *Pottery chaînes opératoires as Historical Documents.* Oxford Research Encyclopedia of African History, 1-41.

Grinsell, L. V. (2012). The Breaking of Objects as a Funerary Rite. *Folklore*, 3(72), 475-491.

Harush, O., & Grosman, L. (2021). Toward the identification of social signatures in ceramic production: An archaeological case study. *PLoS ONE*, 16(7), 1-22.

Hava, S., Ivri, J., & Auslender, M. (2001). Wavenumber-modulated patterns of transmission through one- and two-dimensional gratings on a silicon substrate. *Journal of Optics A Pure and Applied Optics*, 3(6), 1-6.

Hein, A. K. (2018). Modeling of the microstructure of ancient functional ceramics and assessment of their performance. *Procedia Structural Integrity,* 10, 219-226.

Hein, A., & Kilikoglou, V. (2020). Ceramic Raw Materials: How to Recognize Them and Locate the Supply Basins: Chemistry. *Archaeological and Anthropological Sciences*, 180(12), 1-17.

Hein, A., Tsolakidou, A., Iliopoulos, I., Mommsen, H., Buxedai Garrigós, J., Montana, G., & Kilikoglou, V. (2002). Standardisation of Elemental Analytical Techniques Applied to Provenance Studies of Ancient Ceramics. *The Analyst*, 4(127), 542–553.

Hendy, J. et al., 2018. Ancient proteins from ceramic vessels at Çatalhöyük West reveal the hidden cuisine of early farmers. *Nature Communications*, 9, pp. 1-10.

Hermans, J., & Helwig, K. (2022). The Identification of Multiple Crystalline Zinc Soap Structures Using Infrared Spectroscopy. *Applied Spectroscopy*, 1, 1-10.

Incitec Pivot Limited. (2017). *Iron Fact Sheet.* Victoria: Incitec Pivot Fertilisers.

Iordanidis, A. G.-G.-M. (2009). Analytical study of Ancient Pottery from the Archaeological site of Aiani, Nothern Greece. *Minerals Characterization,* 60, 292-302.

Jehlicka, J. (2012). Infrared and Raman Spectroscopy: Forensic Applications in Mineralogy . In J. M. Chambers, *Infrared and Raman Spectroscopy in Forensic Science* (pp. 421-445). John Wiley & Sons, Ltd.

Kazakis, N. A. (2015). Provenance of Ceramics: Methods and Practices. In A. Sarris, *Best Practices of GeoInfromatic Technologies for the Mapping of Archaeolandscapes* (pp. 239-250). Oxford: Archeopress.

Kilikoglou, V. M. (1988). The Effect of Furification and Firing of Clays on Trace Element Provenance Studies. *Archaeometry,* 30, 37–46.

Koupadi, K., Boyatzis, S. C., Roumpou, M., Kalogeropoulos, N., & Kotzamani, D. (2021). Organic Remains in Early Christian Egyptian Metal Vessels: Investigation with Fourier Transform Infrared Spectroscopy and Gas Chromatography–Mass Spectrometry. *Heritage,* 1(4), 3611-3629.

Krivoshein, P. K., Volkov, D. S., Rogova, O. B., & Proskurnin, M. A. (2020). FTIR Photoacoustic Spectroscopy for Identification and Assessment of Soil Components: Chernozems and their Size Fractions. *Photoacoustics*, 18, 1-44.

Leake, W. M. (1830). *Travels in the Morea I*. London.

Leroux, G. (1913). *Lagynos: Recherches sur la céramique et l'art ornemental hellénistiques.* Paris.

Loy, W. G., & Wright, Jr., H. E. (1972). The Physical Setting. In W. A. McDonald, & G. R. Rapp, Jr. (Eds.), *The Minnesota Messenia Expedition: Reconstructing a Bronze Age Regional Environment* (pp. 36-46). Minneapolis: University of Minnesota.

Lund, J. (2013). Cypriot Lagynoi with a Funnel Shaped Mouth and a Twisted Handle. *Studies in Ancient Art and Civilization*, 17, 255-275.

Luraghi, N. (2009). VII. Messenian Ethnicity and the Free Messenians. In P. Funke, & N. Luraghi (Eds.), *The Politics of Ethnicity and the Crisis of the Peloponnesian League*. Washington, DC: Center for Hellenic Studies.

Malapani, E. (2021). Συστάδα ελληνιστικών κιβωτιόσχημων τάφων στην Αίπεια Αρχαίας Θουρίας. *Book of Abstracts: 3rd AEPEL ARCHAEOLOGICAL WORK IN THE PELOPONNESE*, (p. 42). KALAMATA.

Maniatis, Y., & Tite, M. S. (1981). Technological Examination of Neolithic-Bronze Age Pottery from Central and Southeast Europe and from the Near East. *Journal of Archaeological Science*, 8(1), 59-76.

McGovern, P. E., & Hall, G. R. (2015). Charting a Future Course for Organic Residue Analysis in Archaeology. *Journal of Archeological Method and Theory*, 32, 592-622.

McGovern, P. E., Callahan, M. P., Hall, G. R., Petersen, C. W., Cavalieri, D., Hartl, D. L., Lamuela-Raventós, R. (2020). Possible to Identify Ancient Wine Production Using Biomolecular Approaches?". *STAR: Science & Technology of Archaeological Research*, 7, 43-48.

McGovern, P., Jalabadze, M., Batiuk, S., Callahan, M. P., Smith, K. E., Hall, G. R., Ba. (2017). Early Neolithic wine of Georgia in the South Caucasus. *Proceedings of the National Academy of Sciences*, 114(48), 1-10.

McGovern, P., Jalabadze, M., Batiuk, S., Callahan, M. P., Smith, K. E., Hall, G. R., Bac. (2017). Early Neolithic wine of Georgia in the South Caucasus: Supporting Document. *Proceedings of the National Academy of Sciences*, 114(48), E10309-E10318.

Mertens, J. R. (2006). Attic White-Ground: Potter and Painter. In B. Cohen, *The Colors of Clay: Special Techniques in Athenian Vases* (pp. 186-193). Getty Publications.

Mitsopoulos-Leon, V., & Österreichisches Archäologisches Institut (Wien). (2001). Forschungen in der Peloponnes: Akten des Symposions anlässlich der Feier "100 Jahre Österreichisches Archäologisches Institut Athen". *Zweigstelle Athen. Symposion (1998: Athēna)* (pp. 5.3-7.3). Athen: Österreichisches Archäologisches Institut.

Montana, G. (2020). Ceramic Raw Materials: How to Recognize Them and Locate the Supply Basins: Mineralogy & Petrography. *Archaeological and Anthropological Sciences*, 175(12), 1-19.

Munsell Color Company. (1975). *Munsell Soil Color Charts* (Pring Book ed.). Baltimore, Md: Munsell Color.

Musée du Lourve. (2021). *Lagynos*. Retrieved January 2022, from https://collections.louvre.fr/en/ark:/53355/cl010275129

Noble, J. V. (1960). The Technique of Attic Vase-Painting. *American Journal of Archaeology*, 64(4), 307-318.

Oakley, J. H. (2004). *Picturing Death in Classical Athens: The Evidence of the White Lekythoi.* Cambridge: Cambridge University Press.

Odelli, E. R. (2020). Micro-Raman spectroscopy to investigate production techniques: A focus on fine ware potteries. *Journal of Raman Spectroscopy*, 52, 1-9.

Oudemans, T. F. (2007). Applying Organic Residue Analysis in Ceramic Studies in Archaeology. *Leiden Journal of Pottery Studies*, 23, 5-20.

Oudemans, T. F., & Boon, J. J. (1991). Molecular Archaeology: Analysis of Charred (food) Remains from Prehistoric Pottery by Pyrolysis-Gas Chromatography/Mass Spectrometry. *Journal of Analytical and Applied Pyrolysis*, 20, 197-227.

Palamara, E., Zacharias, N., Xanthopoulou, M., Kasztovszky, Z., Kovács, I., Palles, D., & Kamitsos, E. I. (2016). Technology issues of Byzantine glazed pottery from Corinth, Greece. *Microchemical Journal*, 129, 137-150.

Panagiotidis, V. V., Malaperdas, G., Valantou, V., & Zacharias, N. (2019). Environmental aspects of ancient city planning: a pilot study on Ancient Thouria in the Peloponnese, Greece. *STAR: Science & Technology of Archaeological Research,* 5(2), 257-268.

Princeton University. (2022). *White-ground lekythos: woman and youth with lyre at a tomb, ca. 420–400 B.C.* Retrieved February 2022, from Princeton University Art Museum: https://artmuseum.princeton.edu/collections/objects/34520

Rambach, J. (2007). *Investigations of two MH I burial mounds at Messenian Kastroulia* (near Ellinika, ancient Thouria) (Vol. 42). Verlag der Österreichischen Akademie der Wissenschaften.

Richter, G. M. (1953). *Handbook of the Greek Collection*. Cambridge: Harvard University Press.

Roffet-Salque, M., Dunne, J., Altoft, D. T., Casanova, E., Cramp, L. J., Smyth, J., Evershed, R. P. (2017). From the inside out: Upscaling organic residue analyses of archaeological ceramics. *Journal of Archaeological Science: Reports*, 16, 627-640.

Romanus, K., Baeten, J., Poblome, J., Accardo, S., Degryse, P., Jacobs, P., Waelkens, M. (2009). Wine and olive oil permeation in pitched and non-pitched ceramics: relation with results from archaeological amphorae from Sagalassos, Turkey. *Journal of Archaeological Science*, 36, 900-909.

Sachs, G. (2006*). Die Siedlungsgeschichte der Messenier: vom Beginn der geometrischen bis zum Ende der hellenistischen Epoche*. Kovač.

Shepard, A. O. (1956). *Ceramics for the Archaeologist* (Vol. 609). Washington, DC: Carnegie Institution of Washington.

Shillito, L. M., Almond, M. J., Wicks, K., Marshall, L.-J. R., & Matthews, W. (2009). The use of FT-IR as a screening technique for organic residue analysis of archaeological samples. *Spectrochimica Acta Part A: Molecular and Biomolecular Spectroscopy*, 72, 120-125.

Shoval, S., & Beck, P. (2005). Thermo-FTIR Spectroscopy Analysis as a Method of Characterizing Ancient Ceramic Technology. *Journal of Thermal Analysis and Calorimetry*, 82, 609-616.

Simpson, R. H. (1966). *The Seven Cities offered by Agamemnon to Achilles* (Iliad ix. 149 ff., 291 ff.). Annual of the British School at Athens, 61, 113-131.

Simpson, R. H. (2007). Interdisciplinary Survey in Messenia, Southwest Peloponnese, Greece. *Geoarchaeology: An International Journal*, 22(1), 110-120.

Simpson, R. H., & Lazenby, J. F. (1972). Greco-Roman Times: Literary Tradition and Topographical Commentary. In W. A. McDonald, & G. R. Rapp, Jr. (Eds.), *Minnesota Messenia Expedition: Reconstructing a Bronze Age Regional Environment* (pp. 81-99). Minneapolis: University of Minnesota Press.

Skibo, J. M. (2013). *Understanding Pottery Function*. New York, NY: Springer.

Spala, V. (2021). Έγγραφο (2)[4052]- Conservation Record. *Internal Conservation Report: Ephorate of Antiquities of Messinia.* Unpublished.

Stewart, D. (2011). Peloponnese (Archaic to Roman). *Archaeological Reports*, 57, 49-62.

Style, R. (2007). The Evaporation of a Salty Film. *Geophysical Fluid Dynamics Program* (pp. 204-226). Boston: Woods Hole Oceanographic Institution.

The British Museum. (2021). *Lagynos*. Retrieved January 2022, from https://www.britishmuseum.org/collection/object/G_1867-0512-52

The Metropolitan Museum of Art. (2021). *Terracotta Lagynos (oil flask).* Retrieved January 2022, from https://www.metmuseum.org/art/collection/search/254574

Themelis, P. (1965). Α.Δ. ΧΡΟΝΙΚΑ 20. ΗΛΕΙΑ.

Themelis, P. (2010). The Economy and Society of Messenia under Roman Rule. In A. D. Rizakis, & C. E. Lepenioti (Eds.), *Roman Peloponnese III : Society, Economy and Culture under the Roman Empire: Continuity and Innovation* (pp. 89-110). Athens.

Tite, M. S., Freestone, I. C., Meeks, N. D., & Bimson, M. (1982). The Use of Scanning Electron Microscopy in the Technological Examination of Ancient Ceramics. In J. S. Olin, & A. D. Franklin (Eds.), *Archaeological Ceramics* (pp. 109-120). Washington, D.C.: Smithsonian Institution Press.

Tite, M. S., Kilikoglou, V., & Vekinish, G. (2001). Strength, Toughness, and Thermal Shock Resistance of Ancient Ceramics, and their Influence on Technological Choice. *Archaeometry*, 3(43), 301-324.

Valmin, M. N. (1930). Études topographiques sur la Messénie ancienne. *Journal of Hellenic Studies*, 50.

Vandenabeele, P. V. (2016). Raman Spectroscopy and the Study of Ceramic Manufacture: Possibilities, Results, and Challenges. In A. Hunt, *The Oxford Handbook of Archaeological Ceramic Analysis* (pp. 1-15). Oxford University Press.

Villafane Silva, C. R. (2015). *The Perioikoi: a Social, Economic and Military Study of the Other Lacedaemonians*. University of Liverpool, Department of Archaeology, Classics and Egyptology. Liverpool: University of Liverpool Press.

Vogeikoff-Brogan, N. (2000). Late Hellenistic Pottery in Athens: A New Deposit and Further Thoughts on the Association of Pottery and Societal Change. Hesperia: *The Journal of the American School of Classical Studies at Athens,* 69(3), 293-333.

Volkov, D. S., Rogova, O. B., & Proskurnin, M. A. (2021). Article Organic Matter and Mineral Composition of Silicate Soils: FTIR Comparison Study by Photoacoustic, Diffuse Reflectance, and Attenuated Total Reflection Modalities. *Agronomy*, 11(1879), 1-30.

Vranová, V., Marfo, T. D., & Rejšek, K. (2015). Soil Scientific Research Methods Used in Archaeology - Promising Soil Biochemistry: A Mini-Review. *Acta Universitatis Agriculturae et Silviculturae Mendelianae Brunensis*, 63(4), 1417-1426.

Walters, H. B., Forsdyke, E. J., & Smith, C. H. (1925). *Catalogue of Vases in the British Museum.* London: BMP.

Wesley, L. D. (2009). Basic Index Tests, Soil Classification and Description. In *Fundamentals of Soil Mechanics for Sedimentary and Residual Soils* (pp. 27-48). Hoboken: John Wiley & Sons, Inc.

Witkowski, A. (1967). Infrared Spectra of the Hydrogen Bonded Carboxylic Acids. *Journal of Chemical Physics,* 47(9), 3645-3648.

Xi, S., Zhang, X., Luan, Z., Du, Z., Liang, Z., Li, L., Yan, J. (2019). Micro-Raman Study of Thermal Transformations of Sulfide and Oxysalt Minerals Based on the Heat Induced by Laser. *Minerals*, 9, 751-767.

Ancient Bibliography

Homer. (1998). *The Iliad.* Translated by Robert Fagles, Penguin Books. Knox, Bernard. Notes.

Pausanias. (1962). *Description of Greece, Volume II: Books 3-5 (Laconia, Messenia, Elis 1).* Translated by W. H. S. Jones, H. A. Ormerod. Loeb Classical Library 188. Cambridge: Harvard University Press.

Polybius. (1962). *Histories.* Translated by E. S. Shuckburgh. Reprint London: Bloomington.

Thucydides. (1881). *History of the Peloponnesian War, Volume I: Books 1-8.* Translated by B. Jowett. Oxford: Clarendon Press

Appendix A. Instrumental Analysis Methodology

Table A.1: Instrumental Methods. Instrumental techniques of elemental and mineralogical analysis of ceramics based on a table by Kazakis **(2015, p. 244)**.

Method	Type of Analysis	Characterization	Analyte	Sample Size	Sample Pre-Treatment	Sensitivity	Accuracy	Speed
NAA	chemical	multi-element, destructive, bulk analysis	solid, powder	50-100 mg or the whole object	pulverization/pellet or none	major, minor, and trace elements (few ppb)	high	high
XRF	chemical	Multi-element, non-destructive, surface or bulk analysis	solid, powder	100 mg-2g or the whole object	pulverization/pellet or none	major, minor, and trace elements (>50 ppb)	semi-quantitative -high	high
AAS	chemical	single-element, destructive, bulk analysis	solution	10mg-1g	pulverization, acidic digestion	major, minor, and trace elements (few ppb)	high	slow
EMPA	chemical	Multi-element, non-destructive, surface analysis	solid	few g	thin section	major, minor, and trace elements (>100 ppb)	good	high
PIXE	chemical	non-destructive, surface analysis	solid	few mg	pulverization/pellet or none	major, minor, and trace elements	high	high
SEM/EDS	chemical/mineralogical	non-destructive, surface analysis	solid	whole object (up to 10x10x20cm)	none or carbon coating	major, minor, and trace elements (>50 ppb)	good	high
ICP-MS	chemical	multi-element, destructive, bulk analysis	solution	5-100mg	pulverization, acidic digestion	major, minor, and trace elements (>50 ppb)	high	high
PETROGRAPHIC POLARIZING MICROSCOPE	mineralogical	non-destructive, bulk analysis	solid	few g	thin section	-	non-quantitative	slow
XRD	mineralogical	non-destructive, surface or bulk analysis	powder	2-20mg	pulverization	major and minor elements (>1%)	non-quantitative	average
RAMAN	molecular	Molecular, non-destructive, surface analysis	solid, solution, powder	few mg	pulverization/pellet, digestion, or none	major, minor, and trace elements (>100 ppb)	high	high
FTIR	molecular	Molecular, non-destructive, surface analysis	solid, solution, powder	few mg	pulverization/pellet, digestion, or none	major, minor, and trace elements (>100 ppb)	high	high

NAA: Neutron activation analysis
AAS: Atomic absorption spectrometry
PIXE: Proton-induced X-ray emission
ICP-MS: Inductively coupled plasma mass spectrometry
FTIR: Fourier Transform Infrared Spectroscopy
XRF: X-ray fluorescence spectroscopy
EMPA: Electron microprobe analysis
SEM: Scanning electron microscope
EDS: Energy-Dispersive X-ray
XRD: X-ray diffraction

Appendix B. Preliminary Sample Determination

Table B.1: Preliminary Characterization of Samples. A visual analysis of the Sample Group.

Sample	*Smooth Side*	*Rough Side*	*Defining Characteristic*	*Particle Size*	*Texture*	*Color*	*Assumed Position*
A1			flat bottom with coarse appearance	small-fine	smooth on bottom with porous appearance, coarse and friable on top	light brown-yellow	bottom
A2			flat, slightly convex bottom	small-fine	smooth and fine on bottom, coarse and friable on top	light brown-yellow	bottom
A3			flat, slightly convex bottom	fine	smooth and fine on bottom, smooth and flakey on top	light brown-yellow	bottom
A4			concave bottom	fine	flakey and fine on bottom, fine and coarse on top	light brown-yellow	middle
B1			flat bottom and shells on top	small-fine	smooth and grainy on bottom, coarse and friable on top	light brown-yellow	bottom
B2			semi-flat bottom with coarse appearance	small-fine	porous appearance that is rough and friable on top	light brown-yellow	middle
B3			smooth concave bottom	small-fine	smooth and fine on bottom, coarse and friable on top	light brown-yellow	middle
B4			smooth semi-concave with rough appearance	small-fine	semi-coarse appearance that is not friable	light brown-yellow	middle
B5			semi-smooth concave top	fine	smooth and fine on top and bottom	light brown-yellow	middle
B6			smooth and flat on both sides	fine	smooth and fine on bottom, smooth and friable on top	light brown-yellow	middle
B7		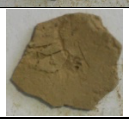	flat, slightly convex bottom and concave top	fine	flakey and smooth and fine on top and bottom	light brown-yellow	middle
B8			flat, slightly concave bottom	fine	Smooth and fine, flakey on top	light brown-yellow	middle
C1			flat convex bottom	fine	smooth and flakey	light brown-yellow	middle
C2			semi-flat concave	fine	smooth and fine and flakey on bottom, coarse and fine on top	light brown-yellow	indeterminate

C3			friable and slightly porous	small-fine	rough and fine and friable	light brown-yellow	indeterminate
C4			smooth and flat on bottom, fine and friable on top	fine	smooth and flat on bottom, fine and friable on top	light brown-yellow	indeterminate
C5			flat and smooth and flakey	fine	smooth and fine on bottom, flakey and fine on top	light brown-yellow	indeterminate
C6			flat and smooth and flakey, slightly concave	fine	smooth and fine on bottom and top	light brown-yellow	indeterminate
C7	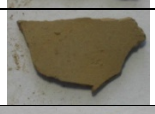		flat and smooth and flakey	fine	smooth and fine on bottom; smooth and rough on top	light brown-yellow	indeterminate
C8			smooth and convex on bottom, rough and fine on top	fine	smooth and flakey on bottom, rough and fine on top	light brown-yellow	indeterminate
C9			flat and smooth and flakey	fine	smooth and fine on bottom, flakey and fine on top	light brown-yellow	indeterminate
C10			flat and smooth and flakey	fine	smooth and fine on bottom, flakey and fine on top	light brown-yellow	indeterminate
C11			small, friable, and fine	fine	friable and fine	light brown-yellow	indeterminate
D1			complete shell	fine	fine and friable	light brown-yellow	indeterminate
D2			partial shell	fine	fine and friable	light brown-yellow	indeterminate
E			remaining loose soil	Medium, small, fine	Small friable clusters and fine loose soil	light brown-yellow	indeterminate
E1[8]			friable and slightly porous and fine	small-fine	friable and fine	light brown-yellow	indeterminate

[8] E1 was not a part of the original sample group but was instead taken from Sample Group E in order to provide elemental values for samples from the interior of the vessel.

Appendix C. Optical Classifications

Table C.1: LED and Munsell Classification of Soil Fabric. A macroscopic analysis of the Sample Group.

Sample	*LED Photo (X50)*	*Munsell Soil Color Chart*	*Frequency of Inclusions*	*Size & Shape of Inclusions*	*Coarseness*	*Porosity*
A1		*2.5Y 6/3 Light yellowish-brown*	*60%*	*small inclusions; granular, angular, subangular; fine to coarse*	*coarse*	*5%*
A2	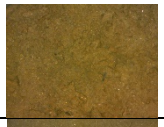	*2.5Y 6/4 Light yellowish-brown*	*15%*	*small inclusion of various colors; granular; fine*	*fine*	*5%*
A3		*2.5Y 6/4 Light yellowish-brown*	*5%*	*very few small inclusions; granular; fine*	*fine*	*0%*
A4		*2.5Y 7/3 Pale Brown*	*5%*	*very few small inclusions; granular; fine*	*fine*	*5%*
B1		*2.5Y 6/3 Light yellowish-brown*	*70%*	*small inclusions; granular, angular, subangular; fine to coarse*	*coarse*	*10%*
B2		*2.5Y 5/3 Light olive Brown*	*70%*	*small inclusion of various colors; granular, angular, subangular; fine to coarse*	*coarse*	*10%*
B3		*2.5Y 7/3 Pale Brown*	*5%*	*very few small inclusions; granular; fine*	*fine*	*0%*
B4	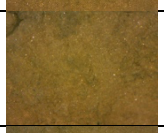	*2.5Y 6/3 Light yellowish-brown*	*10%*	*small inclusion of various colors; granular; fine*	*fine*	*0%*
B5		*2.5Y 6/4 Light yellowish-brown*	*10%*	*very few small inclusions; granular; fine*	*fine*	*0%*
B6	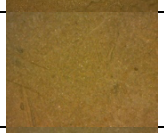	*2.5Y 6/3 Light yellowish-brown*	*10%*	*very few small inclusions; granular; fine*	*fine*	*0%*
B7	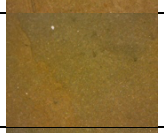	*2.5Y 6/3 Light yellowish-brown*	*5%*	*very few small inclusions; granular; fine*	*fine*	*0%*
B8	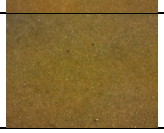	*2.5Y 6/3 Light yellowish-brown*	*10%*	*very few small inclusions; granular; fine*	*fine*	*0%*

C1	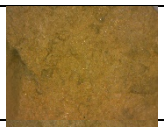	*10YR 6/4 Light yellowish-brown*	*20%*	*very few small inclusions; granular; fine*	*fine*	*0%*
C2		*10YR 6/3 Pale Brown*	*20%*	*very few small inclusions; granular; fine*	*fine*	*5%*
C3		*2.5Y 6/4 Light yellowish-brown*	*30%*	*small inclusion of various dark colors; granular, subangular; fine to coarse*	*coarse*	*10%*
C4	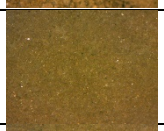	*10YR 6/3 Pale Brown*	*20%*	*very few small inclusions; granular; fine*	*fine*	*0%*
C5		*2.5Y 7/4 Pale Brown*	*10%*	*very few small inclusions; granular; fine*	*fine*	*0%*
C6		*2.5Y 6/3 Light yellowish-brown*	*10%*	*very few small inclusions; granular; fine*	*fine*	*0%*
C7		*2.5Y 7/6 Yellow*	*10%*	*very few small inclusions; granular; fine*	*fine*	*0%*
C8		*10YR 6/4 Light yellowish-brown*	*10%*	*very few small inclusions; granular; fine*	*fine*	*0%*
C9		*10YR 6/3 Pale Brown*	*10%*	*very few small inclusions; granular; fine*	*fine*	*0%*
C10	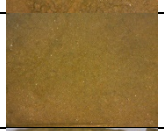	*10YR 7/3 Very Pale Brown*	*5%*	*very few small inclusions; granular; fine*	*fine*	*0%*
C11		*10YR 6/4 Light yellowish-brown*	*30%*	*small inclusion of various dark colors; granular, subangular; fine to coarse*	*fine-coarse*	*50%*
D1		*10YR 6/3 Pale Brown*	*5%*	*very few small inclusions; granular; fine*	*fine*	*0%*
D2	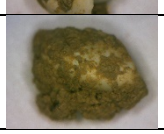	*10YR 6/3 Pale Brown*	*5%*	*very few small inclusions; granular; fine*	*fine*	*0%*
E1		*2.5Y 6/3 Light yellowish-brown*	*10%*	*small inclusion of various dark colors; granular, angular, subangular; fine to coarse*	*coarse*	*40%*

Appendix D. SEM Images

Table D.1: SEM Representative Data of the Refined Analysis Group. A comparison of rough and smooth sides of the samples.

Sample	*Side*	*30x SEM*	*100x SEM*	*200X SEM*
A1	S	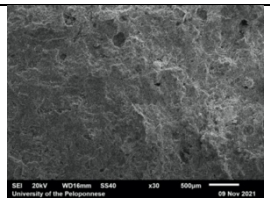	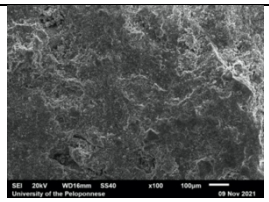	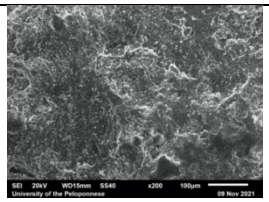
	R	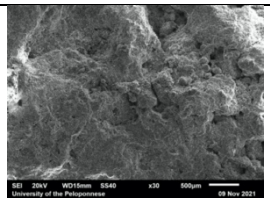	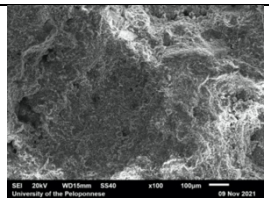	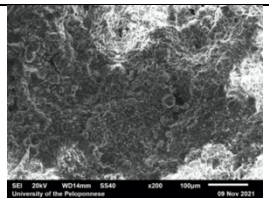
B1	S	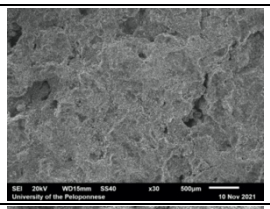	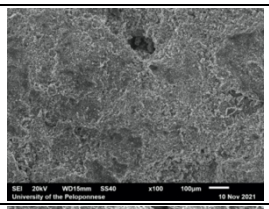	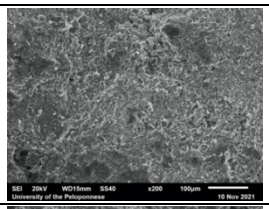
	R	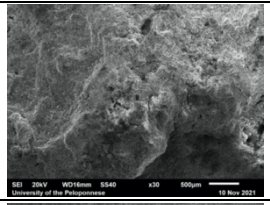	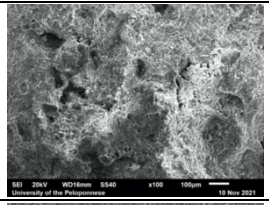	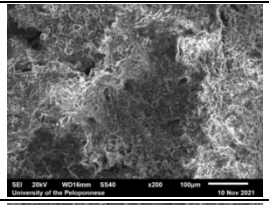
B4	S	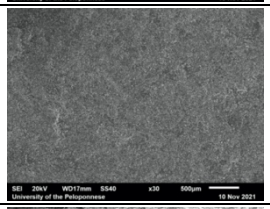	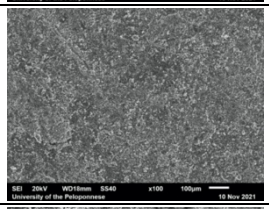	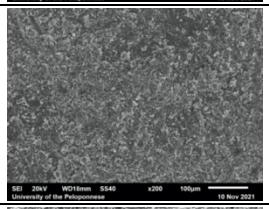
	R	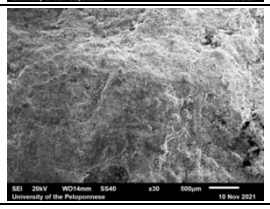	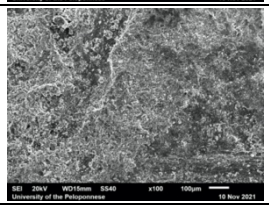	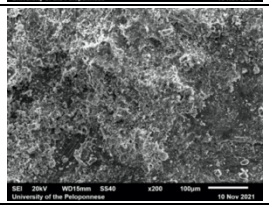

B6	S	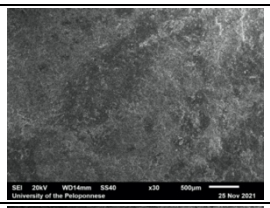	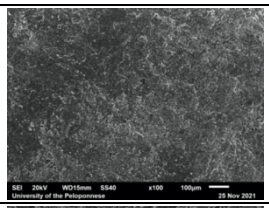	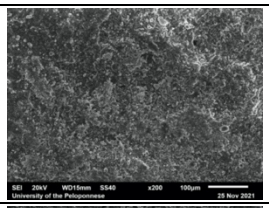
	R	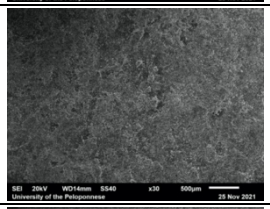	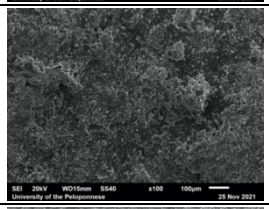	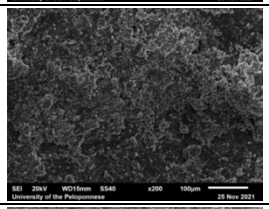
B7	S	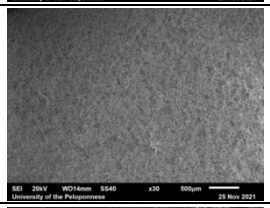	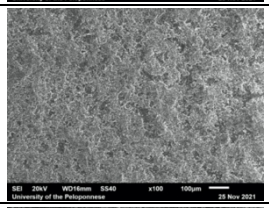	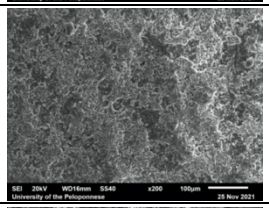
	R	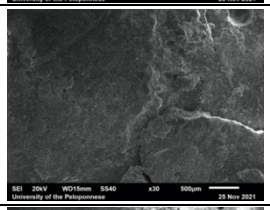	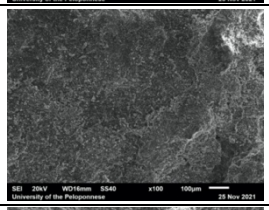	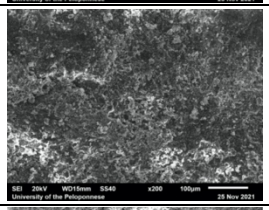
C3	R	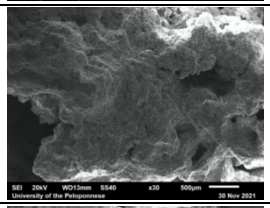	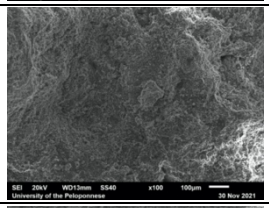	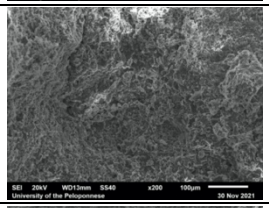
E1	R	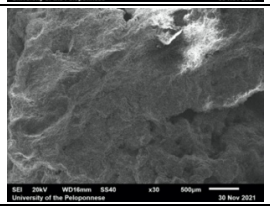	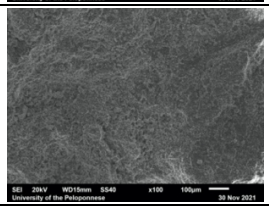	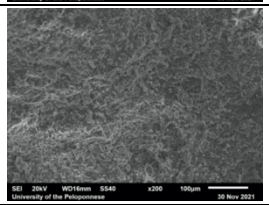

Table D.2: SEM Reference Data of the Reference Group. A comparison of rough and smooth sides of the reference samples.

Sample	*30x SEM*	*150x SEM*	*200X SEM*
REF_A1	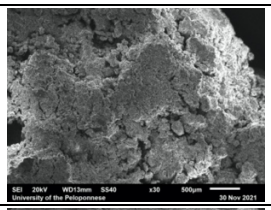	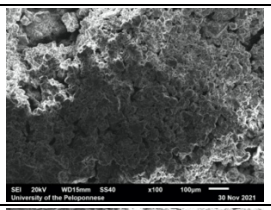	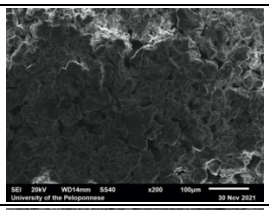
REF_B1	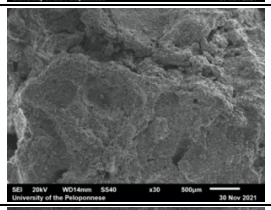	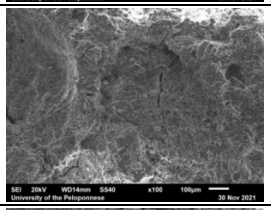	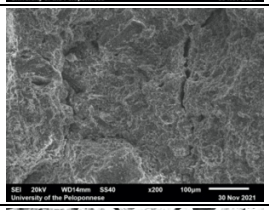
REF_C1	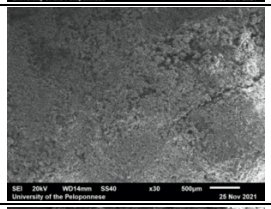	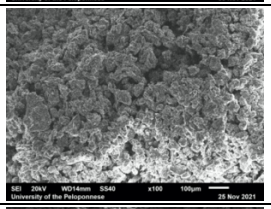	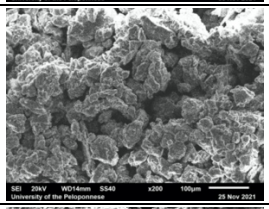
REF_D1	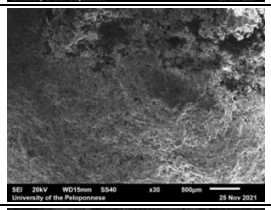	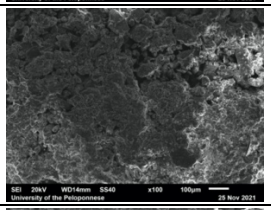	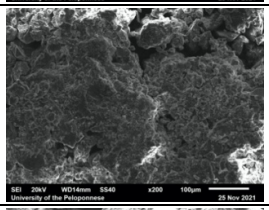
REF_E1	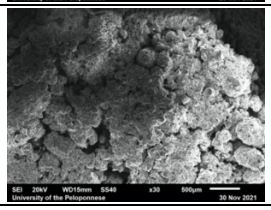	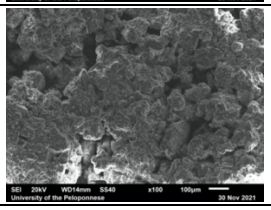	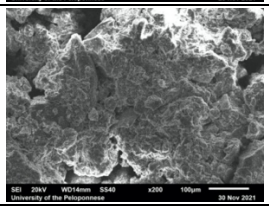

Appendix E. EDS Data

Table E.1: A1 Smooth Side. The group values are given as compound% (normalized to 100%).

	MgO	*Al_2O_3*	*SiO_2*	*K_2O*	*CaO*	*FeO*
Spectrum 4	2.95	14.64	54.77	3.92	18.56	5.16
Spectrum 8	4.21	15.98	47.30	5.67	18.76	8.09
Spectrum 10	3.49	15.89	53.37	4.99	14.47	7.78
Average	3.55	15.50	51.81	4.86	17.26	7.01

Table E.2: A1 Rough Side. The group values are given as compound% (normalized to 100%).

	MgO	*Al_2O_3*	*SiO_2*	*K_2O*	*CaO*	*FeO*
Spectrum 4	3.26	13.10	46.11	3.05	24.81	9.66
Spectrum 7	2.16	13.59	57.25	3.06	18.36	5.58
Spectrum 8	1.99	19.98	49.64	2.09	18.47	7.82
Average	2.47	15.56	51.00	2.73	20.55	7.69

Between the two sides, there are patterns. The smooth side has higher Mg than the rough side. The smooth side has higher K levels than the rough side. The smooth side has lower Ca than the rough side. The Al, Si, and Fe values between the two sides are consistent.

Table E. 3: B1 Smooth Side. The group values are given as compound% (normalized to 100%).

	MgO	*Al_2O_3*	*SiO_2*	*K_2O*	*CaO*	*FeO*
Spectrum 1	2.26	20.74	45.30	4.09	21.09	6.52
Spectrum 4	2.46	14.63	52.03	3.80	19.65	7.43
Spectrum 5	4.24	13.86	49.70	2.78	19.75	9.67
Spectrum 6	3.65	16.56	50.75	3.90	19.01	6.13
Average	3.15	16.45	49.45	3.64	19.88	7.44

Table E.4: B1 Rough Side. The group values are given as compound% (normalized to 100%).

	MgO	*Al_2O_3*	*SiO_2*	*K_2O*	*CaO*	*FeO*
Spectrum 2	3.40	17.71	52.71	3.52	15.88	6.79
Spectrum 3	3.50	16.82	50.14	4.32	18.17	7.04
Average	3.45	17.27	51.43	3.92	17.03	6.92

Between the two sides, there are patterns. The smooth side has lower Al than the rough side. The smooth side has lower Si than the rough side. The smooth side has higher Ca than the rough side. The Mg, K, and Fe values between the two sides are consistent.

Table E.5: B4 Smooth Side. The group values are given as compound% (normalized to 100%).

	MgO	*Al_2O_3*	*SiO_2*	*K_2O*	*CaO*	*FeO*
Spectrum 6	1.77	19.74	55.53	2.96	12.93	7.08
Spectrum 7	4.64	17.29	48.90	3.63	21.33	4.22
Spectrum 8	2.76	20.30	45.85	3.74	20.57	6.79
Average	3.06	19.11	50.09	3.44	18.28	6.03

Table E.6: B4 Rough Side. The group values are given as compound% (normalized to 100%).

	MgO	*Al_2O_3*	*SiO_2*	*K_2O*	*CaO*	*FeO*
Spectrum 3	3.57	17.88	48.10	5.44	17.25	7.77
Spectrum 4	3.74	16.70	50.24	2.92	17.26	9.15
Spectrum 6	2.34	16.47	50.88	4.72	19.54	6.04
Average	3.22	17.02	49.74	4.36	18.02	7.65

Between the two sides, there are patterns. The smooth side has higher Al than the rough side. The smooth side has lower K than the rough side. The smooth side has lower Fe than the rough side. The Mg, Si, and Ca values between the two sides are consistent.